Universitat Politècnica de Catalunya

Departament de Física Aplicada
Departament de Física i Enginyeria Nuclear

Doctoral programme:
Computational and Applied Physics

Dynamics of metallic glasses explored by mechanical relaxation

Thesis submitted by

Chaoren Liu

For obtaining the doctor title by Universitat Politècnica de Catalunya

Directors:

Prof. Daniel Crespo Artiaga

Dr. Eloi Pineda Soler

29th July 2015

Abstract

Dynamic mechanical analysis (DMA) is often used to explore the relaxation dynamics of metallic glasses (MGs). Secondary relaxations in metallic glasses appear as an excess wing, as a shoulder of the primary relaxation peak or as a differentiated low temperature peak on the loss modulus $E''(T)$. In order to differentiate this relaxation from α-relaxation, which is due to collective movement and directly related to the elastic (solid glass) to viscous (supercooled liquid) transition, it is termed as β-relaxation. Its origin and main characteristics are still not clear and the understanding of the β process is still developing.

Early results based on DMA suggested that it is the result of anelastic events, as the system is in a metastable state. It might be originated from diffusion processes, resembling Zener or Snoek relaxation in crystalline materials. In the energy landscape picture it is attributed to jumps between close energy minima separated by a low energy barrier. It is also treated as a process related to the activation of shear transformation zones (STZ) or flow units. In this thesis, the mechanical relaxation of MG is explored by quasi-static measurements like creep and stress relaxation, and by DMA. The current theoretical models and experimental data available in literature are revised and discussed. Following, three different MG systems, namely, $Cu_{46}Zr_{46}Al_8$, $Pd_{42.5}Ni_{7.5}Cu_{30}P_{20}$ and $Fe_{55}Cr_{10}Mo_{14}C_{15}B_6$ are analyzed and it is clarified that the different β-relaxations manifested on the DMA behavior have different origins.

Finally, we discuss the implications of the relaxation dynamics characterization presented in this work on the mechanical properties of these materials. The understanding of the relaxation behavior and some related phenomena like physical aging, mechanical deformation and internal damping is seen as fundamental to improve our knowledge of MGs, this leading to new alloys with improved mechanical performance.

Acknowledgements

I have many thanks for many people who have helped and encouraged me during my dissertation work until its completion.

I would like to express my special appreciation to Professor Daniel Crespo and Dr. Eloi Pineda for the support of my Ph.D. research. This work could not have been finished without their guidance. Daniel started to help me when we were applying for the scholarship. I am extremely grateful for his willingness to take risks with me when I had not yet proven myself. He helped me overcome many difficult problems when designing the experiments. His encouragement of designing experiments, his support for putting many thoughts into practice even in other groups when we can not do it in our own lab has been of great importance for keeping my interest on the research subject. He is also my mentor on Spanish culture. His genius way of solving problems is always inspiring me on my way of life.

Many thanks need to be addressed to Dr. Eloi Pineda. I was introduced to this area by Eloi. My knowledge about relaxation dynamics is obtained by his patient explanation. I am indebted to him for his precious time on discussing all my doubts on the experimental details. His rigorous attitude towards the result is of great importance for the conclusions. Besides research, his affirmative and cheerful character also influenced me. I own many thanks to him for letting me have such good experience on the way of science.

I would like to thank Professor Trinitat Pradell and Dr. Pere Bruna for their helpful discussion on experimental design and analysis. Trinitat's research make me believe that research is not boring experiment on new things or mechanism, but could be very interesting and beautiful. It is very interesting to explore the physical phenomenon in our daily life when Pere prepares the experiments for the graduate students. Many thanks are given to Trinitat and Pere for their amazing stories. I want to thank Doctor Trifon Trifonov from Centre de Recerca en Nanoenginyeria for the X-ray diffraction, SEM as well as focus ion beam experiments. I would like to thank Professor Joan Josep Sunyol and Joan Pere López from Universitat de Girona for their help on the low temperature DMA measurements. I also would like to thank

Mr. Milad Madinehei and Mr. Fuqiang Zhai for discussions on the research topic.

I would like to thank Anna and Ruxandra for their organization of many experiences which made my life more interesting. I am deeply grateful to the people that shared all this time in the office: Araceli, Anna, Enrique, Estel, Francesc, Fuqiang, Gabriela, Maria, Milad, Mitra, Ruxandra and Shervin.

I thank Jing Yang for her belief and tolerance on me. When my self-doubts would exceed my curiosity, she carried me through with effortless grace. I am very gratitude to her for sharing so many memories. I owe everything to my parents, Dechun Liu and Qiugui Liu, for all their love and sacrifice for me.

Financial support from AGAUR is greatly appreciated.

Contents

1 Introduction 1
1.1 Merits of MGs and problems need to be solved 2
1.2 Glass transition and glass forming ability (GFA) 5
1.2.1 Thermodynamics of crystallization and glass transition 5
1.2.2 Parameters related to GFA 8
1.3 Structure of amorphous materials 10
1.4 Stability considerations 13
1.5 Mechanical properties 15
1.6 Forming 18
1.7 Applications of MGs 19
2. Objectives 21
3. Mechanical relaxation of MGs: overview of experimental data and theoretical models 23
3.1 Basics of glass relaxation dynamics 23
3.1.1 Relaxation in the supercooled liquid region 25
3.1.2 Relaxation and aging below T_g 26
3.1.3 Models for glassy dynamics 31
3.2 Mechanical relaxation of glasses 32
3.2.1 Introduction to mechanical relaxation 32
3.2.2 Time and frequency domain response functions 36
3.3.3 Thermally activated models 40
3.3 Mechanical spectroscopy of MGs 42
3.3.1 Secondary relaxations 44
3.3.2 Influence of aging 49
3.3.3 Modelling of the mechanical relaxation spectrum 52
3.4 Relationship between the relaxation and the mechanical properties 60
4. Experimental materials and methods 65
4.1 Sample preparation 65
4.2 Structural, calorimetric and chemical characterization 66

4.3 DMA characterization 75
4.4 Selection of the samples for the mechanical relaxation study 77
5. Characterization of relaxation dynamics of metallic glasses 79
5.1 Relaxation dynamics of $Cu_{46}Zr_{46}Al_8$ MG 80
5.1.1 Thermal analysis 80
5.1.2 Dynamic mechanical analysis 80
5.1.3 Stress relaxation analysis 86
5.2 Relaxation dynamics of $Pd_{42.5}Ni_{7.5}Cu_{30}P_{20}$ MG 91
5.2.1 Thermal analysis 91
5.2.2 Mechanical response of MG under fixed stress 93
5.2.3 Recovery behavior 100
5.2.4 Stress relaxation of $Pd_{42.5}Ni_{7.5}Cu_{30}P_{20}$ 103
5.2.5 Dynamic mechanical analysis 111
5.2.6 Physical aging explored by mechanical relaxation 116
5.3. Relaxation dynamics of $Fe_{55}Cr_{10}Mo_{14}C_{15}B_6$ MG 121
5.3.1 Activation energy spectrum by enthalpy relaxation 121
5.3.2 Mechanical relaxation 124
5.4 Discussion of the experimental results 130
6. Conclusions 139

1 Introduction

A glass is formed when a liquid cooled down below its melting temperature fails to crystallize but instead cools continuously and forms a solid. From the structural point of view, although detailed structure analysis may show differences between the glassy state and the liquid state, the glass inherits the structure of the ancestor liquid. Besides the amorphous structure, the terminology of glass is usually related to substances that show a glass transition on the enthalpy measurement. Structural glasses comprise the families of oxide glasses, polymeric glasses and, more recently discovered, metallic glasses (MGs). In all these families it is found that the crystallization can be suppressed depending on the crystallization kinetics of the particular substance.

As to the particular case of glassy metals, they were first described as "amorphous alloys" where emphasis was put on the structural aspect[1]. In the earlier period, due to the limited glass forming ability of the first discovered alloys, the amorphous alloys were only obtained by high cooling-rate techniques like rapid quenching or atomic deposition. These amorphous alloys, without clear glass transition behavior on the calorimetric measurement, sometimes were not regarded as glasses. The absence of a clear glass transition was because the glassy state was not stable enough and the material crystallized upon heating before the glass transition temperature was completed.

Inoue's systematic works on the stability of supercooled metallic liquids probing different compositions[2–4] broadened the range of alloys that could be vitrified and reduced the required cooling rate. In those new alloys, calorimetric measurements showed a clear glass transition phenomenon at temperatures well differentiated from the crystallization process. Because of this, they were started to be referred as metallic glasses. It was found that in some good glass-forming systems, the critical cooling rate to avoid crystallization could be as low as 10 K/s, for instance in compositional systems like Pd-Ni-Cu-P[5,6] or Zr-Ti-Cu-Ni-Be[7], and they could be cast into parts of centimeters without crystallization by simple copper mold casting

techniques. These easy glass-forming alloys were called as bulk metallic glasses (BMGs)[8,9].

1.1 Merits of MGs and problems need to be solved

Ever since their discovery, MGs have risen great interest, both as a basic research subject in the field of disordered matter and as a potential engineering type of materials. With the continuous research in increasing glass forming ability (GFA), samples with higher stability and more extended supercooled liquid region were obtained. This high glass and liquid stability make it possible to investigate the dynamics and thermodynamics of glass formation and to explore the functional and structural applications. Compared with their counterpart crystalline alloys, glassy metals lacking of long range order endow unusual mechanical, chemical and physical properties.

Until now, the most successful application of MGs are based on their magnetic properties. The families of MGs with soft and hard magnetic properties were reviewed by Inoue[10]. Typical MGs with soft magnetic properties, like $Fe_{72}Al_5Ga_2P_{11}C_6B_4$, have Curie temperatures of 590-600 K, which can increase up to 600-606 K after certain annealing treatments. The saturation magnetization (B_s) is around 1.1 T and the coercive force (H_c) is 2-6 Am^{-1}. The permeability reduces at higher frequency in crystalline metals, while in these soft magnetic MGs the relative permeability can remain as high as 7000-12000 at 1 kHz. The saturated magnetostriction when applied in a transformer core is found to be 2.1×10^{-5} for Fe-Al-Ga-P-C-B-Si alloys which is still high, but is around 30% lower as compared with those of Fe-Si-B amorphous alloys (3.0×10^{-5})[10,11]. This lower magnetostriction is helpful for reducing the noise generated by the transformer. Due to their low coercivity and high permeability, combined with a high electrical resistivity, which is helpful for reducing eddy current losses, soft magnetic MGs are widely used in laminated transformer cores.

As to the hard magnetic properties, MGs like $Ln_{60}Fe_{30}Al_{10}$ (Ln=Nd or Pr) with Curie temperatures T_c around 600 K can be cast into cylinders with diameters up to 15 mm. Typical magnetic properties are 0.13 T for

remanence, 0.15 T for B_s, 280 kAm^{-1} for H_c and 19 kJm^{-3} for $(JH)_{max}$. The magneto-caloric effect and tunable magnetic properties are also of great interest[10].

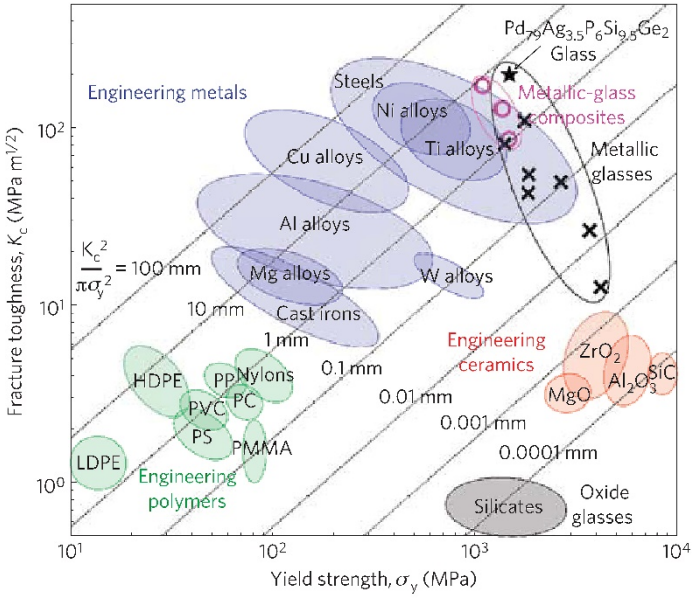

Figure 1-1 Ashby map of the damage tolerance of materials[12].In normal crystalline materials, there is usually a tradeoff between yield strength and toughness due to activation of the dislocations. On the other hand, metallic glasses could possess both high yield strength and fracture toughness.

Regarding to mechanical properties, as the dislocation movement gets activated under stress and accumulated in the grain boundaries, there is a tradeoff between the strength and toughness in crystalline materials. This can be clearly seen from Figure 1-1. As mentioned by Demetriou[12], the dislocation based deformation mechanism makes a low elastic energy threshold for these defects to get activated, which leads to low yield strengths. Dislocation movement also enables extensive plastic shielding ahead of an opening crack, which promotes high fracture toughness. In contrast, materials with amorphous atomic structures, lacking classical microstructural defects like dislocations, can potentially yield plastically at much higher strengths. For example, ductile metals, like low carbon steels, have a low plastic yield strengths of less than 500 MPa and high fracture toughness above 200 MPa·m$^{1/2}$. On the contrary, silicate glass fibers have high yield strengths of up to 3GPa but very limited plasticity ahead of an opening crack tip.

Consequently an opening failure is usually accommodated by unstable crack propagation, resulting in low fracture toughness and often low strength, as shown in the silicates glasses bulk samples where toughness is lower than 1 $MPa.m^{1/2}$. Their failure occurs at less than 100 MPa by brittle fracture which is well below the theoretical yield strength.

Because of the possibility of producing large samples, mechanical properties can be measured in BMGs. A shear sliding mechanism in the vicinity of a flaw under opening stress can blunt the crack, and it is shown that BMGs can possess high yield strength as well as high fracture toughness[12]. As it can be seen in Figure 1-1, BMGs have the advantage of both high strength and high fracture toughness. This makes them potential engineering structural materials. Besides the high elastic limit and strength, ultralow elastic moduli, tension compression anisotropy and strain rate sensitivity have been also found in some specific BMGs[13].

Compared to crystalline metals, MGs show a continuous change of volume during glass formation, the solidification shrinkage is low and high precision is obtained in melt casting processes. Besides, the high viscosity and low strain rate sensitivity of the supercooled liquid permit thermoplastic forming[14]. The ease of precision forming by thermoplastic flow combined with high hardness makes MGs good candidates to be used in mm-scale structures like gears in miniature electric motors[15].

The properties of MGs related to potential applications are summarized in a very nice work by Ashby[16]. Due to the lack of grain boundaries, where initiation of corrosion usually happens, and because of the extension of the solubility region of beneficial anti-corrosion elements some MGs also show an outstanding corrosion resistance. High hardness and corrosion resistance gives durability which is attractive from aesthetic point of view as well as for wear resistance applications.

Although MGs are very promising as potential structural materials, there are several basic as well as practical problems not yet fully understood like formation, structure, thermal stability or brittleness. The solution of these problems is still generating great research efforts in the MG scientific community.

1.2 Glass transition and glass forming ability (GFA)

Practically, the first thing we care about on a specific material is its availability. GFA is an important factor we need to concern about which illustrates the easiness of obtaining MGs. A lower required cooling rate means that a bigger glassy sample can be obtained. MGs are metastable materials formed under the conditions where crystallization is suppressed. Normally, a high cooling rate is required in order to suppress the nucleation and growth of the crystallites. Experimentally, the improvement of GFA can be achieved with composition optimization. This composition optimization is accomplished with the understanding of both the thermodynamics and kinetics of the glass formation and crystallization processes.

1.2.1 Thermodynamics of crystallization and glass transition

Glass is formed when cooling a material under the circumstance that crystallization is avoided. The thermodynamics and kinetics of crystallization play central role in glass formation. Figure 1-2 shows the changes of properties when a liquid is cooled into the solid state. The temperature region could be separated into three parts: the thermodynamically stable liquid, the thermodynamically metastable supercooled liquid and the out-of-equilibrium glassy state. At the highest temperatures, this means region A of figure 1-2, the free energy of the liquid is lower than the crystalline phase, the melt is in equilibrium state and there is no driving force for crystallization.

Cooling into range B (the freezing-melting temperature T_f is where the Gibbs energy of the liquid phase is the same as the crystalline phase), the free energy of the liquid becomes larger than that of the crystalline phase. The melt is metastable and will crystallize if a critical nucleus is provided. This state is called supercooled liquid state. For metallic melts, this temperature region can be separated into two according to the dominating process of crystallization. At the higher temperatures, the critical nucleus size is large and, therefore, the homogeneous nucleation rate is very low. On the contrary, the growth rate is fast at this temperature region. At the lower temperatures of this region, the driving force of crystallization is high enough to produce a

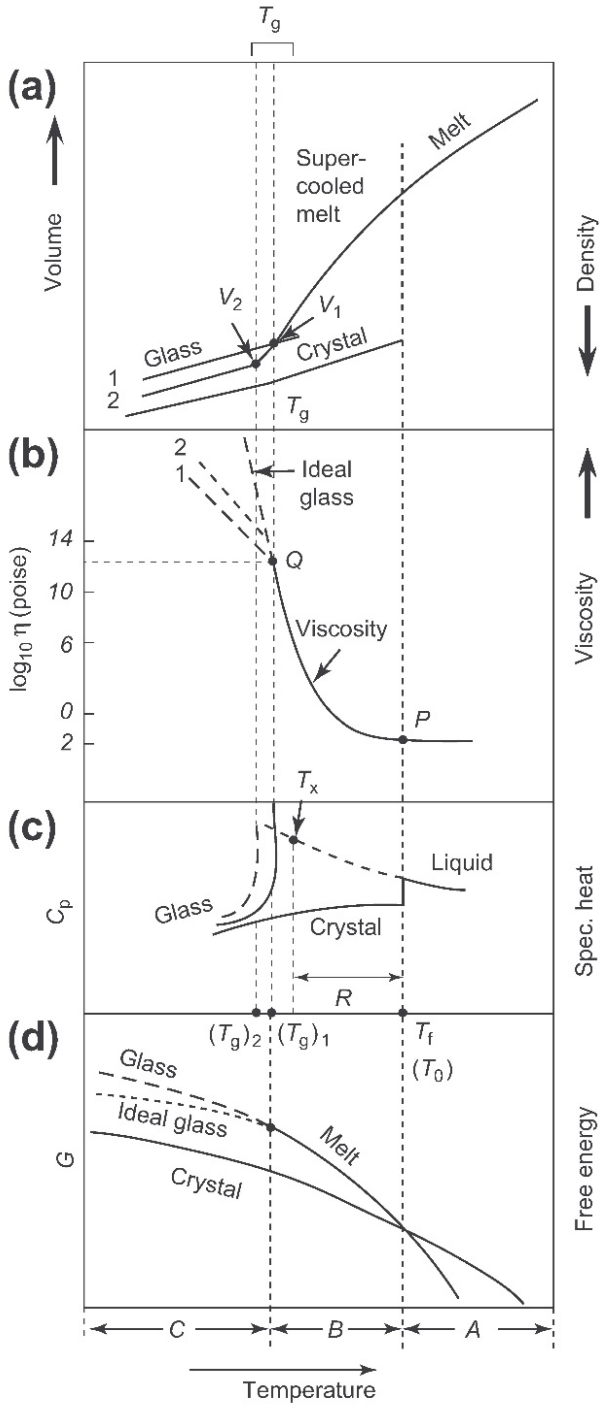

Figure 1-2 Properties of the glassy and liquid state as function of temperature[17]. Properties related are (a) volume or density. (b) viscosity. (c) heat capacity Cp. (d) Gibbs free energy.

high homogeneous nucleation rate but the slow growth of the crystallites, related with the high viscosity and slow diffusion of the atoms, becomes the limiting factor. Crystallization would happen in range B if both the thermodynamic and kinetics conditions for crystal growth are satisfied. If crystallization is avoided on cooling, range C is reached where we called the system is in the glass state.

As shown in figure 1-2, the glass transition manifests on the temperature dependence properties like volume or viscosity of the supercooled liquid. A glass state is characterized by the liquid configuration frozen at the glass transition temperature T_g. It should be noted that unlike T_f which is a thermodynamic parameter, T_g is not but a dynamic related parameter, which depends on the cooling or heating rates applied to the system. In order universally define the glass transition temperature, T_g is defined as the temperature where the viscosity of the supercooled liquid phase reaches 10^{12} Pa·s. However, experimentally, with slow cooling rates, the deviation from the supercooled liquid happens at lower temperatures and a smaller specific volume and higher viscosity of the glassy state are obtained.

From the solidification kinetics point of view, the viscosity of MG forming liquids at temperatures around T_g is of great importance for crystallization. Actually, as it will be explained in chapter 2, the viscosity behavior of the glass is influenced by physical aging and it shows a quite complicated behavior. In the glass state (region C in figure 1-2), annealing of the glass enables the system to evolve towards more stable states and so it becomes densified. This process is referred as physical aging or structural relaxation. Physical aging stabilizes the glass leading it towards a so called ideal glassy state.

This ideal glassy state is represented by an extrapolation of the equilibrium liquid properties. As it can be seen in figure 1-2, extrapolation of liquid properties like volume to lower temperatures would lead to a point where the property of the glassy state would be the same as that of the crystalline one. Kauzmann suggested that the isentropic point at which the extrapolated liquid entropy matches that of the crystal could be taken to represent an ideal glass transition temperature. This ideal glass transition temperature corresponds to

an infinite slow cooling rate and the experimentally observed glass transition from viscosity, calorimetric or other experimental probes is always found at higher temperatures.

1.2.2 Parameters related to GFA

In the early studies, due to limited GFA, researchers were focused on the development of better rapid-quenching techniques for applying higher cooling rates. The pioneer work on stabilizing the amorphous alloys by Inoue showed that, in some alloy systems, the glass could be formed using relatively low cooling rates. Ever since then, much work have been done to explore the range of compositions that do not require high cooling rates but could be formed in bulk MGs with simple mold casting techniques.

Inoue summarized three empirical rules for finding high GFA alloys based on their systematic work on the GFA dependence of composition: a) presence of at least three atomic elements in the system, b) large negative heat of mixing between the elements and c) atomic radius differences larger than 12% between the different components. Besides Inoue's rules, several parameters based on empirical data have been put forward with the aim of understanding the GFA through the characteristic temperatures of the systems.

One of the most used ideas was developed by Turnbull[18], based on the fact that crystallization during cooling is possible only in the supercooled liquid region from the equilibrium melting temperature T_f down to T_g (figure 1-2). Consequently, the crystallization is more easily avoided on cooling if these two temperatures are closer to each other. The liquidus (freezing) temperature T_f is more dependent on composition than T_g which is more constant. At a eutectic composition, the T_f is lowest and thus the two temperatures are closest, increasing the GFA. Compiling results in binary systems, it was suggested that good glass formers are usually found near eutectic points. In order to develop quantitative parameters, GFA was related to the reduced glass transition temperature, $T_{rg}=T_g/T_f$. In multicomponent systems, even deeper eutectics (i.e. with eutectic temperature T_f even closer to

T_g) can be achieved, and this is the basis for the discovery of systems with higher T_{rg} and corresponding higher GFA.

Besides T_{rg}, many other parameters are also used to characterize the GFA from thermodynamic aspects. The stability of the supercooled liquid, determined as $\Delta T_x=T_g-T_x$, which is the temperature difference between T_g and the crystallization temperature T_x is often used. Besides, there are parameters relating two or more characteristics temperatures, like the γ parameter, widely used to characterize the stability of the supercooled liquid and the GFA[19,20]. There are also GFA parameters based on the atomic level characteristics of the alloy. Based on the covalent atomic radii, Ma suggested that a critical electronegativity difference Δx_{cri} correlated the alloy composition with the thermal stability and GFA of Al-Ni-Re ternary MGs[21].

Despite many empirical and theoretical efforts, predicting the GFA is not an easy work. In $Al_{87}Ni_7Gd_6$, the T_{rg} is usually less than 0.5, and the increase of T_{rg} as well as thermal stability against crystallization is obtained with decreasing Al content. Based on the parameters mentioned earlier, the GFA might get improved. However, experimental result show that this is not the case[22]. In fact, the current models are mostly empirical with limited ability to predict GFA. For instance, in binary systems like $Cu_{66}Hf_{34}$[23], with T_{rg}=0.62 and ΔT_x=51 K, fully glassy bulk samples can be obtained. This binary system with large GFA does not fulfills Inoue's empirical rules.

The key for obtaining amorphous metals is the suppression of crystallization at a given cooling rate. The success of Inoue on stabilizing the supercooled liquid has inspired other people aiming to find systems with high GFA. Much effort has been put on optimizing the composition to stabilize the supercooled liquid. Trial and error method is still often employed and nowadays new BMGs are being reported continuously.

This work is focused on three well known MG systems, namely Cu-Zr-Al, Pd-Ni-Cu-P, and Fe-(Mo,Cr)-(C,B).The influence of doping with Al on the thermal behavior of the $(Cu_{50}Zr_{50})_{100-x}Al_x$($3<x<10$) system shows that T_g, T_x and ΔT_x all increase with the concentration of the doping element [24]. Works in other related systems show that with Al addition, the GFA of $Ti_{41}Zr_{25}Be_{34}$

alloy can be enhanced from 5mm to 7mm, and by partial substitution of Cu by Al the system with composition of $Cu_{49}Hf_{42}Al_9$ can be cast into cylinders of 10 mm diameter[25]. A fifth alloying element, Cu addition to Ti-Zr-Be-Al glassy system, can further improve GFA and 10 mm glassy rods have been reported for the $(Ti_{41}Zr_{25}Be_{29}Al_5)Cu_9$ alloy[26].

Pd-Ni-Cu-P and Fe-(Mo,Cr)-(C,B) systems belong also to some of the most studied MG systems. The former one is the system showing the highest GFA ever reporter[6] allowing the production of 7.2 cm bulk parts of completely amorphous metal. The latter one, belongs to the family of the so called amorphous steels. This family is characterized by compositions with a total of 80 at% of transition metal elements (Fe, Mo, Cr, Ni, Co, …) plus a 20 at% of metalloid elements (Si, C, P or B). Amorphous steels are characterized by extremely high hardness as well as good corrosion and magnetic properties for some compositions. The GFA has been optimized and some compositions have been produced in cm-scale bulk parts[27].

1.3 Structure of amorphous materials

Depending on scale, the structure of a material can be viewed from different levels like macrostructure, microstructure, and crystal structure. From the crystal structure point of view, determining the structure of a crystal is to identify the coordinates of all the atoms in the unit cell. The properties of crystalline materials are related to the crystal structures and crystalline defects like point defects, dislocations and crystal boundaries. There are already matured theories on these structure-property relationships. Physical aging's influence on structure and properties of glasses confirms that structure and properties are closely related; a slightly increase in density, which is even difficult to be detectable, leads to a viscosity increase of some orders of magnitude in rapidly quenched MGs. Besides viscosity, the influence of structure is also manifested on other properties like C_p, magnetic properties and electrical resistance.

However, the structure of glasses still remains a great challenge to us. Because of this, the relationship between the structure and properties is far

from being established. From the macroscopic point of view, the glassy structure can be regarded as a featureless single phase solid alloy, without microstructure as it is usually understood. On the microscopic level, there is no crystal lattice and thus no defects such as grain boundaries or dislocations can be defined explicitly. There are no unit cells, and the atomic environments of different species are different, being only possible to describe them on a statistical basis. In this point lies the difficulty of determining and describing the structure of a glass. The goal of structural studies is then limited to identify the physical principles that govern the formation and physical properties of MGs from an statistical point of view[17].

The pair distribution function, PDF, measures the probability of finding atoms as a function of distance r from an average central atom. It is often given in a reduced form $G(r)=4\pi r(\rho(r)-\rho_0)$, where $\rho(r)$ is the number of atoms per unit volume at a distance r and ρ_0 is the average number of atoms per unit volume in the sample as a whole. A common employed structural analysis of glass is based on the PDF which can be determined from scattering experiments using different sources like X-rays, electrons or neutrons. When different types of atoms are not distinguished, the PDF is regarded as radial distribution function (RDF). In this case one set of scattering data is enough to determine the RDF. The RDF analysis ignores the difference between atoms. In the situation where different atoms can be distinguished, a partial pair distribution function (PPDF) is used to describe each type of atom pair.

For a binary alloy AB there are three types of pairs with AA, AB and BB. In order to determine the three PPDFs, it is necessary to perform at least three scattering experiments in which the two types of atom have different relative scattering powers. This can be done in several ways. One way is to use different radiations, such as X-rays, neutrons, and electrons. Another way is to use anomalous dispersion with a wavelength close to an absorption edge of each of the species, to obtain distinct effective atomic scattering factors. There are other techniques also possible which include polarized neutrons (only effective dealing with ferromagnetic sample) or isotopic substitution[28].

The PDFs gives statistic information about atomic ordering with distance, but the information on angular distribution of interatomic bonds is lost from

the diffraction or scattering techniques. This angular distribution could be explored by absorption techniques like X-ray absorption fine structure (XAFS), including the fine structure at or near an X-ray absorption edge. These techniques can give information on the local environments of the particular species of absorbing atoms. It can also be explored by nuclear magnetic resonance (NMR) or Mössbauer spectroscopy. Through the interaction of the nuclear quadrupole moment of the probe atom with the local field gradient, the information on the symmetry of the local environment could be obtained using the Mössbauer spectroscopy.

The obtained experimental structural information can be analyzed on two ways. The first is the direct data analysis. Taking the PDFs as an example, statistic structural information like distance between atoms and coordination number can be obtained by Fourier transform of the scattering factor. The information manifests the peak position, peak width and relative intensity, etc. Another way is to predefine a structural model and simulate the diffraction or absorption spectrum, and compare with the experimental result. The latter is a typical reversal problem where the result depends on the predefined structural model. Normally different configurations are provided and compared with experimental data. By Monte Carlo method, generation of random configurations and minimization of the difference between the simulated and experimental data, the structure could be determined. This methodology is known as Reverse Monte Carlo (RMC) method. The difficulty of this methodology is that the influences of atom positions and atom identities may be difficult to separate. Besides, due to the amorphous nature, there are problems predefining the structural models. Besides the RMC, Molecular dynamics (MD) simulation is also helpful to help us to understand how structure evolves at the atomic scale. The MD results can be verified by the scattering or absorption data which manifest on the PDF or XAFS analysis.

Since the glassy state is congealed directly from the supercooled liquid without ordering, it is logical that its structure might be inherited from the liquid. Bernal modeled the structure of pure metallic liquids as a packing of hard spheres with the same diameter[29]. This dense random packing is statistically reproducible, and the structure can be considered to be made up of

only five simple polyhedra. One important parameter on structural analysis is the coordination number (CN) which is the number of atoms that form the nearest neighbor shell of a given central atom. In glasses with covalent bonding like network glass a low CN value is common while for MGs, with metallic bonding nature, high CNs are observed. It should be noted that the determination of nearest neighbors is arbitrary in glasses when using a distance cutoff method. Other route like Voronoi tessellation analysis is employed to describe the structural motifs.

In addition to the short range Angstrom scale motives dominating the local environment of atoms, glasses are also characterized by nanometer scale fluctuations in the structure. This nanometer scale inhomogeneity is characterized by density as well as elastic and dynamic fluctuations. The presence of soft and hard regions has been observed by TEM and other techniques[30] . This type of structural inhomogeneity is thought to play a central role in the mechanical relaxation behavior of metallic glasses.

1.4 Stability considerations

Due to the metastable nature, a MG is prone to evolving to more stable states. Different aspects like structural relaxation, phase separation and crystallization need to be considered depending on service conditions. They are of especial important when elevated temperature applications are considered.

Here structural relaxation is also referred as physical aging. It has large effect on many properties of the material. The structural effects of physical aging are apparent on the local atomic arrangement, modifying the atomic clusters and the coordination number, and also on the nanometer inhomogeneity. Physical aging is thought to modify the correlation length of density fluctuations thus implying strong changes in the associated properties. A review on the influence and mechanism of structural relaxation is given later in chapter 3.

Although glasses were thought to be homogeneous without phases, Small Angle X-ray Scattering experiments showed that phase separation

phenomenon occur in some MGs like the Ni-Nb-Y systems[31]. This phase separation is also observed in other MGs like Cu-Zr or Fe-B using TEM [32]. It should be noted that not only intrinsic phase separation would introduce phase contrast in TEM, the sample preparation process might also introduce phase contrast when employing TEM techniques. Great care need to be taken when discussing on phase separation of MGs, factors influencing the techniques like surface flatness need to be excluded[33,34].

As for the observed phase separation, it might be related to the miscibility gap in the equilibrium liquid[31]. By adding elements with large positive enthalpy of mixing to one of the main constituent of a glass forming liquid, multi-phase MGs can be obtained in the liquid or in the undercooled liquid. This multi-phase supercooled liquid then can be frozen into a multi-phase MG when further crystallization is limited. The final microstructure depends on the thermodynamics and dynamics when phase separation occurs as well as the processing conditions. Besides Ni-Nb-Y system, Zr-Co-Al-Gd, Co-Cu-Zr, Cu-Zr-Ag systems also show a phase separation phenomenon [31]. The phase separation is claimed beneficial to the mechanical properties as studied in Cu-(Zr,Hf)-(Gd,Y)-Al[35] Cu-Zr-Al-Ti[36] and Cu-Zr-Al-Fe systems[37].

Due to the metastable nature of the glass, crystallization needs to be taken into consideration at elevated temperatures. Since crystallization is a pronounced exothermic process, a method commonly used to determine the nucleation and growth kinetics of crystallization is calorimetric thermal analysis. The crystallization dynamics is usually described by the Kissinger method based on the relationship between the logarithm of the heating rate and the temperature at the maximum of the crystallization rate. Kinetic parameters like activation energy, transformation enthalpy and reaction order can also be obtained from a DSC measurement. For isothermal transformations, kinetic analyses are performed by applying the Kolmogorov-Johnson-Mehl-Avrami (KJMA) formalism. The onset of crystallization is clearly detected in the mechanical relaxation behavior as will be seen in the following chapters.

1.5 Mechanical properties

With the improved GFA, many MGs can be cast into fully glassy state without the need of extremely high cooling rates. These systems of size lager than 1 mm obtained by normal Copper-mold casting, are called BMGs. Some systems can even be cast into rods as thick as several centimeters. Compared with most commonly used crystalline alloys with elastic limit of about 0.2%, BMGs have larger elastic limit, Tian[38] even report a value of 5%. This extremely high elastic limit can make BMGs quite promising in many technological applications. For instance, the amorphous nature without dislocations makes that $Al_{86}Ni_7Y_{4.5}Co_1La_{1.5}$ BMG possesses a compressive yield strength of 1050 MPa[39]. This corresponds to a specific strength of 3.3×10^5 $N\cdot m\cdot kg^{-1}$ and is higher than that of any existing engineering alloys.

On the micro scale, tensile elongation and necking in the in situ deformation of samples of about 100 nm was observed by TEM[40]. However, the macro fracture mode is normally brittle in conditions without constraint[41,42]. Whether the monolithic MG is intrinsically brittle or ductile is still under debate[43], but the evidence is that there is no plastic deformation in tensile deformation mode. The free volume theory and shear transformation zone[44] are commonly employed to describe the deformation mechanisms in MGs. In particular, it is generally accepted that during deformation shear is not homogeneously distributed in the glass; on the contrary, stresses are dissipated in localized small volumes where most of the shear is accommodated. These are the so-called shear transformation zones. Currently, the lack of plasticity has been the main limiting factor for BMGs as engineering materials.

In general, the mechanical properties are related to the microstructure of the material. Recent experimental results found that grain boundaries are not always detrimental to the mechanical properties[45]. As a matter of fact, nanomaterials attract great attention due to the novel properties introduced by the nano-scale grain boundaries. Nanocrystalline materials could be obtained through controlled devitrification of MGs by taking consideration of the crystallization kinetics[46].

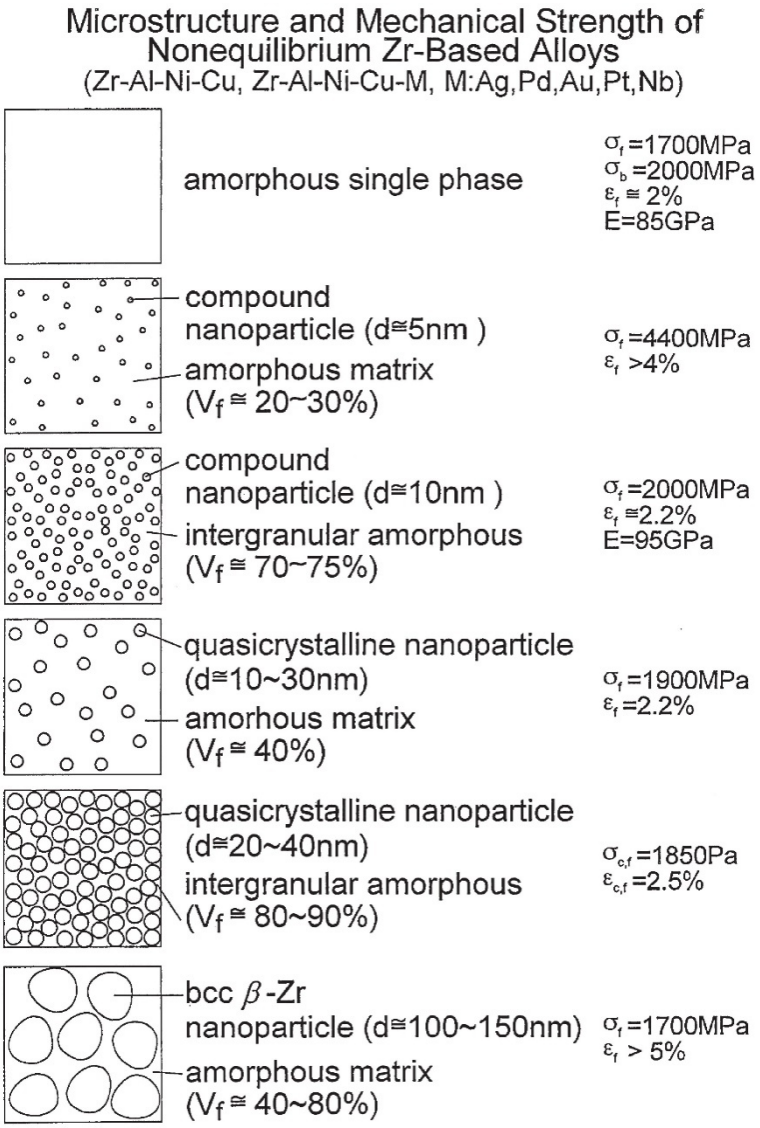

Figure 1-3 Schematic microstructure and mechanical property of Zr based metallic glass composites[45]. The fracture strength and deformation is related to the microstructure of the composite. By appropriate microstructural optimization, comprehensive mechanical properties can be improved.

Composites with microstructures of Al nanocrystals in an amorphous matrix with nanocrystalline volume fractions approaching 20% were obtained in Al rich glasses as shown in figure 1-3[45]. The composite was reported to have improved mechanical properties. Nanocrystalline precipitates are also achieved in Fe based alloy glass systems such as Fe-Nb-B and Fe-Si-B with densities of ~10^{20} m^{-3} [47]. By appropriate microstructure control through

composition optimization and solidification process control, nanostructured matrix/ductile dendritic phase composite with composition of $Ti_{60}Cu_{14}Ni_{12}Sn_4Nb_{10}$ exhibiting plastic strain as high as 14.5% and ultimate stress of 2.4GPa under compression was reported[48]. It was also report that in the Fe based MGs, the fracture strength could reach 3GPa while reaching a plastic strain of more than 30%[49].

Through appropriate microstructure control, the fracture stress and fracture strain could be improved[45]. Compared with the fully glassy ones, BMG composites have better mechanical performance and have gained large attention. The microstructure design mentioned above is referred as *in situ* composite. Besides the nanocrystallization, *in situ* formed continuous second phase and phase separation are also found to be an effective way of adjusting the stress distribution.

The strategy of *in situ* composite is not only effective in compression ductility, but also under tensile stress[50,51]. Extensive toughening and ductility is achieved with control over the shear modulus (G) and size of the dendritic phase in Ti-Zr based BMG composites,showing tensile ductility exceeding 10% at ambient temperature, yield strengths of 1.2-1.5 GPa, K_{1c} up to 170 $MPa{\cdot}m^{1/2}$ and fracture energies for crack propagation as high as G_{1c}=340 $kJ.m^{-2}$. The K_{1c} and G_{1c} values are equal or surpass those achievable in the toughest Ti or even Fe conventional crystalline alloys[51].

Beside the *in situ* formed composite, mechanical properties can be improved through *ex situ* methods like continuous second phases or particles, for example, by addition of particles of TiB_2 into $Mg_{65}Cu_{7.5}Ni_{7.5}Zn_5Ag_5Y_{10}$ MG as reinforcing phase. Without affecting its GFA, when uniformly distributed in the matrix, the BMG composites show plastic behavior under compression with a plastic strain of 2-3% and fracture strength as high as 1.3 GPa[52,53]. By adjusting the interface, the evolution of shear transformation zones could be controlled and thus the plasticity could be improved. Improved ductility in the MGs can not only be achieved by composites but also in foams[54] as well as designed structures[55]. Besides the interface effect, stress induced crystallization[56] and polymorphic transformations might also be employed to improve the mechanical properties.

1.6 Forming

A main feature of MGs is that they possess the high strength of metals while at the same time they flow, still in solid phase, at elevated temperatures. This thermoplastic property could be used as one step forming of the final product. When applying thermoplastic forming to MGs, several aspects need to be considered like crystallization dynamics and, viscosity behavior[57]. Actually, homogeneous deformation should be achieved, as inhomogeneous deformation might lead to failure. Here, the controlling parameter is the temperature dependent viscosity.

Actually, due to the wide range of values of viscosity, which covers as much as 14 orders of magnitude, the theory description is still far from perfect and the description of viscosity of metallic glasses is still a subject of intense research. At high temperatures above the melting point, the configuration of the melt is in equilibrium, i.e. the system can adapt to the new more stable configuration within experimental detectable time. With cooling closer to T_g, the viscosity behavior shows a VFT behavior[58], manifested by the viscosity of $Pd_{82}Si_{18}$, $Pd_{77.5}Cu_6Si_{16.5}$ and $Pd_{40}Ni_{40}P_{19}Si_1$ around the glass transition temperature using creep experiments by Spaepen[59–63]. However, as Mckenna[64] pointed out, a new framework is needed since viscosity described by VFT introduces a T_0 temperature below which viscosity diverges and the system ceases to flow.

Actually, on further cooling, the system congeals into a glass. The structure of the supercooled liquid gets stuck, the system becomes non-ergodic and the viscosity deviates from the VFT behavior. This deviation from the VFT behavior is generally observed in glasses like network glasses and molecular glasses[65,66], and it is also observed in MGs where iso-configurational viscosity show an Arrhenius behavior[67] in $Pd_{82}Si_{18}$ MG. The viscosity behavior could be explained in the framework of the free volume model [60] as performed for $Pd_{43}Ni_{10}Cu_{27}P_{20}$ MG[68].

It should be taken in consideration that recovery of residual stress might also play important role in the final product. For instance, in homogeneously deformed $Cu_{64.5}Zr_{35.5}$ MG, if the strain is not fully recovered before cooling down, anelastic strain will remain in the local structure and this will lead to

structural anisotropy [69]. The homogeneous deformation regime used in thermoplastic forming of metallic glasses is deeply connected with viscosity and the mechanical relaxation behavior which is the main focus of this work.

1.7 Applications of MGs

With the development of new alloys with high GFA, new applications are being investigated. Due to the unique mechanical properties like high elastic strain which allows the material to store more elastic energy, combined with low mechanical damping, BMGs are attractive for springs and some sport products. Actually, golf club heads and tennis racket frames have been commercialized. The high elastic strain limit of MGs makes them attractive for use in strain sensing devices such as pressure sensors. The features like high mechanical strength, large elastic elongation limit, high corrosion resistance and good surface smoothness, have already made Fe-based BMG alloy powders with particle sizes of 0.05 to 1mm been used as shot peening particles[15]. Other applications taking advantage of biocompatibility in niche environment as well as in space exploration are also under investigation by the MG research community[70].

2. Objectives

MGs have attracted great attention due to its unique properties as described above. The deformation mechanisms, such as dislocation and twinning, responsible for plastic deformation of crystalline materials are not valid in the amorphous materials. Therefore, a new deformation mechanism had to be determined for the glassy systems[41]. Closely related to the mechanical properties, the mechanical relaxation of MGs is getting increasing attention[71][72]. Dynamic mechanical analysis, also known as mechanical spectroscopy, is widely used by the metallic glass community to explore the mechanical response. The main objective of this thesis is to investigate the mechanical relaxation of MGs. In order to understand the mechanical response of these materials, an extended review of the relaxation phenomena of metallic glasses is needed. This review and the corresponding discussion will be addressed in chapter 3.

DMA experiments revealed secondary relaxation in BMGs, and this attracted great attention. Wang's work on La-Ni-Y BMGs shows that the activation energy of secondary relaxation is comparable with the activation energy of shear transformation zones. It is believed that the control of the activation of secondary relaxations might be helpful to improve the mechanical properties of MGs[71][73]. Secondary relaxation is known as β-relaxation, this means it is detected as a secondary process on the loss modulus versus temperature profile, $E''(T)$, of MGs. In different systems β-relaxation shows different signatures on the loss modulus. In some cases it is observed as a low temperature peak, in some other cases as a shoulder or excess wing of the primary relaxation peak. One objective of this work is to investigate the nature of this secondary relaxation.

Besides mechanical considerations, due to the softening behavior as temperature is increased, MGs start to flow below the glass transition temperature. This opens a way of forming the material into complex shapes in a single step. In such cases, relaxation dynamics and viscosity are key factors for designing the processing conditions. For instance, the temperature where forming processes like fiber drawing or glass blowing could be performed is

usually when viscosity reaches 10^8 Pa·s. Other techniques like annealing and bubble removal, as employed in oxide glasses, are also closely related to the viscosity behavior. Thus, the knowledge of the mechanical relaxation behavior of MGs is critical to define their technological potential. Besides, it does not only play an important role in technical aspects; as claimed by Gupta[74], the iso-structural viscosity is also of crucial important in testing in detail the proposed models of the glass transition theory. So, the other focus of interest of this thesis is the viscosity behavior of MGs.

The work is structured in 6 chapters. After chapter 3, already described, the experimental materials and methods used in this work are described in Chapter 4. Following, section 5 presents and discuss the results obtained. As for the specific MG systems studied in this thesis, the Cu-Zr-Al MG family is of interest as potential structural material. This is because of the fact that the mechanical properties of the Cu-Zr based MGs are often found promising with minor doping of Al[37,56,75,76], The mechanical relaxation of Cu-Zr-Al will be explored in section 5.1.

The extremely high glass forming ability of $Pd_{42.5}Ni_{7.5}Cu_{30}P_{20}$ MG, with a wide temperature span of the supercooled liquid region and superior stability against crystallization, provides us a good sample to investigate the properties of MGs. The mechanical relaxation of this MG will be explored in section 5.2.

Iron based MGs with relative cheap raw material, acceptable glass forming ability and good corrosion resistance performance[77][78] are extensively used in the transformer cores as well as the antitheft devices taking advantage of soft magnetic properties. They are also promising as structural engineering materials[79][16]. The mechanical relaxation of one amorphous alloy belonging to this MG family will be explored in section 5.3.

The discussion of the experimental results will be addressed in section 5.4. Finally, the conclusions of the work are presented in Chapter 6.

3. Mechanical relaxation of MGs: overview of experimental data and theoretical models

The purpose of this chapter is to give an overview of the relaxation phenomenon in metallic glasses, the techniques to explore it and the influence of relaxation on their properties. This review is addressed to clarify some basic definitions and general behaviors. The terminology of β-relaxation in different contexts will be explained and the general methodology for analyzing the mechanical response will be addressed. The main work of this chapter has been published in reference [80].

3.1 Basics of glass relaxation dynamics

Relaxation is a universal phenomenon driving a system from an excited state towards a more stable one. There are different techniques capable to explore the relaxation response under different stimuli. These techniques comprehend mechanical and dielectric spectroscopy, nuclear magnetic resonance, neutron scattering, and various electromagnetic radiation scattering. They probe the relaxation dynamics through the time behavior of different variables such as density, enthalpy, stress or strain, electric and magnetic polarization, nuclear spin orientation, and mean square and rotational angle displacements.

The relaxation times obtained from different techniques coincide in some systems and time-temperature windows, but not necessary in others as illustrated in figure 3-1[81]. The relaxation time τ_l (liquid structural relaxation-longitudinal) determined from Brillouin scattering, $\tau_{reorientation}$ obtained from vibrational spectroscopy, τ_σ determined from electrical conductivity, τ_s from viscosity and τ_H from differential scanning calorimetry of 0.4 $Ca(NO_3)_2$ 0.6 KNO_3 (CKN glass) split off from each other when temperature decreases, this indicating a decoupling of the relaxation times associated to different structural movements as the supercooled liquid approaches the glass transition temperature (T_g). In the case of MGs some of these experimental techniques cannot be used, as for example dielectric spectroscopy. This opens a hole in the frequency window usually probed,

which is partially filled with the information obtained by mechanical relaxation techniques.

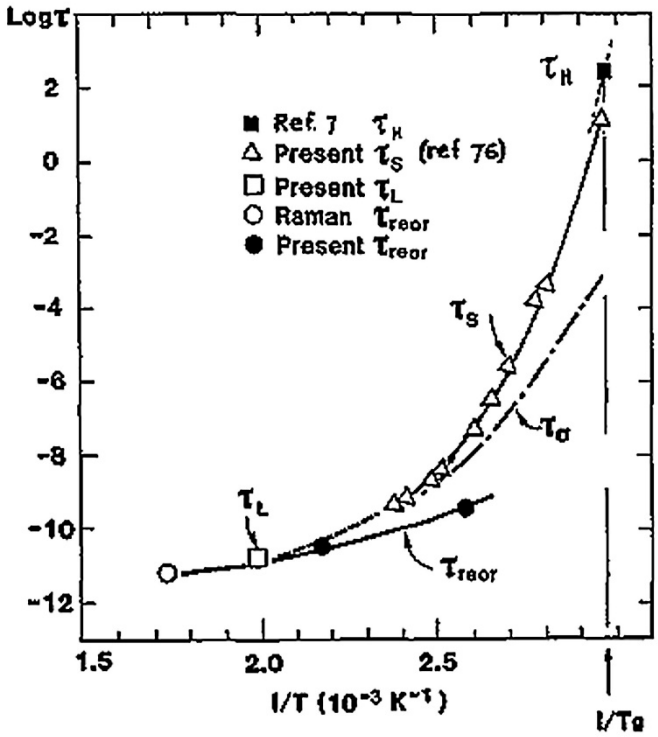

Figure 3-1 Relaxation times associated to different probed properties in CKN glass. Reprinted from ref. [81].

Although there is not yet a comprehensive theory, it is generally accepted that glass formation is not a thermodynamic phase transformation but a kinetic process that freezes the system in an out-of-equilibrium configuration at temperatures below T_g[82–84]. Therefore, glasses are permanently prone to change its configuration towards a more stable state through irreversible atomic movements. This process is called physical aging and it may have time scales much larger than the experimental ones, seeming that the system is stable from the macroscopic point of view. This process is also called structural relaxation, in the sense that the system is relaxing form a higher free-energy configuration towards a lower one. Nevertheless, the structural relaxation understood as the response of the system to an applied external stimulus, is an intrinsic process present both in equilibrium (liquid) and out-of-equilibrium (glassy) states. Of course, in many cases, similar structural movements are responsible for structural relaxation and physical aging.

However, the relaxation response is a well-defined property dependent only on temperature and pressure for a particular glassy configuration while physical aging is a history dependent process driving the system through different glassy states.

3.1.1 Relaxation in the supercooled liquid region

The activation of viscous flow reflects the complete relaxation of the system, accommodating its structure under the application of an external force. Therefore, in structural glasses, viscosity is directly related to the primary relaxation time of the system, the so-called α-relaxation. In the supercooled liquid region, when $T>T_g$, the system is ergodic and the α-relaxation time, τ_α, characterizes how long takes the system to return to internal equilibrium after being excited by an external force or a change in the temperature-pressure conditions. Generally speaking, the viscosity (η) and τ_α deviate from Arrhenius behavior. As summarized by Angell[85], different theories like simple liquid model, mode coupling theory, random walk model, random packed spheres or cooperatively rearranging system model propose different dependences on temperature.

Actually, in the relatively narrow temperature region where most of the experimental viscosity data is obtained, all models fit the data with just two or three parameters and it is difficult to determine which model have superior validity. Experimentally, for many liquids above T_g, the relaxation dynamics can be described in the form of the Vogel-Fulcher-Tammann (VFT) equation for the viscosity

$$\eta(T) = \eta_0 \exp\left(\frac{D^* T_0}{T - T_0}\right) \tag{3.1}$$

D^* and T_0 being the strength parameter and the VFT temperature respectively. In some cases, $D^* T_0$ is described as B. The strength parameter D^* is used to distinguish between strong and fragile liquids; strong liquids are defined by a large D^* and an almost Arrhenius like behavior ($T_0 \rightarrow 0$). On the other hands, fragile liquids are characterized by small D^* and a very rapid breakdown of shear resistance when heating above T_g. Analogous temperature dependence is

also found for τ_α above T_g[86]. The strong-fragile nature of liquids near T_g is also usually characterized by the fragility parameter

$$m = \left.\frac{d\log\eta}{d\left(T_g/T\right)}\right|_{T=T_g} = \left.\frac{d\log\tau_\alpha}{d\left(T_g/T\right)}\right|_{T=T_g}. \tag{3.2}$$

According to the bonding nature, it could be classified as network formers like SiO_2, lonic liquids, van der Walls bonding between molecules and MGs. SiO_2 have a near Arrhenius temperature dependence of viscosity, the parameter m is usually smaller than 30, it is called strong liquid. While organic liquid like o-terphenyl which composed of discrete molecules is fragile with a strongly non-Arrhenius temperature dependence of viscosity and a large m value lager than 100. MG is between strong and fragile liquids with m value between 20 and 80.

In addition to the main α-relaxation, secondary relaxations may be also found in the supercooled liquid region. Below some critical temperature, particular structural movements may be decoupled from the main process giving rise to faster relaxations which usually follow an Arrhenius-like temperature behavior. As discussed below, some models predict the presence of a β-relaxation below a critical temperature (T_c>T_g) as a universal feature of the glass transition process[85,87,88].

3.1.2 Relaxation and aging below T_g

In an intermediate temperature region near and not too far below the glass transition, the situation is complex. The relaxation dynamics cannot be described by the VFT equation anymore, the system is not in an ergodic state and its properties are not uniquely defined by the temperature-pressure conditions; they depend on the particular glassy state reached during the previous history of the system. Furthermore, the degree of aging determine the physical and mechanical properties like density, elastic constants, diffusivity, Curie temperature (for ferromagnetic glasses)[89], electrical resistivity, enthalpy, etc., as well as the relaxation dynamics of the system. In this intermediate region, physical aging must be considered as occurring

continuously on all experimental time scales, but without reaching equilibrium except for very long annealing times (t_a). This complexity might be solved in a first-order approach by introducing a fictive temperature $T_{fictive}$, which is used to define the glassy state of a system[90].

If aging is not considered the glassy dynamics of many systems can be approached as function $T_{fictive}$ using the Adams-Gibbs-Vogel (AGV) model[91,92]

$$\tau_\alpha(T) = \tau_0 \exp\left(\frac{B}{T\left(1 - T_0/T_{fictive}\right)}\right) \tag{3.3}$$

where B and T_0 are empirical parameters, τ_0 the pre-exponential factor and $T_{fictive}$ defines the temperature at which glass Arrhenius-like (AGV) and liquid (VFT) dynamics intersect each other. This fictive temperature evolves as a consequence of aging

$$\frac{dT_{fictive}}{dt_a} = \frac{T - T_{fictive}}{\tau_{aging}} \tag{3.4}$$

with limiting condition of $T_{fictive}=T$ for a completely aged system attaining internal equilibrium.

At low temperatures ($T<<T_g$) the aging time, τ_{aging}, is usually long enough to consider $T_{fictive}$ constant and the glass structure frozen in an iso-configurational state, with properties dependent on T, P and $T_{fictive}$. This low temperature region can be defined as the range where the cooperative stress relaxation (α-relaxation) of the viscous liquid is completely frozen and the structural state of the glass does not change in laboratory time-scale; as $T_{fictive}$ is constant, the glass properties are defined only by the temperature-pressure conditions. Relaxation in this glassy range involves decoupled, localized motion of easily mobile species; this is usually called secondary relaxations. They are sometimes classified further as β, γ, δ-relaxations in polymers where the stepwise freezing of various local degrees of freedom may be associated with specific molecular groups. While remaining in an isoconfigurational

state, relaxations are thermally activated processes with well-defined temperature dependences, $\tau(T)$, usually following Arrhenius-like behaviors.

On the other hand, at intermediate temperatures, the complexity comes from the fact that τ_{aging}, which controls the aging evolution, is at the same time dependent on the degree of aging. Different models have been introduced in order to model this complex behavior. One common approach to model the viscosity, the glassy dynamics and other properties is the Tool-Narayanaswamy-Moyniham (TNM) equation[91,93–95]

$$\tau\left(T, T_{fictive}\right) = \tau_0 \exp\left(\frac{xE_{act}}{k_B T} - \frac{(1-x)E_{act}}{k_B T_{fictive}} \right) \tag{3.5}$$

where x is a dimensionless non-linearity parameter (the TNM parameter), E_{act} is an activation energy and k_B is the Boltzmann constant as usual. Under this approach, the viscosity dependence on time could be described as a function of the change of the fictive temperature with complexity attributed to the non-linearity parameter x. Some models propose different approaches for the time evolution of the α-relaxation time during aging at a given temperature. Lunkenheimer et al.[96] proposed an expression for $\tau_\alpha(t_a)$ assuming that τ_{aging} is equal to τ_α. This assumption is commonly adopted for structural glasses, as it is reasonable to expect the movements accommodating the structure to an external force should be similar to the ones driving the system towards more stable configurations during aging.

The study of physical aging in MGs has been extensively done by calorimetric techniques. Based on Chen's work[97], the aging process characterized by DSC can show a broad distribution of activation energies. The activation energy spectrum can be obtained by plotting the difference between c_p in the as quenched and annealed state versus temperature. Chen's work shows that the spectrum has two separable broad processes, attributed to β and α relaxations respectively[97]. In the $Pd_{48}Ni_{32}P_{20}$ MG the low-energy peak corresponds to an activation energy E=92.4 kJ/mol (0.96 eV). Tsyplakov[98] obtained similar results on the activation energy spectrum using DSC and mechanical relaxation. He interpreted the data by assuming that aging of MGs is a change in the concentration of frozen defects similar to

Dumbbell interstitials in simple crystals[98–100]. In the Dumbbell interstitials model, the activation energy shows a broad distribution of values. Nagel's work on positron annihilation studies of free volume changes during aging of $Zr_{65}Al_{7.5}Ni_{10}Cu_{17.5}$ glass[101] suggests that the isothermal aging kinetics obeys a Kohlrausch-Williams-Watts (KWW) law with β_{KWW} exponent of about 0.3 between 230 and 290 ^{o}C. The effective activation energy was found E~120 kJ/mol.

Below T_g, there is also a reversible thermal relaxation component, faster than the irreversible aging. By thermal cycling, the annealing induced relaxation can be separated into reversible and irreversible components and can be interpreted by chemical short range ordering (CSRO) and topological short range ordering (TSRO) respectively[102,103]. The former could be explained by the activation energy spectrum, while the latter could be explained in terms of free volume theory[102]. Borrego et al.[104] studied aging by monitoring enthalpy and Curie temperature changes in Fe-(Co)-Si-Al-Ga-P-C-B and Finemet glasses. They found that aging can be interpreted as driven by two relaxation times of minutes and hours respectively, in this case they associated the fast process to TSRO and the slow one to CSRO changes. However, it should be noted that this sharp separation between TSRO and CSRO is criticized because CSRO is unlikely without an accompanying TSRO[105,106].

Khonik[107,108] treated plastic flow below T_g as irreversible structural relaxation with distributed activation energies modified by external stress, developing the so called directional structural relaxation (DSR) model. According to DSR model, relaxation and aging involve structural movements generally anisotropic at the atomic level and oriented in different directions. In the presence of a mechanical stress, however, the distribution of the local events may become asymmetric producing a net distortion in the direction of energetically favored orientations. The DSR model is a general approach which includes any relaxation mechanism based on the motion of defects, and it even can be applied to relaxation in crystalline materials. At T~T_g, cooperative atomic motions cause viscous flow, mechanical relaxation and aging. In the DSR model the relaxation centers are divided into irreversible

and reversible ones, the former being responsible for mainly viscoplastic low-frequency internal friction, plastic flow and even for reversible strain recovery, whereas the latter cause anelastic processes seen at higher frequencies. However, in spite of some models, the microscopic mechanisms and dynamics are still far from being understood. Recent work shows that in the microscopic scale, the aging of MGs is a complex process leaded by the release of internal stresses involving both smooth and sudden (avalanche-like) movements of the structure[109].

The activation energies of the processes controlling physical aging in MGs show typical values around 100kJ/mol[97,98,110]. Generally, aging is thought as being driven by thermally activated localized structural rearrangements and then controlled by the same molecular movements responsible of the secondary relaxations. Hu[111] performed a survey of the sub-T_g aging and relaxation data of several MGs obtained by DSC or DMA and they found a common relationship of E_β=26.1RT_g. Although enthalpy changes can be the result of many different types of structural rearrangements while mechanical measurements respond only to shear deformation, comparison between as-quenched and relaxed samples using both enthalpy and mechanical techniques suggest that structural relaxation could be characterized by both of these techniques and the results are consistent[98,112]. However, it should be noted that, as Chen pointed out[113], the secondary relaxation process observed from calorimetry in MGs does not necessarily respond to the one observed by shear deformation. The internal friction measurements probe shear relaxations, while enthalpy relaxation samples all sorts of relaxation processes, chemical and topological.

At still lower T, where the primary structural relaxation is eventually frozen, plastic deformation of MG is controlled either by creep or by highly localized shear banding depending on the applied deformation rate. In this range, secondary relaxations are related to anelastic processes concerning easy mobile species with similar behaviors as in crystalline materials. Maddin[114] suggested that the creep behavior of $Pd_{80}Si_{20}$ MG is governed by a single thermally activated process with an activation energy E=50 kJ/mol (0.52 eV). Based on the calculation of the activation volume of 25 Å, close to the volume

of one constituent atom, they proposed that steady state creep of the MG is due to transfer of atoms across a distance of one lattice spacing in order to relax the applied stress.

3.1.3 Models for glassy dynamics

The free volume model, proposed by Turnbull and Cohen[115], describes quite properly the viscosity dependence on temperature and it was further developed to explain the glass transformation phenomenon[116,117]. The model uses free volume as a parameter to describe the change of physical properties, with the particular achievement of predicting the equivalence of viscosity changes due to temperature or pressure variations in the supercooled liquid state. According to this theory, physical properties are related to the density of the system. The volume in the liquid could be classified into two types; type I is the volume of the elemental unit, type II is the volume where the elemental unit can move freely. Type II is called free volume. It is a small part in the whole volume and it is shared by the elemental units. When the system cools down, both volumes decrease, and when the free volume drops below a certain volume, the elemental units can no longer move and thus form glass. Free volume theory is quite useful and highly accepted in the MG community to explain the glass transition and aging phenomena. The weak point of the theory is that free volume is difficult to measure directly by experiment. Furthermore, later work on the phenomenon of inhomogeneous flow as well as the divergence of the relaxation modes showed that a single parameter model is not enough to describe the properties of a glassy state[84,118].

The potential energy landscape model is often used to interpret the relaxation dynamics[119]. According to the analysis by Johari and Goldstein[87], the atomic and molecular configurations in liquids and glasses change according to motions classified as primary (α) and secondary (β) relaxations. Primary relaxations describe the major large scale irreversible rearrangements responsible for viscous flow. On cooling, the glass transition is reached when the decreasing mobility stifles these rearrangements. On the contrary, β-relaxation could be viewed as a locally initiated and reversible

process. Measurements of the dielectric loss factor in many rigid molecular glasses as well as amorphous polymers show secondary relaxations. According to this evidence, Johari and Goldstein suggested that secondary relaxation could be a near universal feature of the glassy state[87]. From a potential energy landscape perspective, Debenedetti and Stillinger[82,83] have identified the β-transitions as stochastically activated hopping events across sub-basins confined within the inherent mega-basin and the α-transitions as irreversible hopping events extending across different landscape mega-basins.

The mode coupling theory (MCT) is able to explain the experimental evidence that the α-relaxation time diverges from β-relaxation at some critical temperature[88]. By characterizing and classifying the secondary relaxations in many glass formers, Ngai and Paluch identified the class of secondary relaxation that bear a strong connection or correlation with the primary one in all the dynamic properties and called it Johari-Goldstein (JG) β-relaxation[120]. This link between α and β relaxations was initially found in polymers, but at present it is assumed to be universal. According to MCT, the decoupling temperature and the expected effects at much lower temperatures can be calculated. Based on this Ngai suggested the excess wing manifested in mechanical spectroscopy of MGs comes from a JG β-relaxation[121].

3.2 Mechanical relaxation of glasses

3.2.1 Introduction to mechanical relaxation

In general, the self-adjustment with time of a thermodynamic system towards a new equilibrium state in response to a change in an external variable is termed relaxation. When the external variable is mechanical, the phenomenon is known as mechanical relaxation. The measurement of internal friction by dynamic mechanical analysis (DMA), also known as mechanical spectroscopy, is widely used in solid state physics, physical metallurgy and materials science to study structural defects and their mobility, transport phenomena and solid-solid phase transformations. From the mechanical engineering point of view, the internal friction properties are responsible for

the damping properties of materials, including applications of both high damping (vibration and noise reduction) as well as low damping materials (vibration sensors). In MGs, normally, the internal friction behavior is empirically characterized and interpreted as a manifestation of internal relaxation processes, ignoring the details of their physical origins or atomistic mechanisms which are difficult to describe due to the complex structure of glasses.

The relationship between stress, σ, and strain, ε, within the elastic region is given by the modulus of elasticity M

$$\sigma = M\varepsilon . \tag{3.6}$$

For an arbitrary deformation, the stress and strain are second order tensors and Hooke's law is a set of linear equations expressing each component of the stress tensor in terms of all the components of the strain tensor. However, considering an isotropic material and the usual modes of pure shear, uniaxial and hydrostatic loading, M corresponds to shear (G), Young's (E) and bulk (B) modulus respectively. Results of mechanical spectroscopy in MGs are obtained in both shear and uniaxial modes, the latter usually adopted when only thin ribbon-shape samples are available due to a low glass-forming ability (GFA) of the alloys.

The ideal elastic behavior has three conditions to be fulfilled, namely: 1) The strain response to each level of applied stress has a unique equilibrium value, 2) The equilibrium response is achieved instantaneously and 3) The response is linear. In a solid material exposed to a time dependent load, besides the elasticity part there might be also a time dependent part generating internal friction and deviating from Hooke's law. According to the conditions obeyed by the stress-strain relationship, mechanical responses can be classified into the following types detailed in table 3-1[122].

Table 3-1. Classification of mechanical behaviors.

Behavior	Complete recoverability	Instantaneous	Linear
Ideal elasticity	Yes	Yes	Yes
Nonlinear elasticity	Yes	Yes	No
Instantaneous plasticity	No	Yes	No
Anelasticity	Yes	No	Not necessary
viscoplasticity	No	No	Not necessary

So, the internal friction behavior could be the result of all these effects. The work by Nowick and Berry[122] explains in detail the different behaviors observed in the relaxation of solids, focusing mainly in the anelastic one. Experimentally, mechanical relaxation is observable by recording the stress (or strain) change with time when strain (or stress) is modified externally. It can be measured as quasi-static measurements in terms of creep, the elastic aftereffect, or stress relaxation. Quasi-static experiments are used to obtain information on the behavior of materials over periods of several seconds and longer. For information about the behavior of a material in a shorter timescale, dynamic experiments are more appropriate. In these experiments a stress periodic in time, $\sigma=\sigma_0 e^{i\omega t}$, is imposed on the system, and the phase lag ϕ of the strain, $\varepsilon=\varepsilon_0 e^{i(\omega t-\phi)}$, behind the stress is determined. For ideal elasticity, $\phi=0$, the ratio ε/σ gives the elastic compliance of the material J. In the case of viscoelastic contributions, ϕ is not null, and so the ratio ε/σ is a complex quantity called complex compliance, $J(\omega)$, which is a function of the applied frequency ω

$$J(\omega)=\frac{\varepsilon}{\sigma}=J'(\omega)-iJ''(\omega) \tag{3.7}$$

where $J'(\omega)$, the real part, is called the storage compliance and $J''(\omega)$, the imaginary part, is called the loss compliance. In a similar way, we could have regarded the periodic strain as given, and the stress as leading the strain by a phase angle ϕ. The complex modulus $\sigma/\varepsilon=M(\omega)=M'(\omega)+iM''(\omega)$ could be

then defined in a similar way. It should be noted that $J(0)=J'(0)$, and at very high frequencies, $J(\infty)=J'(\infty)$, it follows that $J''(0)=J''(\infty)=0$.

The characterization of the internal friction of materials is commonly done by the damping parameter

$$Q^{-1} = \tan\phi = \frac{M''}{M'} \tag{3.8}$$

which is proportional to the mechanical energy dissipated by the system. Q^{-1} has the advantage of being not influenced by uncertainties of the sample sizes and it is widely used in thermal analysis of substances, for instance in the characterization of T_g in polymeric materials, and in the determination of internal friction at high frequencies by ultrasound spectroscopy. On the other hand, as will be discussed later, the loss modulus peak is more directly related to the frequency spectrum of the mechanical relaxation.

Within the scope of linearity, the mechanical response satisfies the Boltzmann superposition principle: the response of the material to an applied stress is independent on other applied stresses. This means that each response function constitutes a complete representation of the inherent anelastic properties of the solid. Accordingly, any one of the various response functions can be used to specify completely the anelastic behavior of the solid, and further, all other response functions are derivable from the selected one. The classical analysis of mechanical relaxation data uses mechanical models composed of springs ($\sigma=K\varepsilon$, where K is the elastic constant of the spring) and Newtonian dashpots ($\sigma=\eta d\varepsilon/dt$, where η is the viscosity of the dashpot) arranged in different configurations. This allows the derivation of the response of the system from the solution of the differential equations coming from the model. The two elements combined in parallel and series give rise to the Voigt and Maxwell units respectively. The standard anelastic solid is a three parameter model which can either contain a Voigt or a Maxwell unit. The Voigt type model is convenient for the analysis of the creep behavior while the Maxwell type model is convenient for analyzing the stress relaxation.

The general behavior of a standard anelastic solid shows a Debye peak in the loss modulus with the form

$$M'(\omega,T) = M_u - \frac{\Delta M}{1+\omega^2\tau^2(T)}$$
$$M''(\omega,T) = \frac{\Delta M\,\omega\tau}{1+\omega^2\tau^2(T)} \tag{3.9}$$

Where M_u=$M(\infty)$ is the modulus dictating the pure elastic response, and ΔM is the intensity of the relaxation process (i.e. the decay of storage modulus observed between external forces being applied faster or slower than the characteristic time of the process). The peak in the loss modulus is observed when $\omega\tau$=1 and it can be traced either by scanning in ω or in temperature, as $\tau(T)$ is temperature dependent. Glass relaxation involves cooperative movements of atoms in a non-regular structure, and it is far more complex than the simple standard anelastic model. The mathematical functions most commonly used to characterize the mechanical responses measured in both quasi-static and dynamic experiments are detailed in the following section.

3.2.2 Time and frequency domain response functions

Based on the observation of relaxation phenomena, the time dependent properties measured in dielectric or mechanical relaxation of glasses can be usually well-described by a KWW equation, also called stretched exponential

$$\varphi(t) = \exp\left(-(t/\tau)^{\beta_{KWW}}\right) \tag{3.10}$$

$\varphi(t)$ being the time correlation function describing how the system losses memory and returns to equilibrium after being excited by an external stimulus. This expression with only two parameters is widely used to describe time dependent properties in both microscopic and macroscopic scales. Actually, the stretched exponential is known as a complementary cumulative Weibull distribution. The coverage of this equation is not only limited to models based on distributions of relaxation times but also complex correlated processes. The interpretation of the parameter β_{KWW} is of great interest as

discussed by Ngai[123]. When β_{KWW}=1 the function represents a simple exponential decay characteristic of a Debye relaxation with a characteristic time constant, while if $0<\beta_{KWW}<1$ the expression can be regarded as the result of a distribution of individual events with different relaxation times.

In creep-recovery experiments, the strain evolution $\varepsilon(t)$ during the recovery is

$$\varepsilon(t) = \varepsilon_{pl} + \sigma c \varphi(t) \tag{3.11}$$

where ε_{pl} is the residual irreversible plastic deformation, σ is the stress applied during the previous creep period and $\sigma c+\varepsilon_{pl}$ corresponds to the strain at the beginning of the recovery period[124]. On the other hand, in quasi-static stress relaxation experiments, a sudden deformation is applied to the system generating an initial stress σ_0 that decays following

$$\sigma(t) = (\sigma_0 - \sigma_R)\varphi(t) + \sigma_R \tag{3.12}$$

where σ_R is the residual elastic contribution. Both creep recovery and stress relaxation probe the relaxation response function of the system. An example of the expected strain or stress time evolution in these experiments is shown in figure **3-2**.

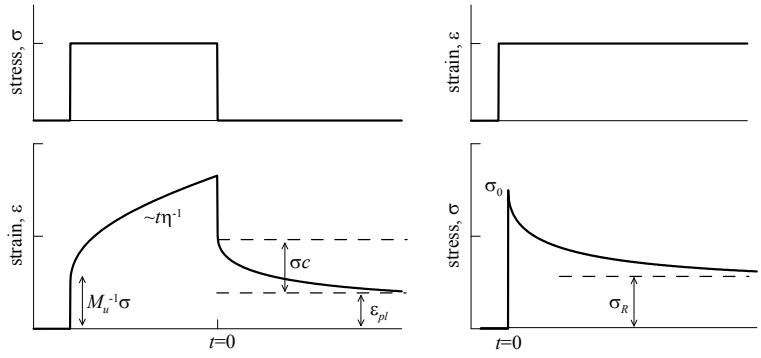

Figure 3-2 Expected behavior for creep-recovery (left) and stress-relaxation (right) quasi-static experiments.

The description with a two parameter stretched exponential is forcedly a simplification of the mechanical response, assuming implicitly an unimodal

distribution of relaxation times. In order to gain further insight, the time response may be analyzed in terms of a distribution of relaxation times

$$\varphi(t) = \sum A_i \exp(-t/\tau_i)$$

or

$$\varphi(t) = \int_0^\infty A(\tau')\exp(-t/\tau')d\tau' \tag{3.13}$$

with factors $A(\tau')$ determining the contribution of each relaxation time to the whole relaxation process. This analysis is able to fit complex experimental responses that may be not well fitted by the two-parameter function. However, $\varphi(t)$ is just the Laplace transform of the intensity of the respective relaxation process and, as it is well known, the computation of the inverse Laplace transform is a very complex mathematical problem where experimental noise or inaccuracies may derive in fuzzy results. In the present case, it might give rise to fictitious relaxation time distributions, so experimental data must be cautiously analyzed.

Jiao[125] analyzed the stress relaxation of a MG by assuming that the relaxation time spectrum had a log normal distribution with the form

$$A(\ln\tau') = k\exp\left(-(\ln\tau' - \ln\tau)^2/s^2\right) \tag{3.14}$$

where τ is the most probable relaxation time, s is the width of the τ' spectrum, and k is a normalizing factor. This model fitted properly the stress relaxation of the $Pd_{40}Ni_{10}Cu_{30}P_{20}$ MG. Besides log-normal distribution, other distribution shapes like box or wedge-like could be also used for the spectrum to fit with experimental data[126]. The activation energy spectrum could be also determined with some approximation by using the data from calorimetric or mechanical relaxation experiments[98].

The correlation function $\varphi(t)$ is related to a complex susceptibility by Fourier transform

$$\chi(\omega) = \chi'(\omega) - i\chi''(\omega) = \int_0^\infty \left[-\frac{d\varphi(t)}{dt}\right] e^{-i\omega t}dt \tag{3.15}$$

which can be probed by dynamical experiments. In case of DMA experiments, the measured complex elastic modulus is

$$M(\omega) = M'(\omega) + iM''(\omega) = M_u - \Delta M \chi(\omega) \tag{3.16}$$

with M_u and ΔM already defined in equation 3.9. It should be noticed that there is no analytical expression for the Fourier transform of the KWW function with a general value of the β_{KWW} exponent and numerical methods have to be employed in order to translate the experimental data from time to frequency domains or inversely. Furthermore, computing of Fourier transform poses numerical problems originating from cutoff effects which yield unwanted oscillations, especially when treating real data with experimental error and noise.

Characterization of the relaxation processes is generally obtained from the analysis of the loss modulus *M''*(ω). The *M''*(ω) peak related to a given relaxation process is defined by four main characteristics: The intensity of the peak (ΔM), the bluntness of the peak, and the power laws defining both the low and high-frequency tails

$$\begin{aligned} \chi''(\omega) &\propto (\omega\tau)^{a} \quad \omega << \tau \\ \chi''(\omega) &\propto (\omega\tau)^{-b} \quad \omega >> \tau \end{aligned} \tag{3.17}$$

where 0<*a, b*<1. In the case of a Debye process *a*=*b*=1, and for a time-domain response defined by a KWW function (equation 3.10) *a*=1 and $b=\beta_{KWW}$. The real loss peak found experimentally shows different degrees of asymmetry. An empirical function widely used for characterizing it is the Havriliak-Negami (HN) function

$$\chi(\omega) = \frac{1}{\left[1 + (i\omega\tau)^{\alpha}\right]^{\gamma}} \tag{3.18}$$

where the exponents α and γ define the broadness and the asymmetry of the peak respectively, and they produce power-laws of the tails given by $a=\alpha$ and $b=\gamma\alpha$. The Cole-Davidson (CD) function and the Cole-Cole (CC) functions, which are also commonly used in relaxation studies, correspond to the HN-

function with α=1 or γ=1 respectively. The CD-function, with peak shape dictated only by the γ exponent, shows an asymmetric peak very similar to the one given by the Fourier transform of the KWW-function[127]. On the other hand, the CC-function results in a symmetric peak with broadening given by the exponent α. Many results show that secondary relaxations of glasses can be generally fitted by using the Cole-Cole equation; the parameter α gives information about how distributed are the relaxation times and normally it increases with the temperature. On the contrary, classical anelastic relaxations in crystalline metals show shapes very close to a Debye relaxation with α and γ~1. It should be recalled here that the $\tau=\tau(T)$ in the previous equation is the average relaxation time of the process at a given temperature.

Other functions, either empirical or coming from physical models, are used to characterize the experimental loss modulus of glasses[128,129]; although here we only describe the most common ones, some of these other models will appear in the next section when discussing the mechanical spectroscopy results in MGs. In any case, however, all the functions have to fulfill similar properties as the ones detailed here for the HN and related functions.

3.3.3 Thermally activated models

As previously stated, internal friction can be interpreted as a combination of anelastic (reversible) and viscoplastic (irreversible) relaxation events. Previous works on crystalline metals show that anelastic relaxation can be well explained by mobility of defects in the crystalline lattice. These models consider interface relaxation (including grain boundary, twin boundary and nano-crystalline metals), dislocation, and point defect relaxation known as Snoek and Zener relaxation[122,130]. That is, most of the known mechanisms of anelastic relaxation in metals have their origin in the thermally activated motion of various kinds of defects.

The amorphous nature of MGs prevents the description of internal friction in terms of these mechanisms. The only mechanism which can be easily extrapolated from crystalline to amorphous structures is that of atomic and defect migrations, directly related to the movement of single atoms inside the

structure. The jump of an atom or point defect from one site to another in a crystal lattice is a simple example of a rate process. The corresponding relaxation time follows a reciprocal Arrhenius equation

$$\tau_\alpha(T) = \tau_0 \exp\left(\frac{E_{act}}{k_B T}\right) \tag{3.19}$$

valid when the rate limiting step of the relaxation process is the movement over an energy barrier.

From the position of the loss peak at a given temperature, $\omega\tau(T)=1$, obtained from dynamic experiments the activation energy is calculated as

$$\begin{aligned} &\ln(\omega_{peak}\tau) = 0 = \ln(\omega_{peak}\tau_0) + \frac{E_{act}}{k_B T} \\ &\ln\left(\frac{\omega_{peak2}}{\omega_{prak1}}\right) = \frac{E_{act}}{k_B}\left(\frac{1}{T_1} - \frac{1}{T_2}\right) \end{aligned} \tag{3.20}$$

In the case of no observable peak, the activation energy could still be calculated using the temperature dependence of a fixed value of the loss modulus as a function of frequency. In a more general way, the temperature behavior of the average relaxation time $\tau(T)$ may be obtained by application of the temperature-time-superposition (TTS) analysis of the mechanical relaxation curves also for non-Arrhenius behaviors[131].

The relaxation processes of glasses may involve cooperative movements much more complex than the defect migration scheme. Besides, even for a well-defined process of atomic or defect migration, the inhomogeneous structure of glasses would generate a broader distribution of activation energies than in a crystalline material. In spite of this, glass relaxations are usually interpreted in terms of the temperature dependence of a main characteristic time $\tau(T)$, which is the average value of the relaxation times distribution, and can be determined by TTS analysis. Of course, if the DMA curves involve the overlapping of different processes with quite different activation energies or $\tau(T)$ behaviors, the TTS analysis will not be applicable.

3.3 Mechanical spectroscopy of MGs

A huge amount of work on mechanical spectroscopy is collected by Magalas[132]. DMA can be performed both in isothermal (scanning frequency at fixed temperature) or isochronal (scanning temperature at fixed frequency) modes. In every solid, there exists a fundamental thermoelastic coupling between the thermal and mechanical states with the thermal expansion coefficient as the coupling constant. The thermoelastic damping contributes to the background of the loss modulus and Q^{-1} isochronal curves; differences between high and low frequency tests may originate from this effect. A detailed discussion on the thermoelastic background could be found in Nowick's book[122]. Other effects may also contribute to the DMA background, which increases in less compact structures and it is then more important for glassy states with higher free-volume. Castellero[133] used the change in the intensity of the Q^{-1} background in order to follow the room temperature aging of Mg-Cu-Y glasses.

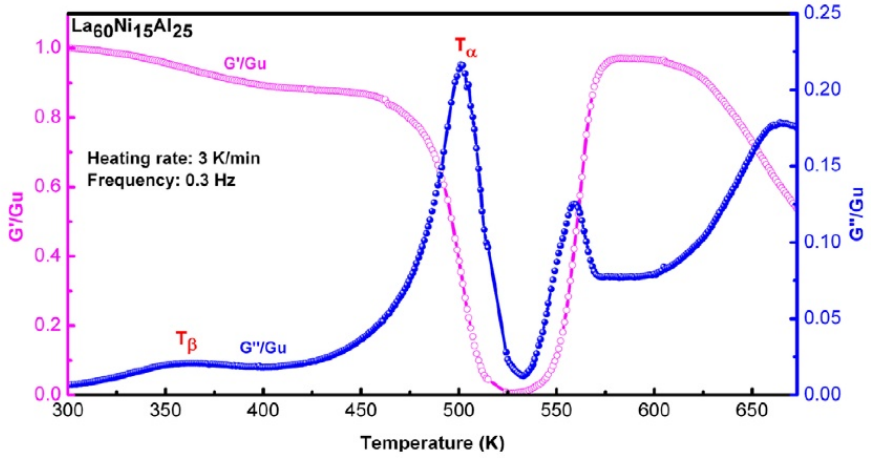

Figure 3-3 Normalized storage shear modulus *G'* and loss modulus *G''* vs temperature in $La_{60}Ni_{15}Al_{25}$ BMG, G_u is the unrelaxed shear modulus. Reprinted from ref.[135].

In addition to the background, the basic features of isochronal DMA curves of MGs are observed in figure **3-3**. At temperatures below T_g, a slight and constant decrease of the storage modulus is expected as temperature increases due to thermal expansion of the structure[134]. In this region, many

MGs also show a secondary relaxation peak in the loss modulus and the corresponding partial step-like decay of the storage modulus. Increasing the temperature, the dynamic glass transition is clearly visualized by the α-relaxation peak of *M''* and a complete decay of *M'* once in the liquid state. At higher temperatures, crystallization returns the system to the solid state increasing again the storage modulus. At even higher temperatures, thermal expansion and softening of the solid reduce again the storage modulus and increases the internal friction.

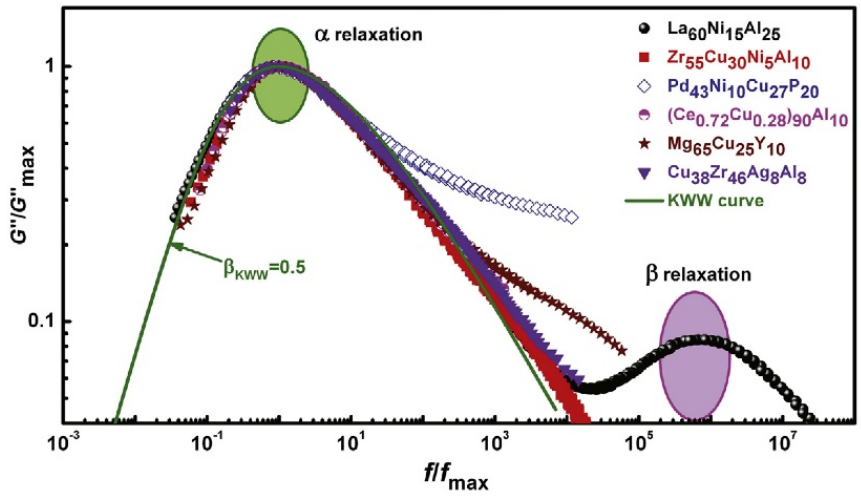

Figure 3-4 Dependence of the normalized loss modulus vs the normalized frequency in typical MGs. The solid line is fitted by the KWW model. Reprinted from Ref.[139].

DMA measurements are usually performed with heating rates of 1-5 K/min and frequencies from 0.01 to 100 Hz. For this range of heating rates and frequencies, the maximum of the α-peak is found in the liquid temperature-region, and the measured temperature dependence of τ_α is in good agreement with the viscosity behavior described by equation 3.1[136]. In many glassy alloys, however, crystallization is very close or even overlapped with glass transition. The decay of the storage modulus is then stopped before reaching a zero value and the α-peak may be cut on its high-temperature side. In this case, the apparent maximum of the peak may not correspond to the real α-relaxation peak maximum. In spite of possible deviations due to crystallization or aging, the α-relaxation process observed by DMA is generally well-understood and it can be characterized by an HN-

function or the Fourier transform of a KWW function with stretched exponent values β_{KWW}~0.5, as seen in figure **3-4**. Wang et al.[137] also found values of β_{KWW} between 0.4 and 0.5 for some of the most representative MGs (PdNiCuP, CeAlCu and Vitreloy), while Meyer's work on $Pd_{40}Ni_{10}Cu_{30}P_{20}$ in the equilibrium state[138] found that the α-relaxation followed the stretched exponential function with β_{KWW}=0.76. On the other hand, secondary relaxations show very diverse characteristics in different MGs and their origin is less clear.

3.3.1 Secondary relaxations

By surveying the relaxation dynamics in organic molecular liquids and fused salts, Johari and Goldstein suggested that β relaxation was a universal feature of glassy systems[87]. In some polymers, as shown in figure **3-5** from the work by Casalini[140], there is a clear picture. On one hand the α-relaxation time becomes arrested in an Arrhenius behavior once in the glass state, it controls the aging and it is coincident with the calculations from the mode coupling model. On the other hand, the β-relaxation times are similar to the primitive τ_α in agreement with the interpretation of a Johari-Goldstein relaxation as a precursor of the structural α-relaxation.

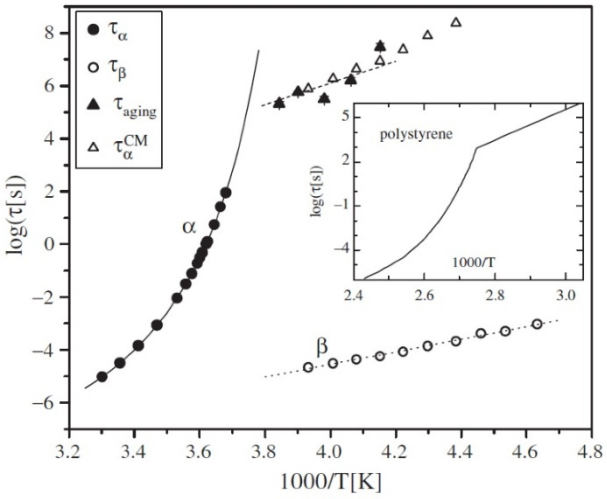

Figure 3-5 Relaxation time for the α and β processes, along with the aging decay time τ_{aging} and the τ_α calculated from coupling model. Reprinted from ref.[140].

Nowadays, it is becoming popular a description of MG dynamics in terms of α and β relaxations. All the peaks below the glass transition temperature are referred as β-relaxation although their origin may not be the same. We will follow this terminology here. However, it should be noted that some β-relaxations detected by mechanical spectroscopy are not Johari-Goldstein relaxations or the ones envisioned from the potential energy landscape model but may come from different origins.

Indeed, this kind of anelastic events in MGs can be dated back to the discovery by Berry that in Nb_3Ge MGs thermal activated anelastic events manifest on an internal friction peak around 250 K[141]. This peak was interpreted as stress induced ordering of a similar nature to the point defect relaxations known in crystalline solids. Although it is not a Debye peak and it shows an asymmetric distribution of activation energies, the typical magnitude of the relaxation time corresponded to a single atomic jump and the intensity of the peak decreases with aging. Actually, later work suggested that in the low temperature region there might be contributions from hydrogen absorption, which exists in quite large range of MGs[142]. Yoon[143] also found these peaks located around 250K with activation energies of E~100 kJ/mol (1.0 eV) in $Fe_{40}Ni_{40}P_{14}B_6$ and $Fe_{32}Ni_{36}Cr_{14}P_{12}B_6$ MGs and they ascribed them to the movement of B atoms. Fukuhara[144] interpreted the low-temperature (150 K) relaxation peak found in $Zr_{55}Cu_{30}Al_{10}Ni_5$ as related to a topological transition or a vacancy-like defect rearrangement.

However, based on the finding of this peak in $Cu_{50}Zr_{50}$, $Co_{35}Y_{65}$ as well as $Co_{35}Dy_{65}$ MG, and after excluding factors like hydrogen or oxygen absorption, Kunzi[145] suggested that the relaxation peak is due to the existence of intrinsic degrees of freedom in the amorphous structure as well as in other glasses such as oxides glasses[146]. It is also observed that cold work might lead to the observation of peaks occurring at temperatures between 100 to 300K[147]. Actually, plastic flow both on cold rolling and hydrogenation occurs via formation and motion of dislocation-like defects which are the reason of the observed anelastic anomalies. It is suggested by Khonik[147] that low temperature internal friction peaks described in the literature for as cast, cold deformed and hydrogenated samples have common origin.

Nevertheless, the characterization of local defects in amorphous structures is a complex, long-standing topic still not fulfilled in spite of many efforts since the early works of Egami[148].

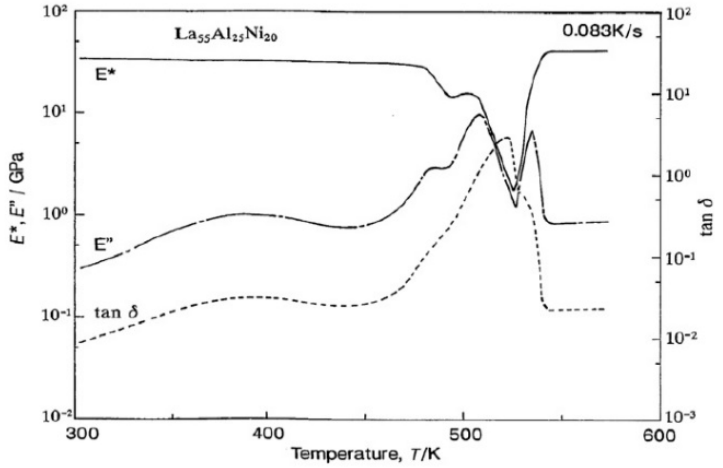

Figure 3-6 Temperature dependence of DMA behavior of $La_{55}Al_{25}Ni_{20}$ MG. Reprinted from ref. [149].

These thermal activated anelastic events might also happen in a bulk MG as first described by Okumura[149] in the analysis of the viscoelastic behavior of $La_{55}Al_{25}Ni_{20}$ MG. As shown in figure 3-3-6, besides the glass transition temperature region, a β-relaxation gets activated at around 400K. Further work[150] showed that aging reduces the magnitude of the relaxation peak but has little effect on the β-relaxation peak position. However, this fact was questioned by Qiao's work, which showed that the β-peak moves to higher temperature after physical aging[151]. The activation energy of the β-relaxation obtained by the time temperature superposition (TTS) shift factor method is E_β~100 kJ/mol (1.0 eV). In calorimetric measurements, the extrapolation of the intensity of β-relaxation associated to enthalpy release when the aging process is completed shows a non-zero intercept, which suggests that the β-relaxation would still remain in the fully relaxed state. Combined with Qiao's result on partially crystallized samples where this peak remains, it seems consistent that β relaxation might be caused by short range atomic relaxation, somewhat similar to Snoek or Zener type processes, as suggest by Okumura. On the other hand, as already stated above, some works have found that the characteristics of the secondary relaxation in some MGs

are well in agreement with the expected JG-relaxation[121]. The debate on the origin of β-relaxation remains open.

Similar behavior of the loss modulus is also observed in $La_{70}Al_{15}Co_{15}$. Wang's work on La-based BMGs shows that the β-relaxation behavior could be tuned by modification of the chemical composition and could also manifest on different fragility parameter[152]. Not only the intensity, but also the temperature is strongly influenced by the composition; the loss modulus dependence on temperature of $La_{70}M_{15}Al_{15}$ with M=Ni, Co or Cu is strongly related to the composition as shown in figure **3-7**. In the case of Ni and Co, there are distinguishable β relaxation peaks, but in the case of Cu the onset of β relaxation is at higher temperature and overlaps with the contribution of the main relaxation, leading to a shoulder or excess wing. This is further explored by Yu[72], affirming that β-relaxation appears if all the atomic pairs have large similar negative values of enthalpy of mixing, while positive or significant fluctuations in enthalpy of mixing suppress β-relaxation. Their conclusion is based on the fact that by substituting Ni by Cu in $La_{70}Ni_{15}Al_{15}$ the loss modulus changes from a separate β-relaxation peak to an excess wing behavior.

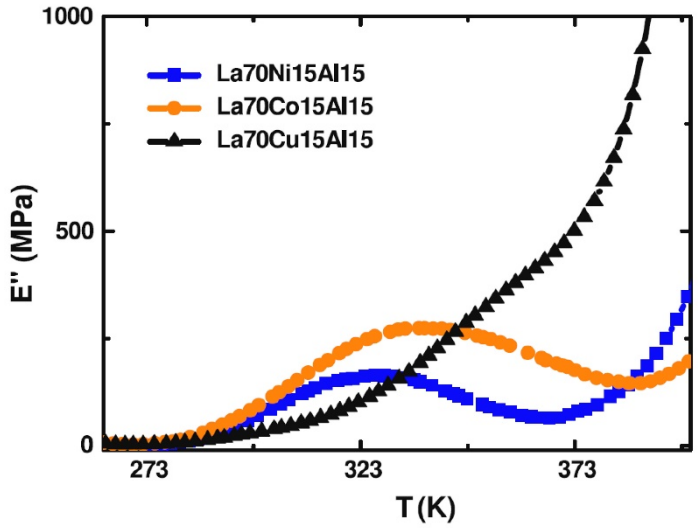

Figure 3-7 The *T* dependence of loss modulus of $La_{70}M_{15}Al_{15}$ with M=Ni,Co,Cu. Reprinted from ref.[152].

The enthalpy of mixing is also used to explain the experimental observation that partially substituting Ni with Cu in $Pd_{40}Ni_{40}P_{20}$ increases the glass transition temperature while lowers the starting temperature of β-relaxation. Furthermore, they suggest that strong and comparable interactions among all the constituting atoms generate string-like atomic configurations, whose excitation emerges as the β-relaxation events.

In systems like $Pd_{77.5}Si_{16.5}Cu_6$, $Pd_{48}Ni_{32}P_{20}$, $Pt_{58.4}Ni_{14.6}P_{27}$ and $Au_{49}Cu_{26.9}Si_{16.3}Ag_{5.5}Pd_{2.3}$ the *sub-*T_g relaxation is detected as a shoulder of the α-peak[153,154] and experiences important changes upon annealing due to aging. Chen pointed out[153] that this sub-T_g relaxation has different features from the JG-relaxation of polymeric and molecular glasses which shows a distinct peak at T_m<0.6T_g (at a frequency of 1Hz) and small effect on the intensity due to thermal stabilization near T_g. In $Zr_{55}Cu_{30}Al_{10}Ni_5$ alloys or $La_{55}Al_{25}Ni_{20}$, $M''(T)$ behavior is more similar to a double α-peak than a peak with a shoulder. These results have been interpreted in terms of double glass transitions related to phase separation in the glass[155] or because of double-stage unfreezing of the mobility of the different species during heating[156].

Cohen[157] simulated the loss modulus of a binary Lennard-Jones potential by molecular dynamics by introducing oscillatory stress. The simulation results showed that the β wing could appear on the loss modulus as a function of temperature. Based on simulated DMA curves performed with different fractions of pinned particles, β process was attributed to cooperative movements different from α relaxation. Yu[158] suggested that cooperative string-like atomic motion might be more appropriate to express β process in MGs since it can explain the diffusion of the smallest atom species. Although with a nature of cooperative movement, they involve only small part of all the atoms in the system. Liu[159] measured the activation energy E_β in ultra-quenched MGs, the relationship E_β=26RT_g suggested that it is a JG-relaxation. X-ray diffraction combined with EXAFS results showed that relaxation originated from short range collective rearrangements of large solvent atoms which could be realized by local cooperative bonding switch. In general, the microscopic mechanisms considered for secondary relaxation are also

associated to aging. A short revision of various microscopic models suggested to be responsible of physical aging is already given in section 3.1.2 above.

3.3.2 Influence of aging

Physical aging makes the structure denser and induces changes in the mechanical, electrical, magnetic, thermal and transport properties. The oldest and widely adopted concept for interpreting aging is that of free volume being progressively reduced. Alternative concepts describe aging as annihilation of various kind of 'defects' of the amorphous structure, comprising interstitial-like, stress inhomogeneities, shear transformation zones (STZ) or other microscopic motives. In MGs aging is usually referred as irreversible structural relaxation and has long been noticed as a strong effect existing even at room temperature. Early experiments[160,161] found that when an as-quenched sample is heated cyclically at a constant rate to successively increasing temperatures, the internal friction in each heating run is reduced. This can be described as if the relaxation spectrum is reduced in its faster part by physical aging. When heating during a DMA isochronal test, physical aging may occur in situ and the relaxation spectrum would not correspond to a single isoconfigurational state[162]. On the other hand, if the sample has been previously properly annealed it may not suffer significant aging during the test and the results become reproducible in consecutive heating-cooling-heating cycles.

The nature of individual movement of small areas is supported by room temperature creep behavior using nanoindentation techniques by Castellero[133]. The creep behavior is viscoelastic and could be fitted by two typical relaxation times, which were found to be around 4 s and 36 s for $Mg_{65}Cu_{25}Y_{10}$ and 2.5 s and 25 s for $Mg_{85}Cu_5Y_{10}$. After aging, the relaxation time of the slow process increases. Comparing with the relaxation time obtained by positron annihilation spectroscopy, Castellero et al. suggested that there are small and large traps where positrons can be annihilated. Smaller defects could be intrinsic open volume regions similar to Bernal interstitial sites, while larger defects are unstable and get annihilated as a consequence of aging. The reduction of these defects, responsible for shear transformations,

lead to an abrupt loss of plasticity and a continuous decrease in the creep deformation rate.

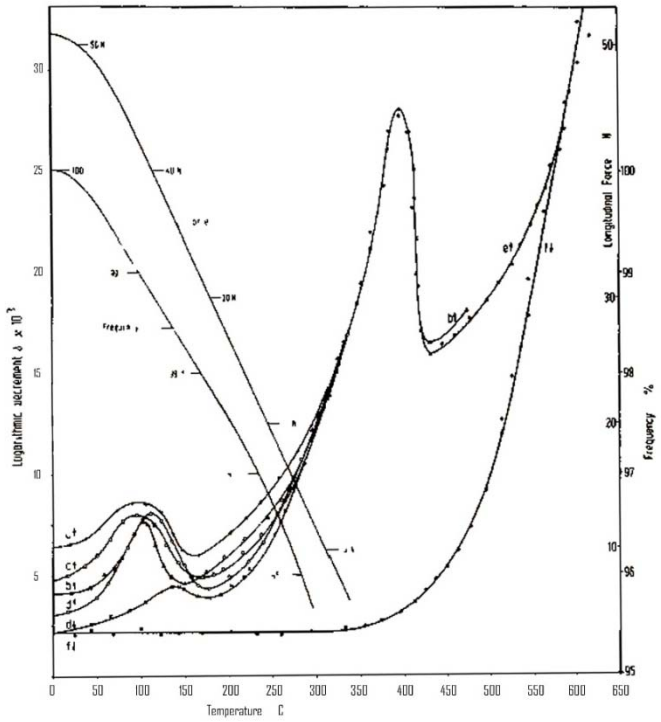

Figure 3-8 Internal friction of an Fe-based MG for different degrees of physical aging. Reprinted from ref.[163].

Kiss investigated the influence of aging on internal friction of FeB and NiP amorphous alloys[164]. Their results on $Ni_{80}P_{20}$ show that annealing decreases the internal friction and increases the storage modulus of MGs. Hettwer's work[163] on influence of heat treatment on the internal friction of $Fe_{32}Ni_{36}Cr_{14}P_{12}B_6$ shows that besides the peak observed around 665 K, there is another small peak in the range between 360 K and 400 K which nowadays could be classified as β-relaxation as shown in figure **3-8**. The intensity of such β-relaxation becomes reduced and shifted to higher temperatures by heat treatment. Using this β-relaxation as a probe, they investigated the aging dynamics by considering that the reduction of the damping is influenced by both temperature and annealing time as $Q^{-1}=\alpha \log t_a + Q^{-1}_0$ where parameters α and Q^{-1}_0 are functions of the temperature.

Tests at higher frequency (280 Hz) on the same composition by Haush[165] show a similar behavior, a strong secondary relaxation peak shift to higher temperature. However, Morito[166,167] observed that the β-relaxation reported by Hettwer is not always reproducible, and he suggested that it might come from inappropriate loading. Morito and Egami's work[160,167] on the same composition shows the influence of aging on internal friction. After an extended period of annealing, the glass reaches an internal pseudo-equilibrium state revealed on the internal friction. The decay kinetics can be expressed by first order kinetics with a log normal distribution of time constants, and the pseudo-equilibrium state is a function of the annealing temperature. A change in the annealing temperature results in a reversible change from one such state to another.

The work by Deng and Argon on $Cu_{59}Zr_{41}$ and $Fe_{80}B_{20}$ shows that besides the α-relaxation, there is another relaxation process which gets activated at lower temperatures[32,168], the peak position of the β-relaxation is near 500 K. This peak shifts progressively to higher temperatures as aging continues and is used as a probe to study the aging process. Unlike the $Fe_{32}Ni_{36}Cr_{14}P_{12}B_6$, where quasi-equilibrium structures can be achieved and altered reversibly by annealing at different temperatures, in the $Cu_{59}Zr_{41}$ MG these quantities continued to change until the onset of crystallization. By fitting the peak temperature at different frequencies, the activation energy for the sample aged at 573K for 34 hours is 46 kJ/mol (0.48 eV), with a frequency factor of 1.9×10^5 s^{-1}. Considering the connection between activation energy of shear transformations and the level of free volume at the transforming cluster site, they affirm that the aging related shifting to higher temperatures without change in height is a result of reduction of free volume in a specific local atomic environment existing in this composition.

The activation energy spectrum of the change of internal friction associated with aging can be obtained by subtracting the internal friction curve of the fully relaxed material from that of the as received one, in a similar way as the data obtained by calorimetric measurements. It is important to keep in mind that the activation energy of internal friction is different than the activation energy of irreversible structural relaxation or aging. A well-

known fact is that the relaxation time from internal friction tests is frequency dependent. However, for example in $Fe_{32}Ni_{36}Cr_{14}P_{12}B_6$, the aging characteristic time at 473 K is around 135 minutes and almost the same for 573 K[166].

3.3.3 Modelling of the mechanical relaxation spectrum

The temperature dependence of internal friction or loss modulus can be modelled with the methodologies described in section 2.2.2. Debye relaxation is normally used to describe the anelastic behavior, and the distribution of relaxation times can be related to a spectrum of activation energy. Ignoring the microscopic origin of the E distribution, the time-temperature relaxation spectrum $M''(\omega,T)$ can be modelled by combining a frequency response function (HN, CD, CC or other) with a temperature dependence of the main relaxation time $\tau(T)$, in what is called time temperature superposition (TTS) method[169]. In this approach, the shape of the response function describes the effect of the relaxation time spectrum, i.e. the deviation from a Debye process. In the case of HN, CD or CC functions, this shape is determined by the exponents α and γ of equation 3.18 with values obtained from fitting the experimental data. Therefore, $\tau(T)$ describes the temperature dependence of the average or main relaxation time of the process and is commonly found to follow an Arrhenius-like behavior for $T<T_g$.

If the system shows various relaxation processes well differentiated in the time scale, each one of these processes can be modelled by the corresponding response function χ_i and intensity ΔM_i as

$$M(\omega,T) = M_u - \Delta M_1 \chi_1(\omega,T) - \Delta M_2 \chi_2(\omega,T) - \ldots \qquad (3.21)$$

where the temperature dependence of χ_i is given by the corresponding $\tau_i(T)$. Of course, if the activation energy spectrum of one of these processes is very broad, a $\tau(T)$ defined by a single activation energy and a $\chi(\omega)$ function with constant shape will not be able to reproduce the whole time-temperature spectrum and the modeling will have to take into account the explicit distribution of activation energies, computing the frequency-domain response

function by numerical calculation of equations 3.13 and 3.15. Finally, it should be taken into account that M_u, and sometimes ΔM_i, usually shows a slight temperature dependence[134] that may has a significant effect if the modelling expands over a large temperature window.

The master curve analysis is often used in the interpretation of DMA data using TTS principle; the master curve is constructed using isothermal multi frequency DMA data. Within this methodology, the temperature dependence of the shift factor follows an Arrhenius relationship with different activation energies below and above T_g. Pelletier[170] investigated the apparent activation energy in Pd-Ni-Cu-P using this method and obtained E_β=1.1 eV and E_α=3.4 eV respectively. Jeong[171,172] analyzed the mechanical relaxation of $Mn_{55}Al_{25}Ni_{10}Cu_{10}$ and $Zr_{36}Ti_{24}Be_{40}$. For $Mn_{55}Al_{25}Ni_{10}Cu_{10}$ glass, the activation energy of the alpha relaxation was found E_α=78 kJ/mol (0.81 eV) and E_α=323 kJ/mol (3.3 eV) respectively below and above T_g. For $Zr_{36}Ti_{24}Be_{40}$, the activation energies were $E_\alpha(T<T_g)$=93 kJ/mol (0.96 eV) and $E_\alpha(T>T_g)$=392 kJ/mol (4.1 eV). Guo's work[173] on mechanical relaxation studies of α and slow β processes show that $Nd_{65}Fe_{15}Co_{10}Al_{10}$ have a distinct β relaxation in the temperature region between 320K and 420K. The activation energy is found E_β=98 kJ/mol (1.0 eV) with the $\tau_{\beta 0}=10^{-14.5}$. Since there is a relationship $E_\beta=24RT_g$ which is close to the suggested by mode coupling theory[174], they claim that β relaxation is intrinsic in MGs. Activation energy data of α and β relaxations of many MG systems can be found in Wang's work[175].

In a narrow range above T_g, the VFT behavior of $\tau(T)$ can be approximated to an Arrhenius law with an apparent activation energy of the liquid

$$E_{\alpha,liquid} = mRT_g \ln(10) \tag{3.22}$$

This gives values between 200 and 600 kJ/mol depending on the fragility and the T_g of the system. On the other hand, the activation energies of both α and β relaxations at $T<T_g$ are usually found between 80 and 160 kJ/mol. These E values of the mechanical relaxation processes below but not far from T_g coincide with the activation energy commonly found for physical aging in this

temperature region, as already stated above, the same microscopic origins are expected for both processes.

Here it is interesting to note that $E_\beta \sim 26RT_g$ and E_α given by the AGV approach (equation 3.3) give very similar values. For instance, considering typical values for MGs of $T_g=T_{fictive}$=600 K, T_0=450 and $B=D^*T_0$=4500, equations 3.1, 3.2, 3.3 and 3.22 give $E_\alpha(T>T_g)$=440 kJ/mol, m=38, $E_\alpha(T<T_g)$=128 kJ/mol while $E_\beta=26RT_g$=130 kJ/mol. Therefore, the expected values of the average activation energies controlling both primary and secondary relaxations in the glassy phase are very similar for MGs. This poses difficulty in interpreting both phenomena with the potential energy landscape picture in terms of sub and mega-basin transitions.

Concerning the shape of the relaxation function, Liu and Wang[176,177] fitted the DMA behavior of Ce-based and Zr-Ti-Cu-Ni-Be glasses assuming that $\tau(T)$ follows a VFT behavior and relaxation can be described by the KWW function. The loss modulus was computed by Fourier transform finding that in the temperature region higher than T_g the experimental data was well reproduced; however, in the lower temperature region, the fitting was poorer. In $Ce_{70}Al_{10}Cu_{20}$ and Zr-Ti-Cu-Ni-Be glasses the excess wing was fitted by considering α and β relaxations. They suggested that β relaxations arise from the small scale translational motions of atoms which are hindered in its metastable atomic positions by solid-like islands.

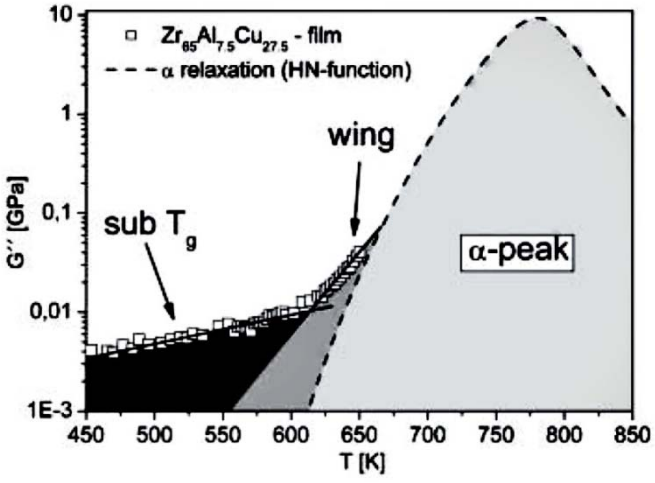

Figure 3-9 Low temperature side of the loss modulus peak of ZrAlCu glass. Reprinted from ref.[178].

In many MG compositions, mechanical relaxation below T_g is only perceived as an excess wing of the main α-peak (see figure **3-9**). In other cases, a shoulder or a secondary peak is detected in as-quenched samples but vanishes after thermal cycling in more stable glassy states. Description of $M''(\omega,T)$ along the whole temperature range by consistent relaxation functions and $\tau(T)$ behaviors is maybe the main tool in order to discern if a secondary relaxation is present and what are its main characteristics.

Using a CC-function, Hachenberg et al.[179,180] showed that the α-peak of $Zr_{65}Cu_{27.5}Al_{7.5}$ and $Pd_{77}Cu_6Si_{17}$ is well described by the VFT equation and the excess wing is better fitted when taken in consideration a β-relaxation. By observing the heating rate dependence of the onset and turning point of storage modulus dependence on temperature, Hachenberg determined E_β to be 0.67±0.11eV and 0.59±0.39 eV for $Pd_{77}Cu_6Si_{17}$ and $Zr_{65}Al_{17.5}Cu_{27.5}$ respectively. He ascribed this change on the storage modulus as a result of β-relaxation with a cooperative nature. Since these two different glassy systems have quite different strong-fragile liquid behavior (m=52.8-77 for Pd-Cu-Si and m=36.4-38.4 for Zr-Al-Cu) they suggested β-relaxation might be a universal feature of MG dynamics. Combining the dependence on the heating rate of α peak and MCT predictions they explained the merging of α and β relaxations.

The analysis of DMA behavior of $Mg_{65}Cu_{25}Y_{10}$ glass show that the deviation from VFT behavior combined with the in situ aging manifested a shoulder on the loss modulus as shown in figure **3-10**. [162]. In this case, the CC-function used for fitting the relaxation spectrum showed a significant change of the broadening parameter due to aging. The study of room temperature aging of the same system[110] shows an average activation energy coherent with the $\tau_\alpha(T<T_g)$ behavior found from DMA, implying that in this system aging is driven by molecular movements belonging to the high-frequency tail of a broad α-peak.

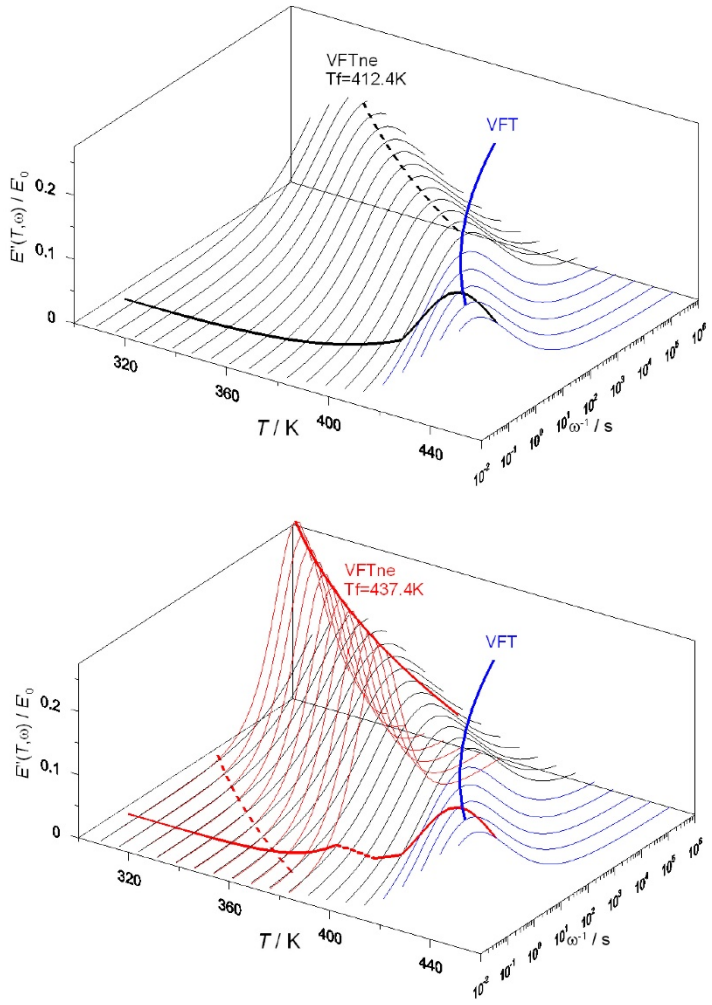

Figure 3-10 Thick solid line is the expected isochronal DMA behavior of $Mg_{65}Cu_{25}Y_{10}$ for different fictive temperatures. Reprinted from ref.[162].

In some MG compositions, especially Pd and La-based ones, the secondary relaxation appears as a prominent peak well-separated from the α-peak and present also for well-aged samples. Based on Cavaille's work on rheology of glasses and polymers[181], Pelletier analyzed the dynamic mechanical behavior of $Pd_{43}Ni_{10}Cu_{27}P_{20}$ in a hierarchical correlation concept[170]. Following Gauthier's[182] work on quasi point defects, three different contributions exist in the mechanical response as elastic, viscoelastic and viscoplastic parts. Qiao[183] analyzed and fit the temperature dependent internal friction behavior of $Zr_{55}Cu_{30}Ni_5Al_{10}$ using the same model.

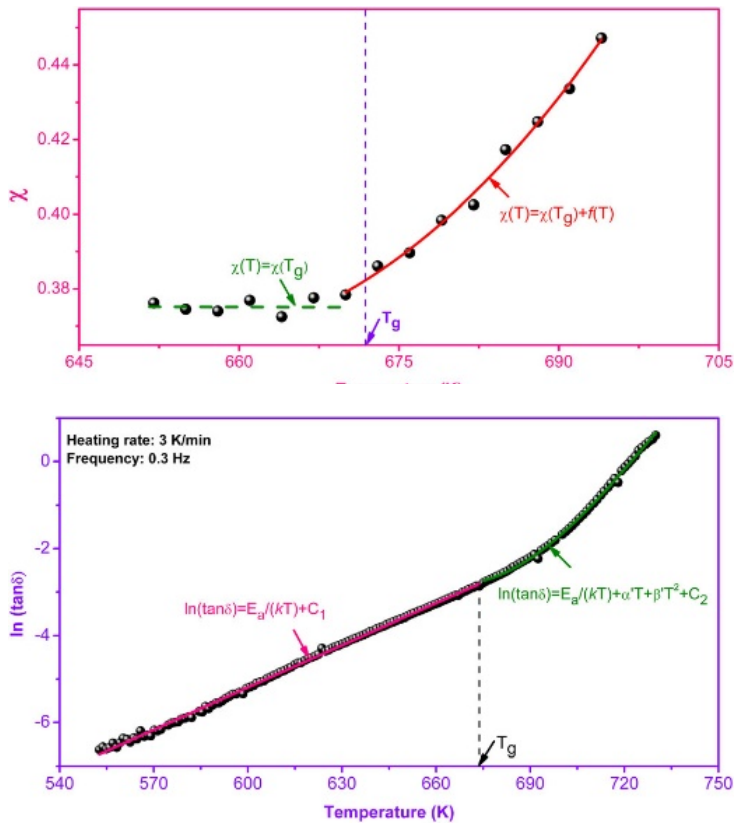

Figure 3-11 Internal friction modeled by the quasi-point defect theory and χ dependence on temperature. Reprinted from ref.[183].

In this model, the important parameter χ is a correlation factor between 0 and 1 linked to the quasi point defect concentration. χ=0 corresponds to a maximum order, when any movement of a structural unit requires the motion of all other units, while χ=1 represent maximum disorder when all the movements are independent of each other. With this methodology, in the low temperature range, when the χ is constant (~0.38 in the case of $Zr_{55}Cu_{30}Ni_5Al_{10}$), the loss factor can be easily fitted by a simple Arrhenius equation. At higher temperatures, the parameter χ is a function of temperature, and it was found that it could be fitted with a parabolic function (see figure **3-11**). In the point defect model, the key-question is how the order parameter χ changes with temperature. The behavior of χ is related to the viscosity change and Qiao's work shows that the quality of the fitting depends on an appropriate description of the viscosity behavior. However, due to the many

orders of magnitude change within a relatively narrow temperature region, the description of viscosity behavior is still an open problem[84,184,185].

Wang[186] showed that the DMA behavior can be fitted in the whole temperature range by coupling two KWW equations in Fourier transforms. The temperature dependence of τ_α shows a VFT equation while τ_β has an Arrhenius-like dependence. For $La_{70}Ni_{15}Al_{15}$, the pre-factors $\tau_{\alpha,0}$ and $\tau_{\beta,0}$ are 10^{-13} s and 10^{-15} s respectively and β_{KWW}=0.42. Qiao[151] fitted the relaxation dynamics of $Pd_{40}Ni_{10}Cu_{30}P_{20}$ as well as $La_{60}Ni_{15}Al_{25}$ by combining the Fourier transform of the KWW function for the α-relaxation and the CC-function for the β. From a microscopic point of view, α-relaxation could be interpreted as collective movement of all the atoms, while β relaxation could be understood by the quasi-point defect theory which relates relaxation to thermally activated jumps of a structural unit[135]. Later on, they described the β process using a coupling model in a very similar form[151].

Mechanical spectroscopy data can also unveil the underlying distribution of relaxation times. This means obtaining the distribution of relaxation times $A(\tau')$ defined in equation 3.13. Kursumovic[124,187] and Ocelik[188] analyzed creep recovery and found a trimodal distribution of τ' with maximums of the distribution peaks around 10 s, 100 s and 1000 s at temperature 50-100 K below T_g (figure **3-12**). The details of the $A(\tau')$ allowed them to propose different TSRO and CSRO corresponding to each mode of the distribution, the slowest one corresponding to annihilation of free-volume by cooperative motions. Ju and Atzmon applied direct spectrum analysis to strain relaxation data on $Al_{86.8}Ni_{3.7}Y_{9.5}$ at room temperature[189] and later to DMA isothermal curves of $Zr_{46.8}Ti_{8.2}Cu_{7.5}Ni_{10}Be_{27.5}$ near T_g [190]. In both cases they obtained a multimodal distribution of times, and interpreted it as associated to the activation of shear transformation zones (STZs) involving different number of atoms. The direct time spectrum analysis of mechanical spectroscopy permits to unveil more details about the microscopic movements involved in the relaxation process.

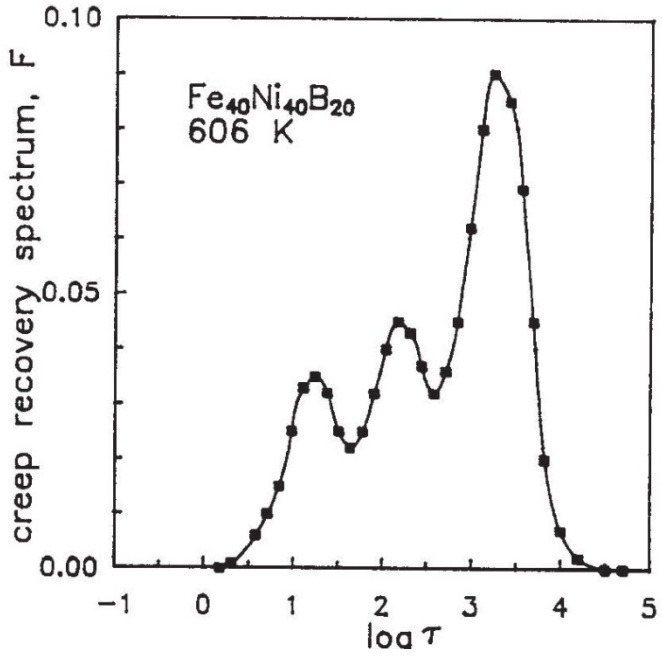

Figure 3-12 Time spectrum of anelastic relaxations of $Fe_{40}Ni_{40}B_{20}$ glass at $T<T_g$. Reprinted from ref. [187].

In addition to get insight to the microscopic origin of glassy dynamics, the determination of the relaxation spectrum $M''(\omega,T)$ by appropriate response functions and average $\tau(T)$ dependences is, per se, an important characterization of MGs due to its consequences on the mechanical properties. The relationship between mechanical relaxation processes and mechanical properties will be briefly introduced in the following section.

3.4 Relationship between relaxation and mechanical properties

On the macroscopic scale, bulk MGs can show plasticity depending on the temperature and the strain rate. At room temperature, depending on the specific system, the length scale of the plastic process zone ranges from 100 nm to 100 μm. Based on the relationship found between the measured plastic zone size and the stress intensity factor K_{IC}, Xi[191] suggested that fracture of MGs can be regarded as a flow process at different length scales. As reviewed by Schuh[41], physical aging affects all mechanical properties, from Young's modulus to impact toughness. This is often explained in the framework of the free volume theory; the free volume decreases during annealing, the shear to bulk moduli ratio increases and the glass becomes more brittle. In general, the mechanical behavior of MGs is interpreted in terms of shear transformation zones (STZs) or of the more recently developed cooperative shearing model (CSM) as reviewed by Chen[79]. As discussed above, the β-relaxation measured by mechanical spectroscopy is interpreted as micro-events activated at temperature lower than T_g. The main point here is to describe the relationship between these events and the mechanical properties.

Kahl investigated[192] the aging paths below T_g of $Pd_{40}Ni_{40}P_{20}$ glass via ultrasonic measurements. Figure **3-13** shows the changes in shear modulus due to decrease in free volume after various annealing treatments. The structural changes causing the process have been attributed to JG-β relaxations. In a similar material ($Pd_{43}Ni_{10}Cu_{27}P_{20}$), Harmon[193] identifies these secondary β-relaxation events with reversible anelastic excitations within the elastic matrix confinement, while the α-relaxation event was identified with the collapse of the matrix confinement and the breakdown of elasticity.

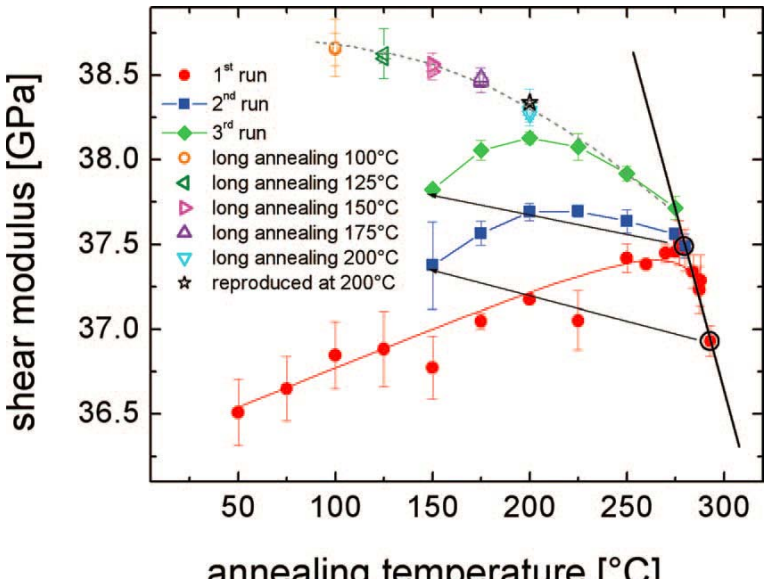

Figure 3-13 Shear modulus vs annealing temperature of a freshly prepared $Pd_{40}Ni_{40}P_{20}$ MG and subsequent annealing procedures. Reprinted from ref. [192].

Okumura[149] investigated the mechanical behavior of $La_{55}Al_{25}Ni_{20}$ MG at different temperatures. As can be seem from figure 3-**3-14**, there is an increase of maximum elongation around 385K that corresponds to the activation of β-relaxation in figure 3-3-6. As pointed out by Spaepen[63,194], stress or thermal activation in MGs transforms nanoscale soft regions - with larger free volume - into flow units able to accommodate deformation. Below the yield stress, the resulting atomic rearrangement is reversible. Above the yield stress the flow units overcome a certain energy barrier and the atomic reconfiguration becomes irreversible. Macroscopic plastic deformation is thus the result of simultaneous irreversible microscopic shearing events. Under this approach, shear banding is a consequence of a localized high density of flow units. Single flow units promote the activation of near flow units, in a cooperative mechanism which eventually results in the nucleation of a shear band.

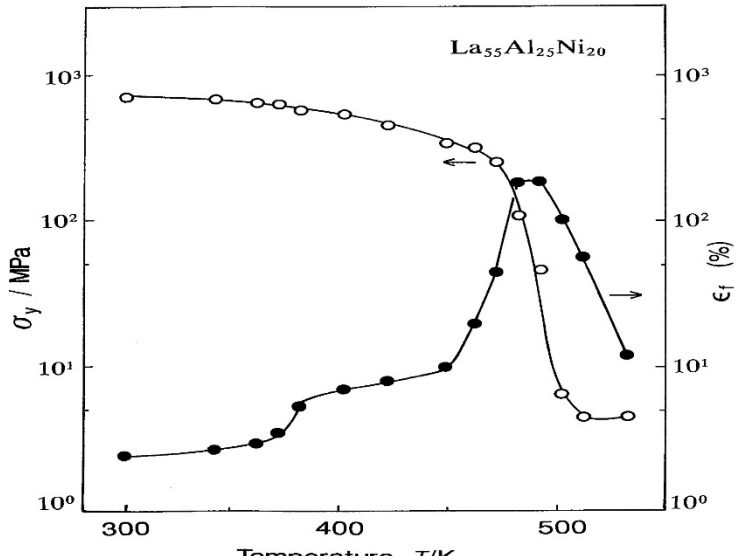

Figure 3-14 Changes in the yield stress and fracture elongation with testing temperature for $La_{55}Al_{25}Ni_{20}$ glass. Reprinted from ref.[149].

Based on potential energy landscape and the theory of shear strength in dislocation free solids, Johnson[195] proposed the CSM with the aim of understanding the rheological mechanisms and mechanical properties of MGs. According to it, the volume of STZs, Ω, is proportional to their activation energy, W^*, and the number of atoms participating in the flow unit can be estimated from the model. Using this model and treating the observed shoulder or β-peak of $M''(\omega,T)$ as a thermal activated process, the activation energy of the process can be determined by DMA. Zhao et al.[196] obtained the E_β of several different MGs. They obtained a relationship of $E_\beta = 27.5RT_g$ which is close to $24RT_g$ accepted for nonMG formers. They ascribe this difference to the different type of bonding and suggest that this is the Johari-Goldstein β relaxation in MGs. Using the same methodology, Yu[73] determined the activation energy of more MG alloys and found $E_\beta = 26RT_g$. By an appropriate choice of parameters and using the CSM model they found that the activation energy of β-relaxations and the potential energy barriers of STZs are the same. Liu[197] determined the activation energy of the β relaxation in La-based bulk MGs and assuming that this was the activation energy of STZs they obtained Ω=5.5(0.1) nm^3 and the number of atoms involved in an STZ, n=178(10), of $La_{60}Al_{25}Ni_{15}$. By compiling data of E_β ,

they found that the flow unit volume of various MGs range from 2.36 to 6.18 nm^3 and n goes from 170 to 250. These values are in agreement with Pan's[198] estimation based on nanoindentation experiments.

The importance of the Poisson's ratio on the design modern materials is highlighted by Greaves[199]. Besides, it is generally accepted that Possion's ratio is a good indicator of the ductility of MGs. With small deviations on the exact value, it is widely accepted in the literature that there exists a critical value which divides plasticity (higher ν values) from brittleness (lower ν values)[43]. For values of ν larger than 0.32, the shear band tip tends to extend rather than induce crack initiation, allowing formation of multiple shear bands and leading to the observed macroscopic plasticity. The exact mechanism is still obscure, but it is suggested that the ductile/brittle nature of metals (in amorphous or crystalline form) is related to the viscous time dependent properties of their liquid precursors, either constrained in MG shear bands or in polycrystalline grain boundaries. The analysis on STZs suggest that the average flow units also correlates with the Possion's ratio; as the value of Ω increase from 2.36 to 6.18 nm^3, the value of Poisson's ratio drops from 0.404 to 0.304.

Unlike previous work where plasticity could only be observed in constrained conditions like bending or compression, Yu[200] found a pronounced macroscopic tensile plasticity in a $La_{68.5}Ni_{16}Al_{14}Co_{1.5}$ MG using ribbon samples. Even at room temperature, the stress strain curve deviates from linear relationship under the strain rate of 1.6×10^{-6} s^{-1}. By determination of the strain rate of ductile to brittle transition (DBT) at different temperatures, the activation energy of the DBT is determined to be 103 kJ/mol. This is a similar value to the E_β determined by DMA. Furthermore, by using nuclear magnetic resonance (NMR), Yu[158] determined the temperature dependent atomic (diffusive) hopping rates of P atoms in $Pd_{40}Ni_{10}Cu_{30}P_{20}$ and Be atoms in $Zr_{46.75}Ti_{8.25}Cu_{7.5}Ni_{10}Be_{27.5}$. They found that their activation energies are very close to E_β. Since the P and Be are the smallest atoms in the respectively MGs, it is suggested that the β relaxation and self-diffusion of the smallest atoms are closely related.

It is generally accepted that the microstructural origin of the MGs plasticity can be explained by flow units or STZs. By utilizing a mandrel winding method which deform in the bend mode, Lu[201] realized homogeneous plastic deformation at room temperature for Zr, Fe, Mg, Al, and La based MG ribbons. Assuming E_β=26RT_g and choosing MGs with different T_g, they found that plastic deformation is higher for lower E_β. By annealing the sample, physical aging decreases the density of flow units and then both the β-peak of internal friction and plastic deformation get reduced. From the results, they suggest that when the loading time is longer than the relaxation time or if enough energy is applied to activate a sufficiently high density of flow units, homogeneous plastic deformation of MGs can occur at room temperature.

4. Experimental materials and methods

This section presents the sample preparation and characterization methods used during the PhD project. Some representative results and a list of all the different samples prepared and characterized during the project are given.

4.1 Sample preparation

Master alloys with different nominal composition were prepared by arc melting a mixture of constituent elements with purity above 99.9% under a Ti-gettered Argon atmosphere. The arc melting furnace used is an Edmund Bühler GmbH model MAM-1. The master alloys were re-melted twice to ensure compositional homogeneity.

After cooling, the master alloy is transferred into a Melt spinning device (SC model of Edmund Bühler GmbH). The melt spinner is first vacuumed below 10^{-3} Pa through combination of mechanical and turbo-molecular pumps. Then the chamber is filled with Argon gas at the desired pressure. The master alloy is loaded in a pure silica glass crucible and melted by an induction coil while temperature is monitored and controlled by an optical pyrometer device. The melt is quenched by injecting on a copper spinning wheel. The injection is obtained using a pressure difference between the crucible and the chamber. A pressure difference of 0.4 bar is usually employed. For all the samples presented in this work, the velocity of the wheel is set as 650 rpm. Taking in consideration the radius of the copper wheel, the lineal velocity is around 40m/s. At this conditions, ribbon samples with thickness of 30 ± 5 μm and a width of 1.5 ± 0.5 mm are obtained.

$Pd_{42.5}Ni_{7.5}Cu_{30}P_{20}$, $Ti_{36.2}Zr_{30.3}Cu_{8.3}Fe_4Be_{12.2}$, $Zr_{70}Ni_{16}Cu_6Al_8$ master alloys were kindly supplied by Prof. Jichao Qiao. The MG ribbons with nominal composition $Fe_{55}Cr_{10}Mo_{14}C_{15}B_6$ were kindly offered by Mr. Milad Madinehei while $Pd_{77.5}Cu_6Si_{16.5}$ ribbon were kindly offered by Dr. Eloi Pineda. These two latter compositions were produced by the same equipment and methods.

During the PhD project, several batches of samples of the following compositions were prepared: $Cu_{48}Zr_{48}Al_4$, $Cu_{46}Zr_{46}Al_8$, $Mg_{65}Cu_{25}Y_{10}$,

$Al_{85}Ni_7Y_8$, $Pd_{42.5}Ni_{7.5}Cu_{30}P_{20}$, $Ti_{36.2}Zr_{30.3}Cu_{8.3}Fe_4Be_{12.2}$, $Zr_{70}Ni_{16}Cu_6Al_8$, $Fe_{87}Zr_7B_5Ag_1$, $Fe_{20}Zr_{80}$, $Fe_{25}Zr_{75}$, $Fe_{30}Zr_{70}$, $Fe_{33}Zr_{67}$, $Fe_{40}Zr_{60}$, $Fe_{90}Zr_{10}$. Table 4-1 describes the purpose and information collected of each of the samples.

Table 4-1 Compositions explored within the Ph.D. thesis scope4.2 Structural, calorimetric and chemical characterization

System prepared: $Cu_{50-x}Zr_{50-x}Al_x$	
Objectives: Study of relaxation behavior and influence of Al content on properties.	Results: Main results of the relaxation behavior presented in chapter 5. Study of the crystallization kinetics in experiment HC-643 at ESRF (Grenoble).
System prepared: $Mg_{65}Cu_{25}Y_{10}$	
Objectives: Study of microscopic dynamics and structural changes during physical aging.	Results: Main results are not included in this PhD thesis but published in ref. [202]
System prepared: $Al_{85}Ni_7Y_8$	
Objectives: preparation of ex-situ composite MGs (Al_2O_3+MGs), study of mechanical properties of the composite.	Results: The composite was not obtained due to the low wetting behavior between the Al-Ni-Y melt and Alumina, and possible high reactivity between Cu-Zr-Al and Alumina. Normal melting casting of the composite as well as previous ball milling were tried as production techniques. Amorphous samples with composition of $Al_{85}Ni_7Y_8$ were obtained as manifested on XRD and DSC results.
System prepared: $Pd_{42.5}Ni_{7.5}Cu_{30}P_{20}$	
Objectives: Study of relaxation behavior and physical aging.	Results: Main results are presented in chapter 5.
System prepared: $Zr_{70}Ni_{16}Cu_6Al_8$	
Objectives: Study of relaxation behavior.	Results: DMA results show similar behavior to the Cu-Zr-Al MG analyzed in chapter 5.
System prepared: $Ti_{36.2}Zr_{30.3}Cu_{8.3}Fe_4Be_{12.2}$	
Objectives: Study of relaxation behavior.	Results: DMA result show similar behavior to the Cu-Zr-Al MG analyzed in chapter 5.
System prepared: $Fe_{20-90}Zr_{80-10}$	
Objectives: Fe-Zr MGs were explored to clarify whether β-relaxations are originated from movements of small atoms.	Results: DMA result is currently under analysis.

System prepared: $Fe_{87}Zr_7B_5Ag_1$	
Objectives: Analysis of thermal and electrical transport properties	Results: Amorphous material was produced but the solid solution of Ag atoms in the glass was not attained.
System prepared: $Pd_{77.5}Cu_6Si_{16.5}$	
Objectives: Study of the microscopic dynamics during physical aging.	Results: Study of the microscopic dynamics by X-Photon Correlation Spectroscopy in experiments HD-607 and HC-1147 at ESRF (Grenoble). Results under analysis.

The amorphous character of the obtained MGs was checked by X-ray diffraction (XRD) in a Bruker D8 Advance X-ray diffraction with Cu-K radiation (λ = 0.1541 nm) over a 2θ range from 20° to 100° with a scanning step of 0.02°. The basic objective of the XRD diffraction was to determine the amorphous character of the prepared alloys. An example of the obtained XRD patterns are shown in figures 4-1 to 4-4.

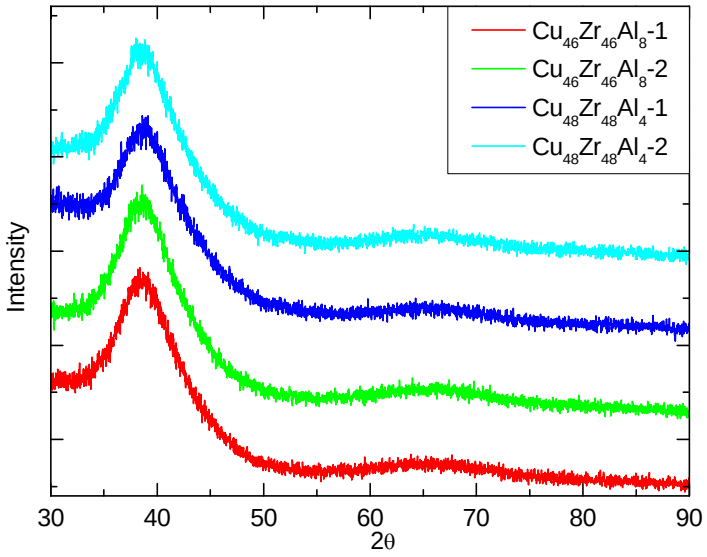

Figure 4-1 XRD result of $Cu_{46}Zr_{46}Al_8$ and $Cu_{48}Zr_{48}Al_4$ metallic glass. No difference is observed between different batches. Diffraction intensity is shift in order to clarify the figure.

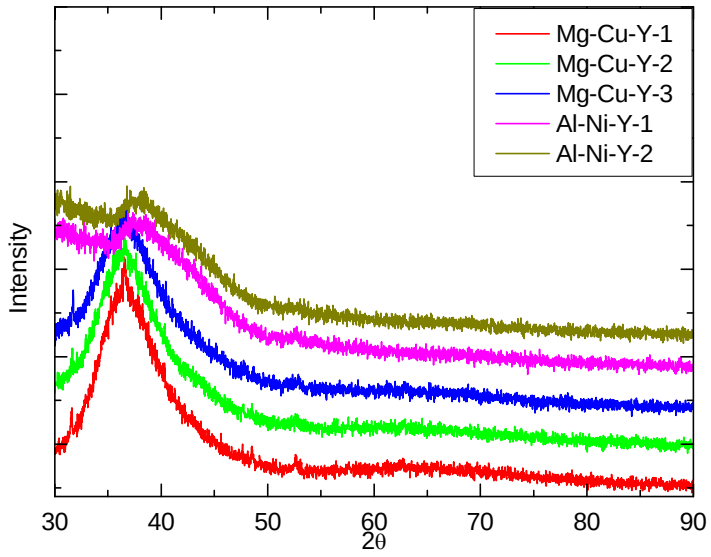

Figure 4-2 XRD of $Mg_{65}Cu_{25}Y_{10}$ and $Al_{85}Ni_7Y_8$. Diffraction intensity is shifted in order to clarify the figure. No difference is observed between different batches.

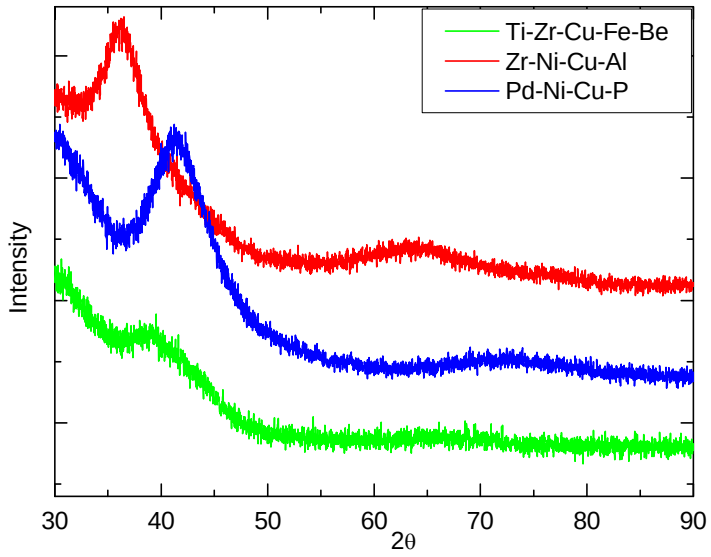

Figure 4-3 XRD of $Pd_{42.5}Ni_{7.5}Cu_{30}P_{20}$, $Ti_{36.2}Zr_{30.3}Cu_{8.3}Fe_4Be_{12.2}$, and $Zr_{70}Ni_{16}Cu_6Al_8$ MGs.

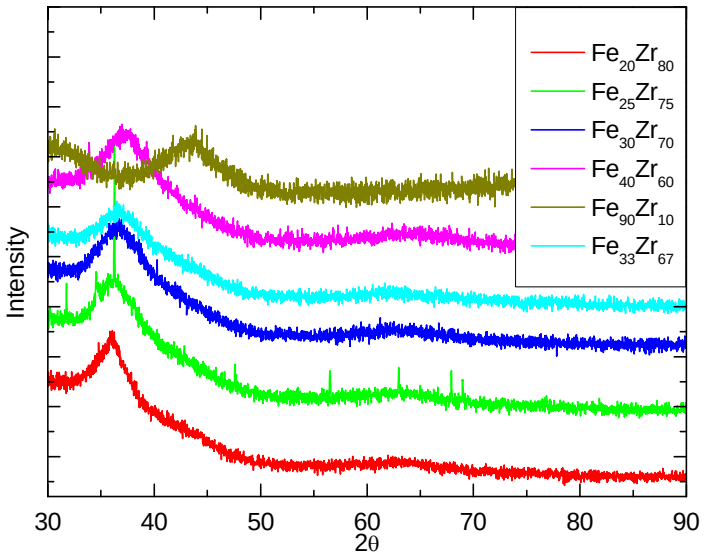

Figure 4-4 XRD of several Fe_xZr_{100-x} binary MGs. Compositions are listed in the legend of the figure. $Fe_{25}Zr_{75}$ was found crystallized.

The XRD patterns obtained and shown in the figures above show the contribution of the sample holder as a reflection at 2θ~25°. Indications of partial crystallinity are observed for example in Mg-based samples in figure 4-2. This crystallinity may come from crystallization during the rapid melting process or the presence of oxides or other inclusions.

Differential scanning calorimetry (DSC) was performed using NETZSCH 404 F3 equipment. Some selected results are shown in figures 4-5 to 4-8. From low to high temperature, the expected phenomenon to be detected by DSC scanning of metallic glasses are structural relaxation of the glass (exothermic), glass transition (change of C_p), supercooled liquid crystallization (exothermic) and melting (endothermic). In multicomponent alloys the crystallization of the supercooled liquid usually involves precipitation of multiple crystalline phases. The crystallization reaction may be a single sharp process, as in Cu-Zr-Al or Mg-Cu-Y samples in figures 4-5 and 4-6, or a multiple stage process with consecutive crystallization reactions, as for instance in the Al-Ni-Y of figure 4-6 or the glassy alloys shown in figure 4-7. Even in the case of a single sharp process, the crystallization usually involves nucleation and growth of various phases in a eutectic-like reaction.

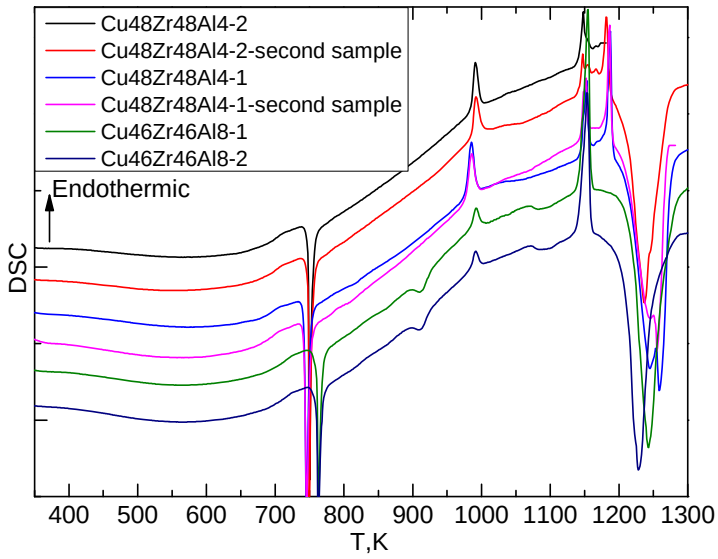

Figure 4-5 DSC of $Cu_{46}Zr_{46}Al_8$ and $Cu_{48}Zr_{48}Al_4$, at a heating rate of 10K/min. Different samples in the same batch show repeatable results. The two $Cu_{46}Zr_{46}Al_8$ batches show the same DSC behavior, while $Cu_{48}Zr_{48}Al_4$ show minor difference on the starting crystallization temperature which differ from 743K to 736K. In the case of $Cu_{46}Zr_{46}Al_8$, crystallization starts from 753K with a maximum at 763K. Vertical axes are shifted in order to clarify the figure.

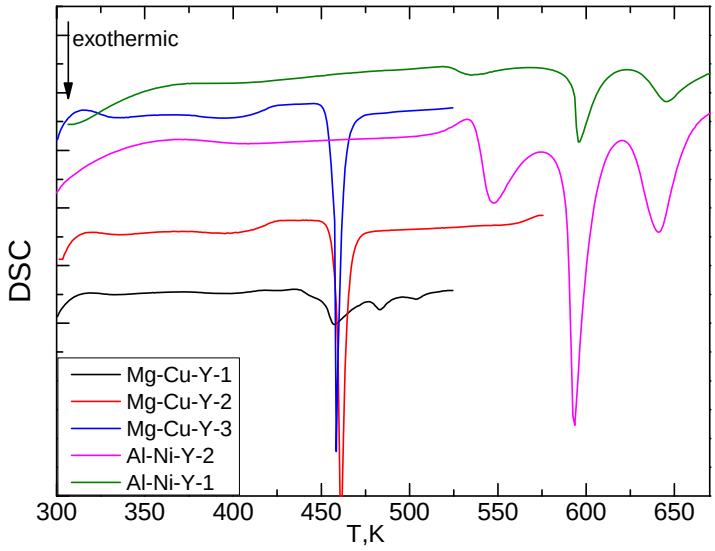

Figure 4-6 DSC of $Mg_{65}Cu_{25}Y_{10}$ and $Al_{85}Ni_7Y_8$ MGs. Al-Ni-Y is measured at a heating rate of 20K/min while $Mg_{65}Cu_{25}Y_{10}$ at 5K/min. Vertical axes are shifted in order to clarify the figure.

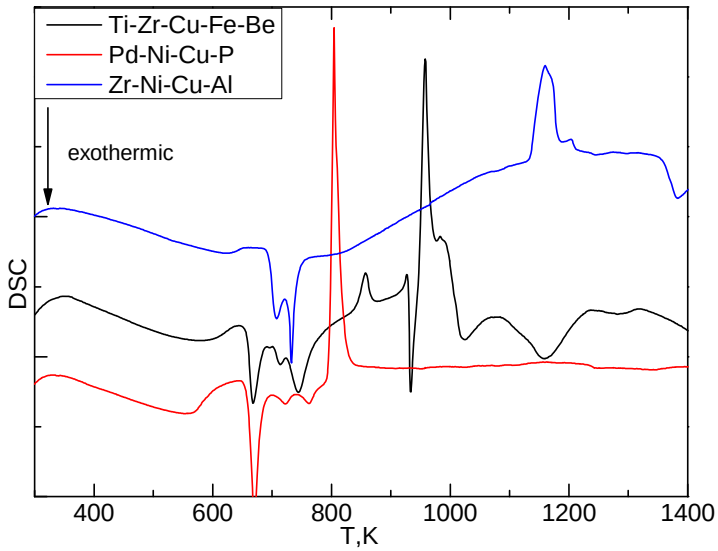

Figure 4-7 DSC of $Pd_{42.5}Ni_{7.5}Cu_{30}P_{20}$, $Ti_{36.2}Zr_{30.3}Cu_{8.3}Fe_4Be_{12.2}$, $Zr_{70}Ni_{16}Cu_6Al_8$ MGs, obtained at a heating rate of 20K/min. Vertical axis are shifted in order to clarify the figure.

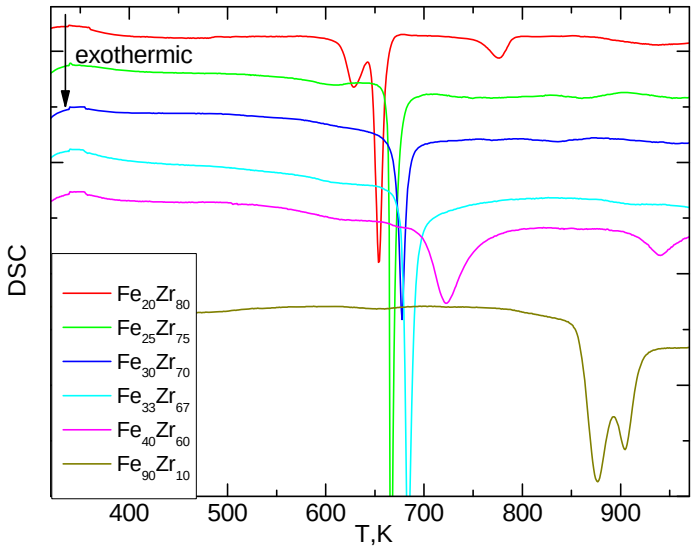

Figure 4-8 DSC of Fe_xZr_{100-x} MGs at a heating rate of 20K/min. No obvious glass transitions were observed in these binary MGs. Vertical axes are shifted in order to clarify the figure.

The glass transition, T_g, crystallization, T_x, melting, T_m and liquidus, T_f, temperatures were determined from DSC curves at 10-20 K/min. The T_g was determined as the position of the onset of the glass transition while T_x is

defined as the onset of the first crystallization reaction. The following table details the characteristic temperatures corresponding to all the samples analyzed during the project:

Table 4-2 Thermal characterization of MGs , Temperature in *K*, heating rates in K/min

Composition	T_g	T_x	T_m	T_f	Heating rate
$Cu_{48}Zr_{48}Al_4$-1	677	734	974	-	10
$Cu_{48}Zr_{48}Al_4$-2	674	740	981	-	10
$Cu_{46}Zr_{46}Al_8$	672	744	982	-	5
$Cu_{46}Zr_{46}Al_8$	695	749	982	-	10
$Cu_{46}Zr_{46}Al_8$	696	760	982	-	20
$Mg_{65}Cu_{25}Y_{10}$	408	450	-	-	5
$Mg_{65}Cu_{25}Y_{10}$	412	460	-	-	10
$Al_{85}Ni_7Y_8$	-	534	902	938	20
$Pd_{42.5}Ni_{7.5}Cu_{30}P_{20}$	553	620	-	-	2
$Pd_{42.5}Ni_{7.5}Cu_{30}P_{20}$	567	650	792	838	20
$Ti_{36.2}Zr_{30.3}Cu_{8.3}Fe_4Be_{12.2}$	601	651	839	-	20
$Zr_{70}Ni_{16}Cu_6Al_8$	628	687	1132	-	20
$Fe_{20}Zr_{80}$	-	609	-	-	20
$Fe_{25}Zr_{75}$	-	569	-	-	20
$Fe_{30}Zr_{70}$	-	657	-	-	20
$Fe_{33}Zr_{67}$	-	662	-	-	20
$Fe_{40}Zr_{60}$	-	690	-	-	20
$Fe_{90}Zr_{10}$	-	852	-	-	20
$Fe_{90}Zr_{10}$	-	866	-	-	50

All the DSC measurements were performed under flow of N_2. All the ribbons containing Zr react with N_2 after melted, this is manifested as an exothermic event on the temperature profile which is heating rate dependent. As to the $Cu_{46}Zr_{46}Al_8$, the reaction starts from 1200K under heating rate of 10K/min. As to Ti-Zr-Cu-Fe-Be and Zr-Ni-Cu-Al, the corresponding reactions start at 926 and 1356K at a heating rate of 20 K/min. Under these circumstances, the determination of the freezing (liquidus) temperature cannot be performed.

In the case of $Fe_{25}Zr_{75}$, X-ray diffraction results show that it is already crystallized. Here the crystallization temperature detected in the DSC scan may result from normal growth of crystals or a recrystallization processes.

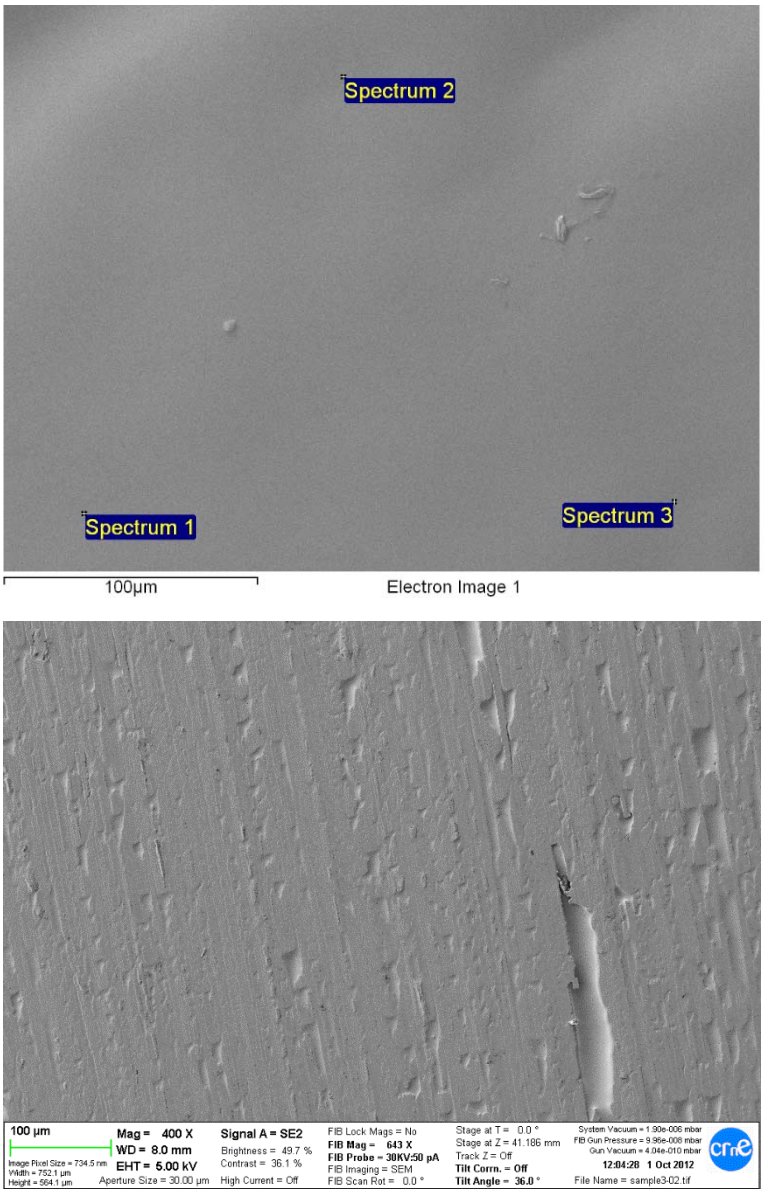

Figure 4-9 SEM of $Cu_{46}Zr_{46}Al_8$ MG.Up: air side of the ribbon. Down: side contacting with the copper wheel.

The morphology of the samples was characterized by a SEM microscope, model Zeiss Neon 40. Typical morphology of MGs ribbons is shown in figure 4-9. On the side contacting with cooper wheel, there are grooves on the surface.

Composition analysis was performed by energy dispersive X-ray spectroscopy (EDS) with the INCAPentaFETx3 detector equipped within the SEM.

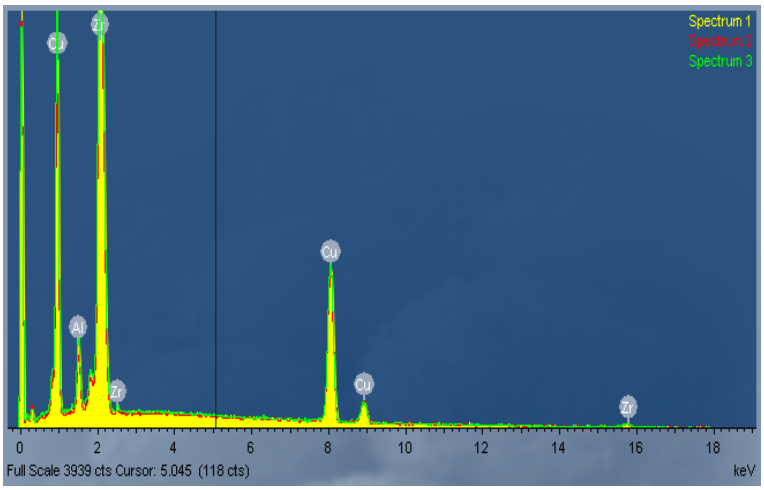

Figure 4-10 EDS of a Cu-Zr-Al MG. Horizontal axis shows X-ray energy and vertical axis number of counts.

Several different points were chosen on each of the samples in order to assess the compositional homogeneity of the samples. A typical EDS result is shown in figure 4-10. Since the X-ray intensities are measured by counting photons the precision obtainable is affected by statistical error. The result obtained for this sample is listed in table 4-3. No differences between different points were observed since the overall analytical accuracy is commonly near 2%.

Table 4-3 EDS analysis of $Cu_{46}Zr_{46}Al_8$ MG.Percentage in atomic%. All element analysis (normalised).

Spectrum	Al	Cu	Zr
Spectrum 1	7.69	42.55	49.76
Spectrum 2	7.69	42.95	49.37
Spectrum 3	7.52	44.17	48.31
Mean	7.6	43.2	49.1
Std. deviation	0.1	0.9	0.8
Max.	7.69	44.17	49.76
Min.	7.52	42.55	48.31

There is a minor difference between the nominal composition and the result obtained by EDS. EDS was performed on the different samples, each sample is scanned on at least three points; the mean results of each sample are

listed in table 4-4. The EDS analyses have been systematically performed in order to assess any possible errors during the production method of the amorphous ribbons.

Table 4-4 composition determined by EDS. All results in atomic%

Norminal composition	Result by EDS
$Cu_{48}Zr_{48}Al_4$-1	$Cu_{44.9}Zr_{51.3}Al_{3.8}$
$Cu_{48}Zr_{48}Al_4$-2	$Cu_{44.7}Zr_{51.3}Al_4$
$Cu_{46}Zr_{46}Al_8$	$Cu_{43.2}Zr_{49.1}Al_{7.6}$
$Cu_{46}Zr_{46}Al_8$	$Cu_{43.6}Zr_{48.9}Al_{7.5}$
$Mg_{65}Cu_{25}Y_{10}$	$Mg_{61}Cu_{25.9}Y_{13.1}$
$Pd_{42.5}Ni_{7.5}Cu_{30}P_{20}$	$Pd_{44.1}Ni_{7.3}Cu_{27.9}P_{20.7}$
$Zr_{70}Ni_{16}Cu_6Al_8$	$Zr_{71.5}Ni_{14.9}Cu_{5.8}Al_{7.8}$

4.3 DMA characterization

Dynamic mechanical analysis in the temperature region between 170 K and 330 K was measured with a SDTA861e DMA designed by METTLER TOLEDO. The low temperature mechanical relaxation of several MGs was explored as illustrated in figure 4-11.

Dynamic mechanical analysis above room temperature and up to the glass transition and crystallization regions was performed on the ribbons with a TA Instruments Q800 DMA in tension mode. In the DMA, the storage modulus and loss modulus were obtained and analyzed. A multi frequency range between 0.1 Hz to 50 Hz was applied to the samples. By choosing appropriate amplitude and preload force, the mechanical spectroscopy is recorded in constant heating mode, the range of heating rates applied varied from 0.5 to 5 K/min. The ribbon shape samples allowed us to explore the difference between ultra-rapidly quenched and relaxed samples, thus surveying the relaxation dynamics in very different glassy states. The use of thin ribbons, however, restricted the range of forces used in the DMA. In order to prevent too much viscous flow in the glass transition region the amplitudes and

preload forces had to be carefully chosen. The range of strain amplitudes and preload forces applied was from 0.5 to 5 μm and from 0.1 to 2 N respectively.

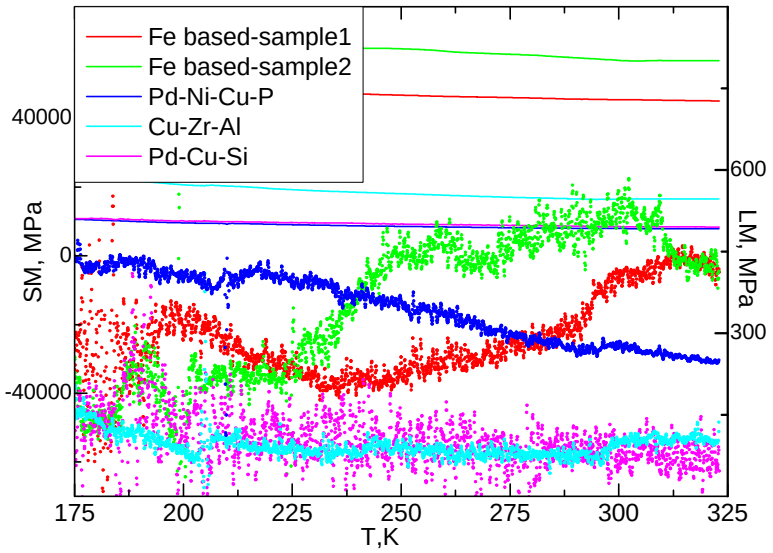

Figure 4-11 DMA measurement at low temperatures. Sample geometry is set as 10.5mm×2mm×30μm. Amplitude is chosen as 5 μm. Frequency employed is 1Hz. No secondary relaxation is were observed in $Pd_{42.5}Ni_{7.5}Cu_{30}P_{20}$, $Cu_{46}Zr_{46}Al_8$, $Pd_{77.5}Si_{16.5}Cu_6$ MGs in the temperature region explored. Secondary relaxation was found in the Fe based MGs, while the peak on E'' (ω) profile varies between different samples.

The quasi stationary tests were also performed by the TA Instruments Q800 DMA. In the case of creep, a stress of 30 MPa is fixed and the corresponding time dependent strain is analyzed. After a certain period, the stress is removed and the strain changes are monitored during the recovery process. In the stress relaxation measurements, a strain of 0.1% is fixed and the stress change with time is analyzed. After a certain time, the strain is removed and the stress recovery is also recorded. The 'instantaneous' stresses applied in this quasi-stationary step tests decay from around 30 MPa. These values of stress and strain fall within the elastic region of metallic glasses. The quasi-static tests were performed under isothermal conditions at different temperatures ranging from room temperature up to the glass transition region.

4.4 Selection of the samples for the mechanical relaxation study

The main objective of this thesis is to investigate the secondary relaxation of metallic glasses. As discussed in chapter 3, the presence of secondary relaxation has been attributed to different origins and shows different appearance on the $E''(\omega)$ profile. The DMA measurements and basic structural and thermal characterizations were performed in all the systems prepared and listed in section 4-1. From all these systems, the MGs with nominal compositions of $Cu_{46}Zr_{46}Al_8$, $Pd_{42.5}Ni_{7.5}Cu_{30}P_{20}$, $Fe_{55}Cr_{10}Mo_{14}C_{15}B_6$ were selected in order to perform the analysis and interpretation of the mechanical relaxation spectrum.

The selection was decided in order to study glasses showing different secondary relaxation behaviors. The three selected systems are representative of a system with secondary relaxation appearing as an excess wing, a system with obvious secondary relaxation but partly overlapped with the glass transition and, finally, a system showing a secondary relaxation of relatively low intensity and very well separated from the glass transition region. The relaxation behavior of these systems is analyzed and discussed in the following chapter.

5. Characterization of relaxation dynamics of metallic glasses

As described in chapter 3, mechanical spectroscopy reveals the presence of β-relaxations in MGs. Actually, some systems show a prominent β-relaxation peak while other systems do not show an evident secondary relaxation but just a low-temperature excess wing of the main relaxation peak.

One of these systems is the family of Cu-Zr-Al alloys, where the relaxation below T_g is perceived as an excess wing of the $E''(\omega,T)$. The origin of this excess wing is still not clear. In section 5.1 of this chapter, the relaxation dynamics of $Cu_{46}Zr_{46}Al_8$ is studied combining mechanical spectroscopy and static stress-relaxation tensile measurements. Preliminary tests on other compositions of the Cu-Zr-Ni-Al system were performed during the project, they all showed similar behaviors. From this set of compositions the $Cu_{46}Zr_{46}Al_8$ was selected for performing the detailed analysis of the relaxation spectrum which is described in section 5.1. The main results have been published in [203].

In section 5.2, the mechanical response of $Pd_{42.5}Ni_{7.5}Cu_{30}P_{20}$ in the temperature region from room temperature to glass transition temperature is explored by quasi-stationary measurement like creep, recovery and stress relaxation as well as by DMA. The DMA behavior is analyzed and related to the static measurement. The viscosity behavior is also explored by elongation experiments. This alloy has been selected as a representative of metallic glasses showing a prominent secondary relaxation. In the Pd-based family of glassy alloys, the secondary relaxation observed by internal friction at the typical frequencies of mechanical spectroscopy (0.01-100 Hz) is observed as a distinctive shoulder, more or less overlapped with the primary relaxation depending on the composition[129].

The relaxation dynamics of a stainless type of amorphous steel $Fe_{55}Cr_{10}Mo_{14}C_{15}B_6$ is explored in section 5.3. The physical aging is explored by enthalpy measurement. Mechanical relaxation is explored by DMA. The viscosity is obtained by treating the material as a Maxwell fluid. Finally, discussion of the characterization results in presented in section 5.4.

5.1 Relaxation dynamics of $Cu_{46}Zr_{46}Al_8$ MG

5.1.1 Thermal analysis

Figure 5-1 shows the DSC curves obtained for $Cu_{46}Zr_{46}Al_8$ as-quenched and relaxed (pre-annealed) ribbons. They show distinct shapes of the glass transition signal, with the expected overshooting in the relaxed glass, while the crystallization at higher temperatures is not affected by the pre-annealing protocol as the memory of the system is lost once heated above the glass transition. The characteristic temperatures of this alloy are listed in table 4-2. The as-quenched ribbons show the exothermal signal of structural relaxation or physical aging due to the release of excess free volume. This release of heat is detected in the DSC curves from above 600 K until the glass transition region.

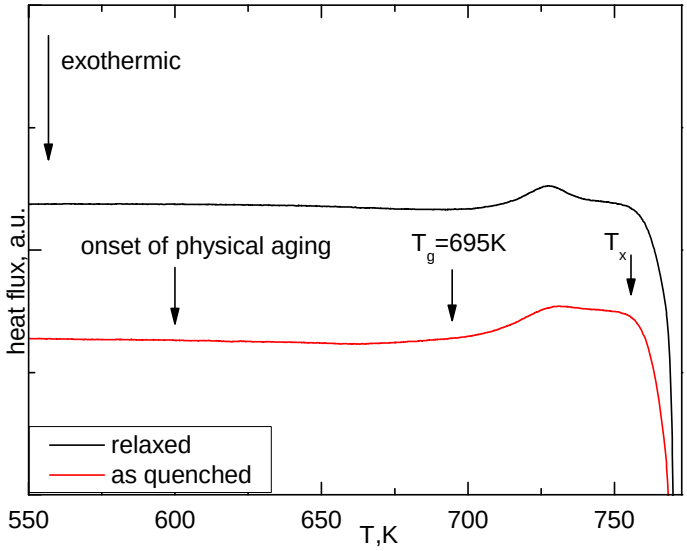

Figure 5-1 DSC scans of the relaxed (black line) and as-quenched (red line) ribbons. The scans were performed at 10 K/min.

5.1.2 Dynamic mechanical analysis

The tensile DMA measurements were performed on melt spun ribbons applying a heating rate of 1 K/min and frequencies between 0.1 and 50 Hz. The frequency response was obtained by applying oscillating tensile strains of 1 μm amplitude on pieces of ribbon of about 10 mm length.

The difference between as quenched state and relaxed state is explored. The relaxed state is obtained by performing a DMA measurement isothermally for 30 minutes at 693K and a posterior cooling down inside the DMA furnace. The onset of glass transition is found at T_g = 695 K (figure 5-1). Therefore, the annealing protocol is expected to drive the system to a sufficient relaxed state as to avoid significant structural changes below ~690 K while heating at 1 K/min. This ensures the mechanical response $E^*(\omega,T)$ corresponds to an isoconfigurational glassy state.

Figure 5-2 shows the imaginary part of $E^*(T)$ of the as quenched and relaxed state, showing the reduction of the excess wing by annealing. As commonly found in metallic glasses and widely discussed in chapter 3, physical aging drives the system towards more stable and compact structures thus reducing the internal friction. The $E''(T)$ behavior of the as-quenched samples is expected to show the in situ effects of aging when increasing temperature. On the other hand, the internal friction of the relaxed sample is expected to characterize the relaxation spectrum of a unique glassy state.

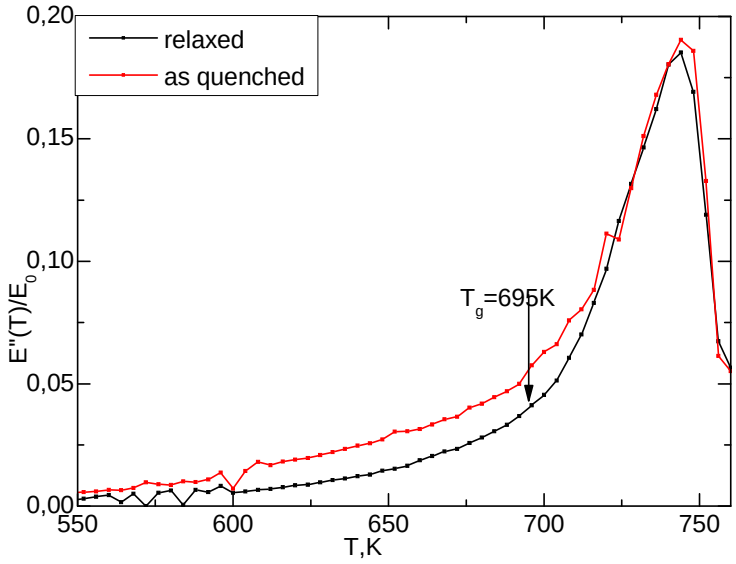

Figure 5-2. Internal loss peak measured at 1 Hz and 1 K/min. Comparison between relaxed (black symbols) and as-quenched (red symbols) ribbons.

$E''(\omega,T)$ of the relaxed ribbons as a function of temperature for different frequencies is shown in Figure 5-3. The expected drift to higher temperature

increasing frequency is clearly observed. At the lowest probed frequencies, the complete α-relaxation peak can be measured. Applying higher frequencies the dynamic frequency-dependent glass transition moves closer to the crystallization temperature. At the highest frequencies, the onset of crystallization inhibits a complete measurement of the primary relaxation peak.

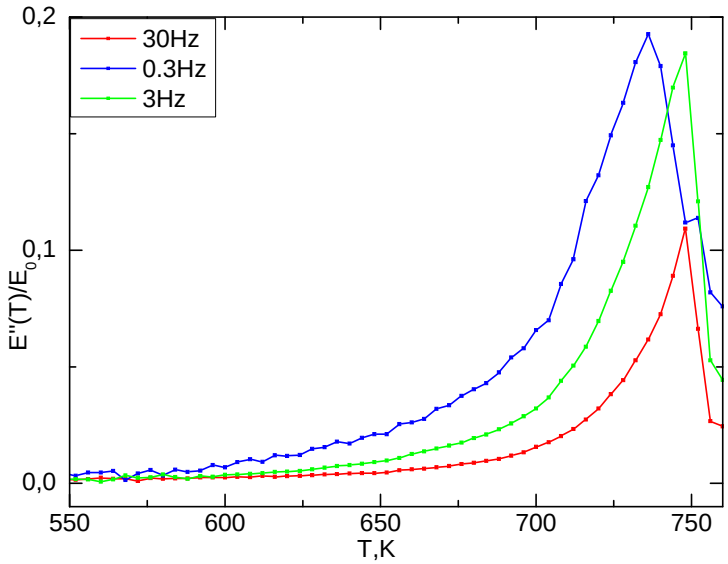

Figure 5-3 Internal loss (normalized loss modulus) of the relaxed samples as function of temperature measured at 0.3, 3 and 30 Hz with heating rate of 1 K/min.

Loss modulus data under different frequencies were taken at temperature steps of 4 K from 500 K up to 750 K. The data sets obtained at each temperature were fitted to the CC-function (equation 3.18 with asymmetric parameter γ=1). The value of $E_0(T)$ in equation 3.18 is taken constant and equal to $E_0=E'(T=500\text{K})$ when the loss modulus contribution is practically zero. The infinite frequency elastic response is therefore considered constant during the whole temperature range. Due to thermal expansion $E_0(T)$ is expected to show a slight monotonous decrease. Fixing a constant value may induce a slight error in the fitting but reduces the fitting parameters to just only the broadening parameter $\alpha(T)$ and the average relaxation time $\tau(T)$.

The fitting CC-functions and the experimental data at some selected temperatures are shown in figure 5-4 for the relaxed samples. The calculated

values of α(*T*) show some dispersion around an average value α=0.35 ± 0.06 with no clear tendency to increase or decrease with temperature. As shown in the figure, the CC-function with constant broadening parameter is able to reproduce the high frequency tails of the *E''*(ω,*T*).

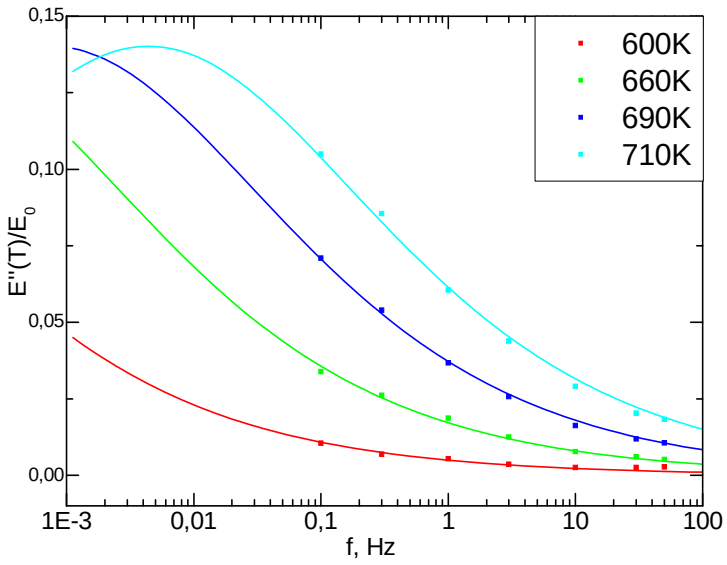

Figure 5-4 Internal loss as function of frequency at different temperatures (symbols) and the corresponding fitted CC-functions (solid lines).

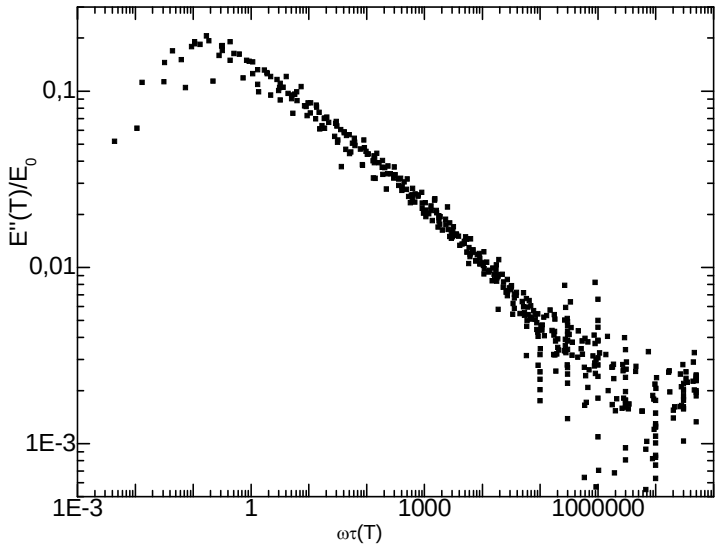

Figure 5-5 Internal loss of the relaxed ribbons as a function of ωτ(T).

In order to assess the validity of the fitting, the loss modulus values collected for all frequencies and temperatures are depicted in figure 5-5 as function of $\omega\tau(T)$. Inspection of equation 3.18 shows that if the values of the α and γ exponents do not change with T a master curve can be obtained as function of $\omega\tau(T)$. This means applying the TTS principle as already discussed in chapter 3. Within the frequency and temperature window explored, the data is well described by a single peak with no observable change in the slope of the high-frequency wing, which would be indicative of a change in the broadening parameter or of a merged secondary process.

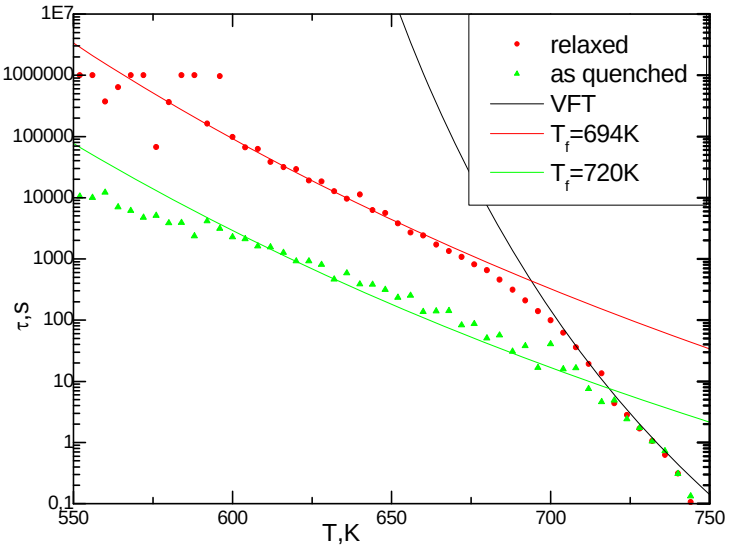

Figure 5-6 Relaxation times calculated by DMA (symbols). Lines correspond to the VFT and AGV functions describing the τ(T) behavior of the relaxed samples. Red and green lines correspond to AGV functions with $T_{fictive}$ = 694 and 718K respectively.

The τ(T) values obtained by fitting a CC function to the experimental data are depicted in figure 5-6. For the case of the relaxed samples, the glass transition, defined as $\tau(T_g)$ =100s, is found at T_g =692K. The change from equilibrium to non-equilibrium dynamics is also clearly seen, the solid lines correspond to VFT and AGV functions (equation 3-1 and 3-3 respectively) with parameters $\tau_0=6\times10^{-13}$s, $D^*T_0=B$ =6220, T_0=512 K and $T_{fictive}$ = 694K. The fragility parameter, calculated from the slope of the equilibrium curve at T_g, is found to be m=57. The glass transition temperature and the fragility

correspond well with the result obtained from enthalpy measurements reported in ref. [204].

As seen in figure 5-5, at temperatures well below T_g the DMA data covers only a small part of the high frequency tail of the relaxation peak. Thus, an equally good description of data could be obtained with another relaxation function or a combination of two merged peaks as described in chapter 3, where the loss modulus is fit with an HN function or the combination of an HN function and the Fourier transform of a stretched exponential KWW function. Since the extra parameter γ in the HN function influences basically on the low frequency side of the peak (or correspondingly the high temperature side), our fitting with CC function is enough to describe the frequency dependent loss modulus profile obtained experimentally. The use of an HN function would imply a third fitting parameter, thus reducing the robustness of the method.

For the case of the as-quenched glass, the DMA measurements in the non-equilibrium region (T<700K) do not correspond to a single isoconfigurational state. As the temperature rises the sample undergoes structural changes. In DMA measurements with tensile geometry this changes are readily observed by the increase of the storage modulus $E'(T)$ due to structural relaxation. This implies that in equation 3.18 the value of $E_0(T)$ does not only change because of the slight thermal expansion of the glass structure but also because of the structural differences between different glassy states.

In order to model the relaxation response of the as-quenched samples by a CC function taking into account the structural changes, we define two temperature regions:T<675K and$T$>700K. In the first region, we fix $E_0=E'_{aq}(T=500\text{K})$, i.e. the storage modulus measured in the as-quenched samples before structural changes are detected. In the second region, T>700K, we fix $E_0=E'(T=500\text{K})$ measured for the relaxed glass, which is 15% higher than $E'_{aq}(T=500\text{K})$. The region between 675 and 700K, where the system shows the more intense structural changes, is not fitted.

The $\tau(T)$ values obtained for the as-quenched ribbons using this method are shown in figure 5-6. The as-quenched glass coincides with the relaxed samples in the equilibrium region, while below T_g the relaxation times are

more than one order of magnitude shorter. The broadening parameter of equation 3.18 is found to be α=0.39±0.06. The as-quenched $\tau(T)$ points do not follow an AGV function with a constant $T_{fictive}$ because of the *in-situ* structural changes taking place when heating at 1 K/min. Indeed, the relaxation times of the as-quenched samples can be interpreted as crossing isoconfigurational lines with decreasing $T_{fictive}$ as shown in figure 5-6.

5.1.3 Stress relaxation analysis

In order to validate the measured $\tau(T)$, static stress-relaxation measurements were performed applying 'instantaneous' tensile deformations of amplitude $\varepsilon \sim 10^{-3}$, corresponding to an initial elastic stress of $\sigma_0 \sim$50–60 MPa, and then measuring the stress decay during 1 h. A typical protocol and result is illustrated in figure 5-7.

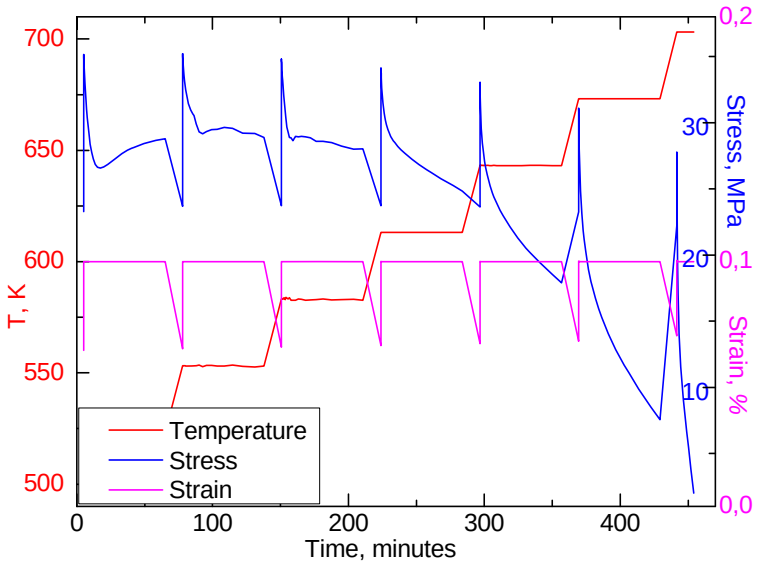

Figure 5-7 Stress relaxation of relaxed Cu-Zr-Al MG in static deformation measurements. Strain 0.1%. Preload force:0.2N.

The comparison of stress relaxation between as-quenched and annealed sample at the same temperature is illustrated in figure 5-8. The time-evolving stress can be well modeled by a stretched exponential (equation 3.10) where β_{KWW} is the Kohlrausch–Williams–Watts exponent. As discussed in chapter 3, when transformed to the frequency domain, equation 3.10 corresponds to a

relaxation peak with a high frequency tail following a power law similar to that given by a CC-function (equation 3.18) with $\alpha \approx \beta_{KWW}$.

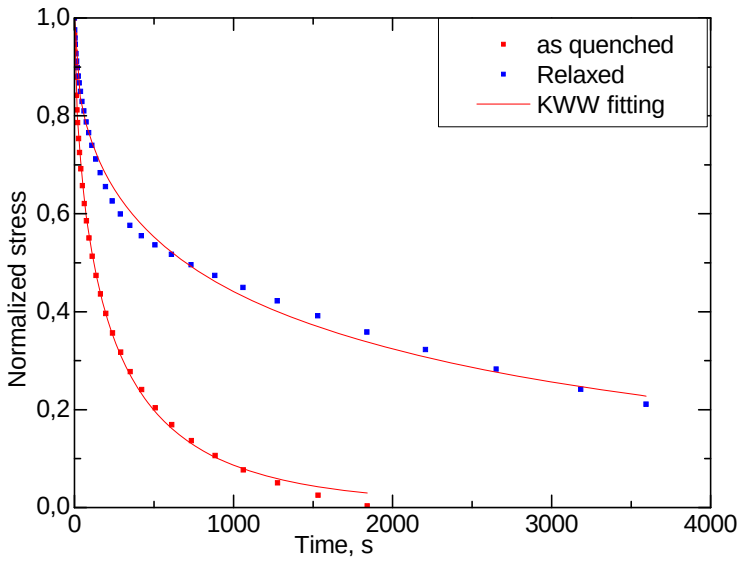

Figure 5-8 Relaxation of stress as function of time in static deformation measurements. Measured stress at 673 K for relaxed (black diamonds) and as-quenched (red diamonds) ribbons. Solid lines correspond to the fitted stretched exponential decays.

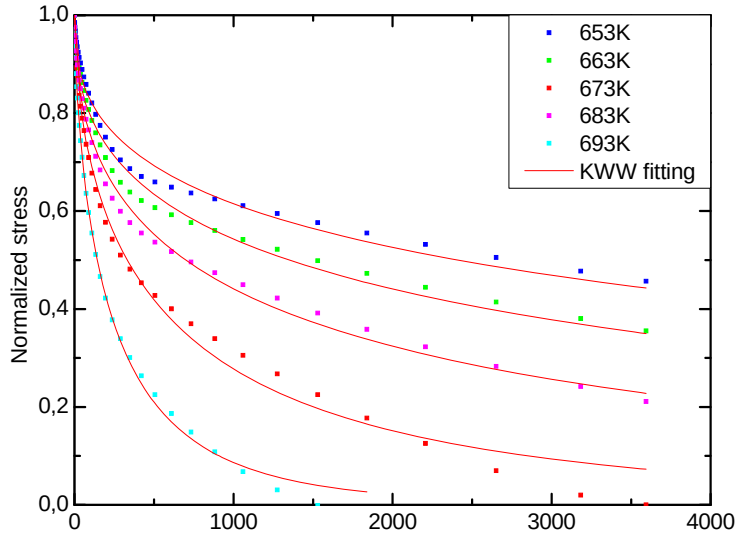

Figure 5-9 Relaxation of stress as function of time in static deformation measurements. Stress relaxation of the relaxed ribbons measured at 653, 663, 673, 683 and 693 K.

Table 5-1 Parameters of KWW functions fitted to stress relaxation data of as quenched Cu-Zr-Al MG.

T (K)	β_{KWW}	τ (s)
523	0,309	12100
553	0,433	7065
583	0,451	3789
613	0,481	1494
643	0,535	618
673	0,598	224

Table 5-2 Parameters of KWW function fit with stress relaxation measurement of relaxed Cu-Zr-Al MG.

T (K)	β_{KWW}	τ (s)
633	0,423	7294
643	0,367	9788
653	0,404	5967
663	0,424	3204
673	0,463	1544
683	0,559	641
693	0,648	252
583	0,295	555720
613	0,361	120111
643	0,401	18415
673	0,44675	3198
703	0,54	308

The values of α and β_{KWW} exponents did not show significant changes between as-quenched and relaxed samples and, contrary to what was observed in $Mg_{65}Cu_{25}Y_{10}$alloy[162], the as-quenched samples do not show a significant change of the α parameter during the transition from non-equilibrium to equilibrium dynamics. The stress relaxation measurements of the relaxed $Cu_{46}Zr_{46}Al_8$ MG at different temperatures are illustrated in figure 5-9. The experimental result is fit with KWW function. The fitting parameters of the as quenched and relaxed state are list in table 5-1 and 5-2 respectively.

The fitted temperature dependent relaxation distribution parameter $\beta_{KWW}(T)$ is illustrated in figure 5-10. The values of the stretching exponent show a tendency to increase with temperature, the average value is found

β_{KWW}=0.5±0.1. It is similar to the values found in other MGs[205] and it is slightly higher than the α parameter obtained for the CC-function.

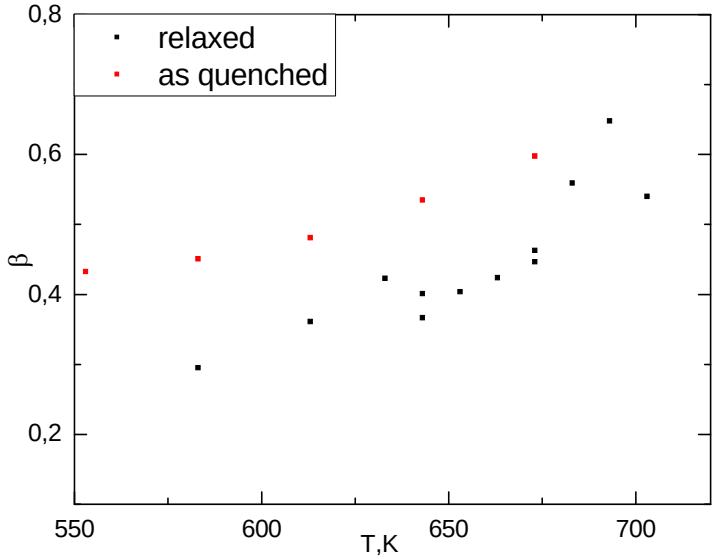

Figure 5-10 Temperature dependend KWW parameter β_{KWW} for Cu-Zr-Al MG.

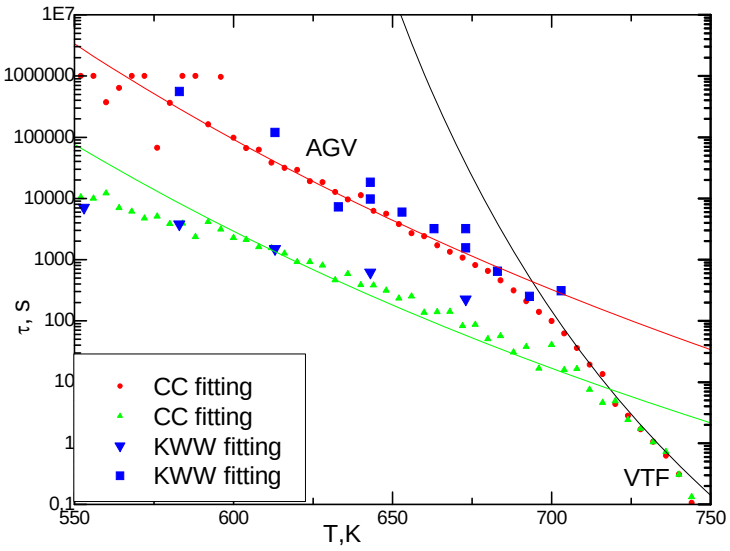

Figure 5-11 Relaxation times calculated by DMA and static stress-relaxation measurements. DMA results are fit with Cole-Cole function while stress relaxation results are fit with KWW function. Relaxed samples are compared with as-quenched ribbons. Black line correspond to the VFT functions describing the τ(T) behavior of the samples. Red line correspond to AVG function with $T_{fictive}$=694K. Green line correspond to AGV functions with $T_{fictive}$ = 718 K.

The fitted temperature dependent relaxation time is illustrated in figure 5-11. The data of $\tau(T)$ obtained fitting the DMA result with Cole-Cole function are also shown in the same figure. The values of $\tau(T)$ obtained from the static measurements are in good agreement with those obtained by DMA. The coincidence of the two methods indicates that between 500K and 675K a CC-function with an approximately constant E_0 and $\alpha=0.39\pm0.06$ is a good description of the frequency domain response of the as-quenched samples, at least within the temperature-frequency window probed.

5.2 Relaxation dynamics of $Pd_{42.5}Ni_{7.5}Cu_{30}P_{20}$ MG

5.2.1 Thermal analysis

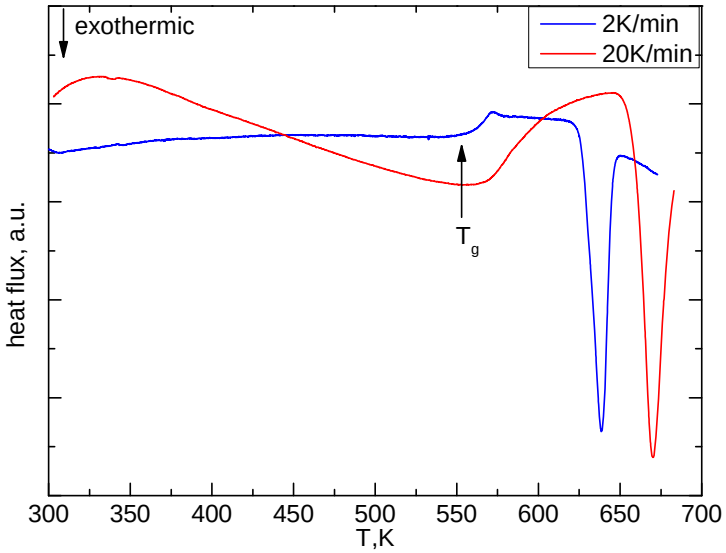

Figure 5-12 DSC of $Pd_{42.5}Ni_{7.5}Cu_{30}P_{20}$ with heating rate of 20 K/min (red) and 2 K/min (blue)

DSC scans on $Pd_{42.5}Ni_{7.5}Cu_{30}P_{20}$ samples were performed at different heating rates, as it is shown in figure 5-12. The onset of the glass transition, as well as crystallization, is heating rate dependent in metallic glasses. With a heating rate of 2K/min, the T_g determined is 553 K and crystallization starts at 620 K. Applying a heating rate of 20 K/min, T_g is detected at 567 K and crystallization at 650 K as detailed in table 4-2. As expected in a Pd-Ni-Cu-P alloy, the thermal stability of the supercooled liquid phase above the glass transition is very high. The temperature span between glass transition and crystallization is T_x-T_g>60 K even for the tests performed with the slowest heating rates. This stability allows us to explore the properties of the liquid phase close to the glass transition even by using long tests.

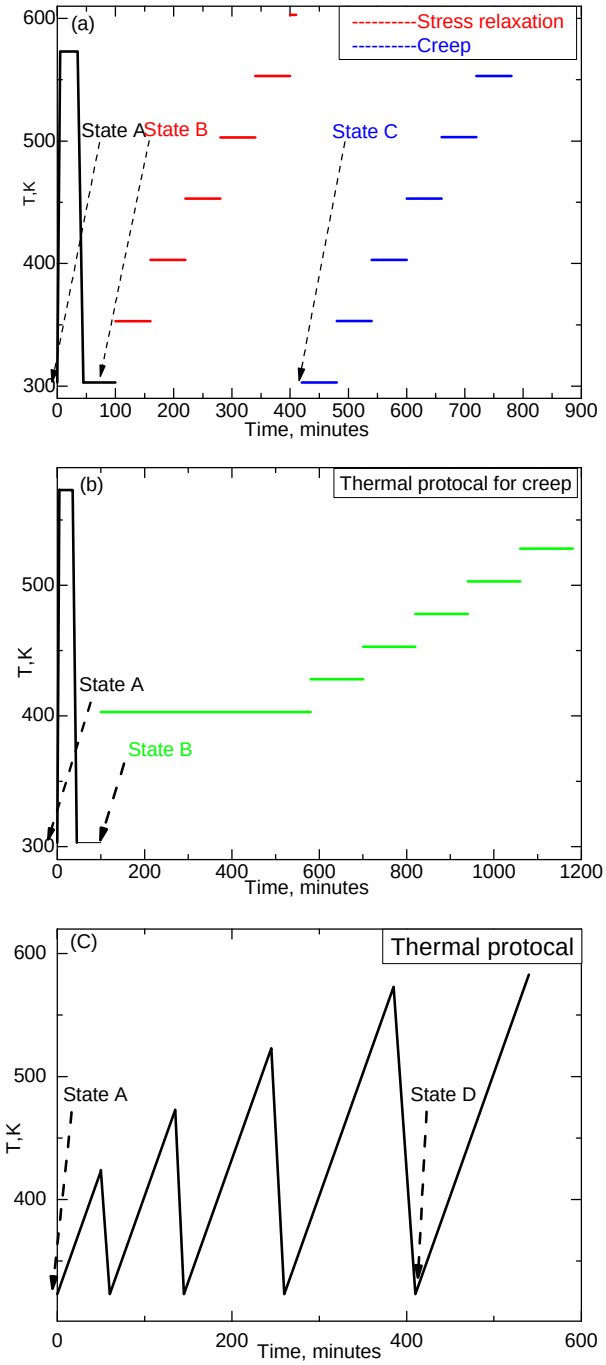

Figure 5-13 Thermal protocol employed in this section. (a): Protocol used for stress relaxation and creep measurements. At each isothermal temperature 30 minutes of stress relaxation or creep measurement is performed and followed by a recovery process of 30 minutes. (b): Creep measurements, when isothermal at 403 K a creep of 240 minutes is performed and followed by a 240 minutes recovery. At higher isothermal temperatures both creep and recovery times are 120 minutes. (c): Continuous heating ramps with a heating rate of 2 K/min followed by furnace free-cooling conditions.

Figures 5-13 a) and b) show the thermal protocols applied during the mechanical tests. The isothermal stress-relaxation and creep tests are performed after a relaxation step above glass transition region. This relaxation step is performed in order to release the excess free volume and internal stresses quenched-in during the rapid solidification production of the ribbons. The high stability against crystallization of the $Pd_{42.5}Ni_{7.5}Cu_{30}P_{20}$ glass and supercooled melt allows us to perform long tests of several hours even at temperatures within the glass transition region. The details of the protocol are detailed in the caption of the figure.

The viscosity and mechanical properties of glasses are state dependent and influenced by physical aging. Different structural states are obtained based on thermal history. In this section, several samples in different glassy states will be investigated. The different states will be termed as states A, B, C and D: State A is the as quenched sample; State B is the sample relaxed at 573 K for 30 minutes; State C is the sample after a series of stress relaxation measurements at different temperatures following the protocol shown in the figures above; State D is the sample employing a thermal protocol composed of a series of heating ramps as illustrated in figure 5-13.

5.2.2 Mechanical response of MG under fixed stress

Under loading, the alloy shows a deformation behavior different from the ideal elastic behavior. As explained in chapter 3, these quasi-static experiments in disordered systems may show exponential or non-exponential relaxations, which are quite often explained in the framework of viscoelasticity with a distribution of relaxation times. According to whether the recovery is complete or not, the behavior can be classified as anelasticity or viscoplasticity. Actually, if the relaxation time is long enough and cannot be determined within the experimental window, the viscoplastic part may be viewed as part of the anelastic response. The anelastic part can be modeled in different ways as performed by Ulfert[206].

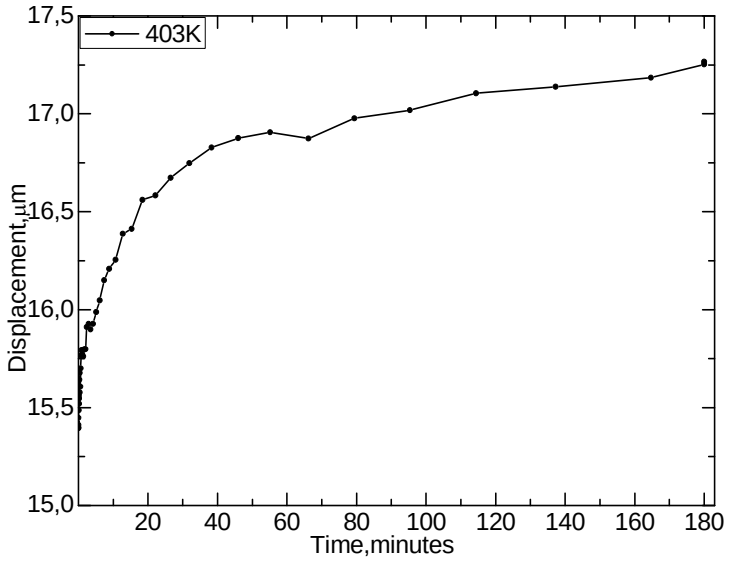

Figure 5-14 Mechanical response of $Pd_{42.5}Ni_{7.5}Cu_{30}P_{20}$ at 403K. Stress employed is 30.MPa.The relaxation dynamics can be described by equation 5.1.

Creep and recovery measurement is performed to investigate the mechanical response of $Pd_{42.5}Ni_{7.5}Cu_{30}P_{20}$ MG. Sample at state B is measured at 403 K, the creep behavior is shown in figure 5-14. The creep reaches a steady state after approximately 30 minutes at 403 K. During the rest of the 3 hours of creep test, strain increases linearly with time indicating a steady state viscous flow. Similar steady state flow is found at 428 K and 453 K within 120 minutes tests. The total displacement during the creep tests can be expressed in the form of:

$$\varepsilon = \varepsilon_0 + A\left(1 - e^{-t/\tau}\right) + kt \tag{5.1}$$

where τ is the relaxation time of the anelastic part and k is related to the viscous flow which is temperature dependent.

Creep and recovery measurements were performed to samples in state C under different temperatures as shown in figure 5-15 and 5-16 where the latter is in log-time scale.

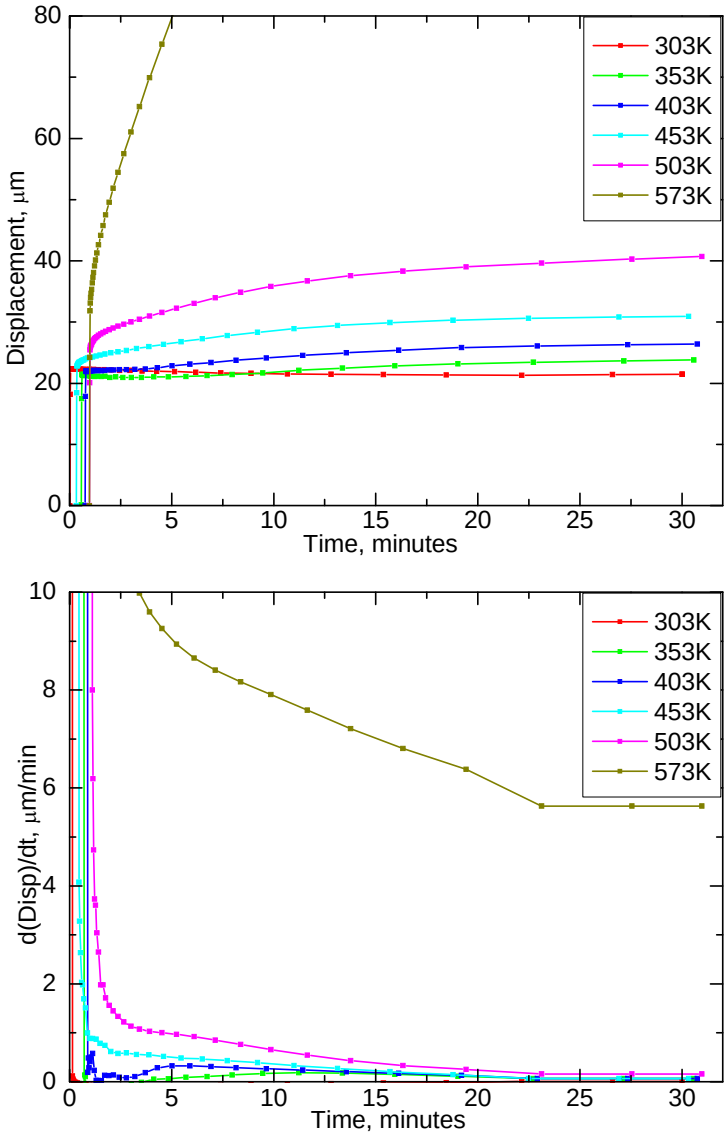

Figure 5-15 Temperature dependent mechanical response of $Pd_{42.5}Ni_{7.5}Cu_{30}P_{20}$. Measurement is performed under fixed stress of 30 MPa. Top:Total displacements. Down: Calculated displacement rates

As can be seen from figure 5-15, above T_g the strain rate is very high an almost reaches a steady state after few minutes. On the other hand, compared with the anelastic part, the viscoplastic part (i.e. the continuous increase of strain) is small at temperatures below 500 K. The mechanical response could be viewed as basically anelastic under these conditions.

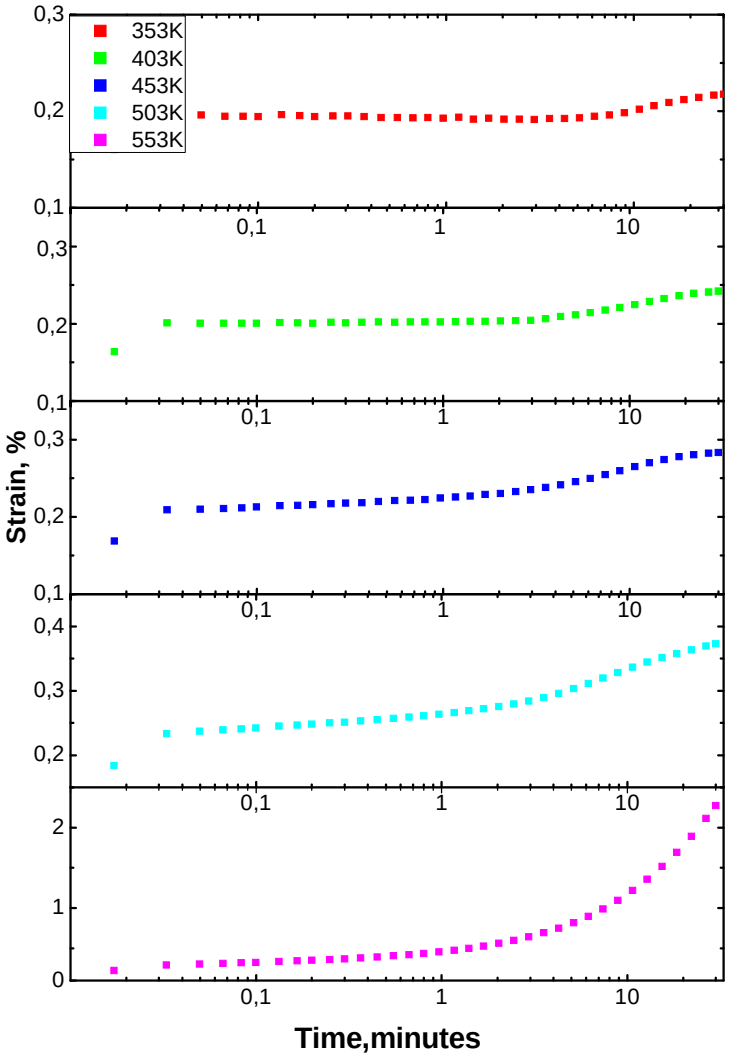

Figure 5-16 Mechanical response of $Pd_{42.5}Ni_{7.5}Cu_{30}P_{20}$ at different temperatures. Below 503 K the mechanical response can be approximated as anelastic behavior with a single relaxation time. At 553 K, the viscoplastic part is important and need to be considered.

5.2.2.1 Anelastic response

The deformation rates are calculated and illustrated in figure 5-15. At 303 K no obvious flow is detected; the viscosity is too high to be determined under the applied stress. On a short time scale of about 20 minutes, the time dependent displacement (or equivalently the strain) can be well fitted with and

exponential growth function with a single relaxation time. This behavior suggests that it may be regarded as anelastic deformation at these temperatures. The anelastic relaxation response, described by the exponential function of equation 5-2, was fitted to the creep data obtained isothermically at different temperatures. The fitted parameters employing a single relaxation time functions are listed in table 5-1. Increasing temperature, the intensity of the anelastic events gets increased while the relaxation time decreases.

At 553 K, besides the anelastic part, the contribution of viscous flow is obvious. No fitting is performed at such high temperature since the anelastic model is no longer valid.

Table 5-3 fitted parameters of anelastic behavior

T (K)	ε_0	A	τ (minutes)
353	0.186	0.049	27
403	0.199	0.057	20
453	0.216	0.071	9
503	0.245	0.128	8

5.2.2.2 Viscous flow

Although through small displacements, the creep measurements show that the strain of the samples is still increasing after 20 minutes at 353 K, 403 K and 453 K, when the anelastic behavior is finished. This implies the behavior is not purely anelastic but has a viscous flow contribution. The viscous flow at temperatures far below T_g is ascribed to activation of flow units[205]. Actually, at lower temperatures, the viscous flow can be seen more clearly at longer. After the anelastic response finishes, the displacement increases linearly with time and, therefore, the deformation rate reaches a steady value. The deformation rate is close to each other at 353, 403 and 453 K. At 503 and 553K, after 23 minutes, the system also reaches a steady state flow, in these cases with a much higher deformation rate.

In the framework of a Newtonian fluid, viscosity is defined as the ratio of stress to strain rate

$$\eta = \frac{\sigma}{\dot{\varepsilon}} \tag{5.2}$$

where σ is the applied stress and $\dot{\varepsilon}$ is the deformation rate. The viscosity is a tensorial quantity that can be decomposed in different ways into two independent components. One commonly employed way is to decompose it into shear and volume viscosities.

In the case of measurement through elongation, shear viscosity is obtained through

$$\eta_s = \frac{\sigma}{3\dot{\varepsilon}} \tag{5.3}$$

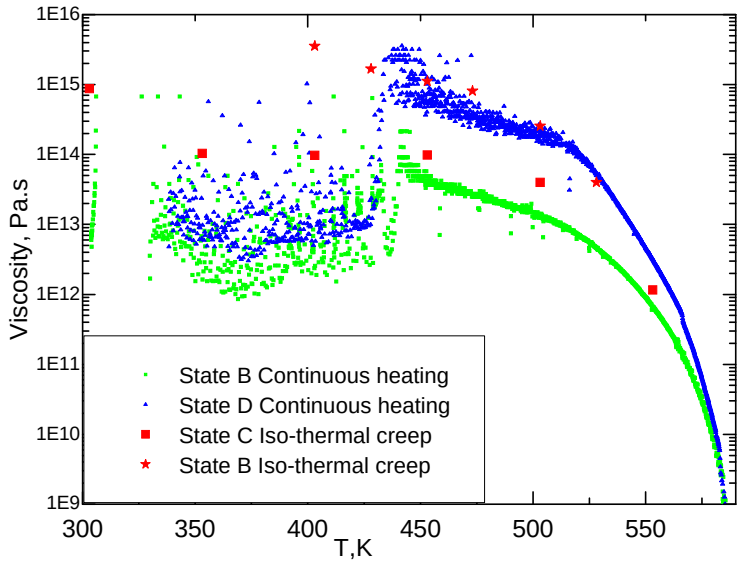

Figure 5-17 Viscosity obtained by continuous heating with heaing rate of 2K/min, a constant preload force of 0.8N (green and blue point) and isothermal steady creep (red points). Different states are employed. Red star: state B, red square: state C, green: state B, blue: state D. In the temperature region below 440K, the viscosity obtained by continuous heating is not valid.

As investigated by Chen and Goldstein[207], when the stress is in the range between 0.6 and 30 MPa, the viscosity obtained from equation 5.3 is valid. The flow is still Newtonian viscous under a shear stress of 82 MPa[60], while at higher shear stresses of 300 MPa it enters the non-linear region[208]. In this thesis, creep is measured employing a stress of 30 MPa at different temperatures and we will assume this assures the validity of equation 5.3. The

viscosity obtained by steady state viscous flow using equation 5.3 is shown in figure 5-17.

According to equation 5.3, the viscosity can be determined through stress and strain rate. The apparent viscosity can also be calculated using stress and apparent displacement obtained during the DMA measurements with a continuous heating procedure and constant preload force. The results, together with the data obtained from the steady state creep measurements explained above, are illustrated in figure 5-17. In both cases, different glassy states are achieved by different thermal history and they become apparent on the $\eta(T)$ behavior.

The viscosity obtained from continuous heating measurements show minor differences compared with isothermal creep measurements. This is due to the fact that the cross-section area of the ribbons is not regular and, the true stress might be slightly different from one sample to another. However, the $\eta(T)$ of the same state from isothermal and continuous heating coincides when an appropriate factor is employed. Besides, according to Berlev and Csach's work on $Zr_{52.5}Ti_5Cu_{17.9}Ni_{14.6}Al_{10}$ and $Pd_{40}Cu_{30}Ni_{10}P_{20}$ glasses[209,210], who compared the effect of different states resulting from different cooling rates during glass formation, the heating rate during creep measurement plays also an important role on the viscosity behavior.

From the $\eta(T)$ relationship, the T_g determined by a viscosity equal to 10^{12} Pa·s is around 555 K, which agrees with the DSC measurements. Near the glass transition, temperature changes of tenths of degrees of magnitude imply changes of 3 or 4 orders of magnitude in viscosity. In order to describe this temperature dependent viscosity behavior, many different models have been proposed; some of them just fit empirical models to the experimental data while others are derived from more physical interpretations. However, these models can only fit partially the experimental data.

As mentioned before, the VFT model is quite generally employed to describe the temperature dependence of equilibrium viscosity, this is above T_g. In the lower temperature region, viscosity deviates from the VFT behavior. It can be viewed as if the system changes from equilibrium to the non-equilibrium glassy state where the configuration is non-ergodic. At

temperatures far below T_g the $\eta(T)$ relationship can be described by an Arrhenius temperature dependence. As to the samples in state B, within the temperature region between 450 and 500K, the apparent activation energy considering an Arrhenius behavior is found to be 41 kJ/mol while the sample with state D shows an activation energy of 50.7 kJ/mol. This is close to the reported result in the $Pd_{80}Si_{20}$ MG (50 kJ/mol).

One thing should be noted, at temperatures lower than 440 K, the viscosity is very high and the deformation is too slow to be detected in this dynamic heating mode. The displacement is comparable to the experimental noise and the obtained viscosity is not valid.

5.2.3 Recovery behavior

Annealing is a usual route employed in materials engineering to relief the internal stresses and to modify the mechanical properties. Experimental results show that, in glasses quenched without time enough for recovery, there are residual stresses congealed in the system. This remaining residual stresses may even lead to anisotropy of the elastic and mechancial properties[69,211]. Here the recovery behavior of $Pd_{42.5}Ni_{7.5}Cu_{30}P_{20}$ is explored.

The sample in state B is creeped at 403 K applying 30 MPa for 4 hours, after this the recovery is monitored for another 4 hours. The recovery behavior at 403 K is plot in figure 5-18. As seen in the figure, the recovery seems to be close to saturation after 4 hours on normal time scale, but when examined on the logarithmic time scale, it is shown that a slow recovery process is still in progress. The recovery can be fitted with a KWW relaxation function as often employed. Using the KWW function, the relaxation time obtained is around 260 minutes but, as manifested by the low β_{KWW} value of 0.23, the process seems to involve a quite wide relaxation times distribution.

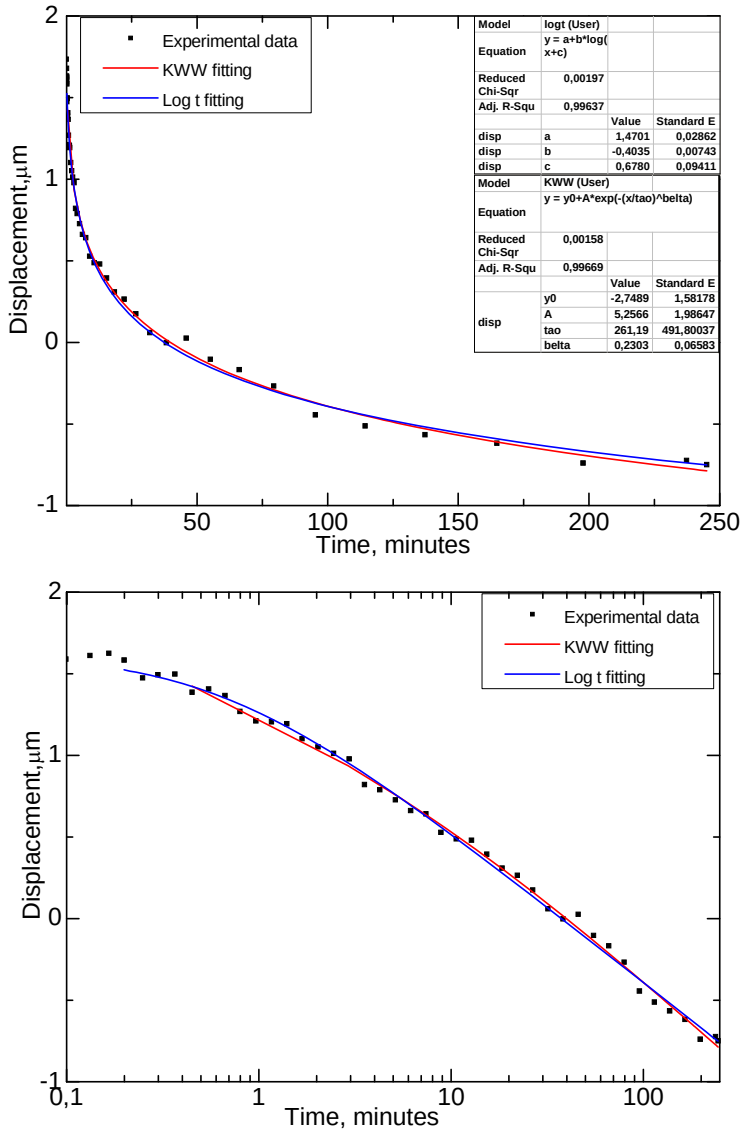

Figure 5-18 Recovery of $Pd_{42.5}Ni_{7.5}Cu_{30}P_{20}$ at 403K on normal (up) and log time scale (down). The fitting is performed using KWW function as well as log *t* function. It is found that both functions can fit the recovery behavior within the experimental window.

Recovery was performed isothermally at different temperatures after each creep measurement. An example of a sample subjected to a procedure of 30 minutes creep and a subsequent recovery time is illustrated in figure 5-19.

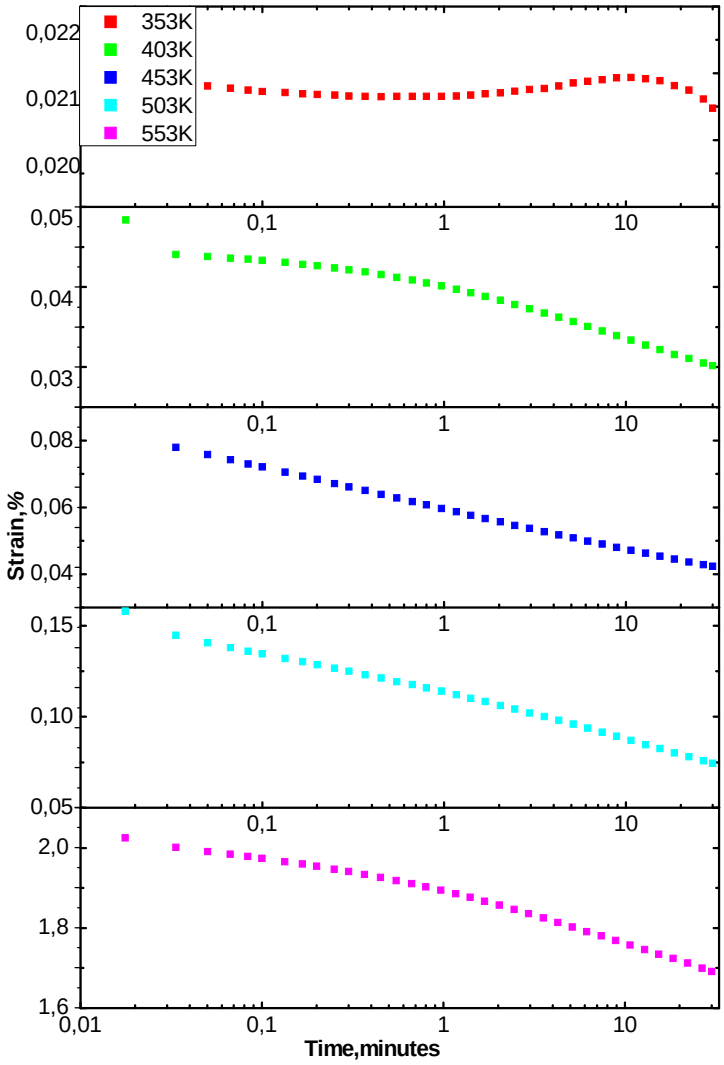

Figure 5-19 Recovery of $Pd_{42.5}Ni_{7.5}Cu_{30}P_{20}$. The sample was in state C with thermal protocol as defined in figure 5-13(a).

If we consider that the recovery is not finished within this time scale, it can be fitted with a three parameters equation:

$$\varepsilon(t) = a - b\log(t + c) \tag{5.4}$$

The parameters fitted with this log(t) behavior are listed in table 5-4. The fitting using equation 5.4 is better than the KWW in this time region. In the case of KWW function, it is a two parameter function when the final state is

determined. In the current situation where final state is not possible to determine in such short range time scale, the KWW function does not allow a robust fitting anymore. Compared with KWW function, the log (t) function has three parameters; this allows a much better fitting. As Gibbs pointed out[212], the log time relaxation kinetics is not anything fundamental, but it is due to the limited range of time and temperature chosen for the experiment.

Table 5-4 Parameters of equation 5.4 fitted in recovery experiments of $Pd_{42.5}Ni_{7.5}Cu_{30}P_{20}$

T (K)	a	b	c
403	0.041	0.003	0.407
453	0.060	0.005	-0.005
503	0.114	0.011	0.042
553	1.905	0.062	0.226

As shown in figure 5-17, the recovery is not finished even after 200 minutes. Although without a solid physical interpretation, equation 5.4 can characterize the relaxation dynamics quite well. This recovery behavior has implications for deformation of MGs under high temperatures. If not enough time is given to the system to recover before quenching to a lower temperature, the deformation might remain in the system leading to internal stresses. This log(t) fitting model seems to be a good approximated tool to estimate the remaining strain to be recovered using experimental feasible time windows of 30 minutes.

5.2.4 Stress relaxation of $Pd_{42.5}Ni_{7.5}Cu_{30}P_{20}$

While creep tests are performed under a fixed stress, stress relaxation tests are also quite often used in determining the relaxation behavior of glasses. They are performed setting a fixed strain while monitoring how stress evolves with time. The stress relaxation probes presented here were performed applying an ‘instantaneous’ strain of 0.1%. Compared with the creep measurements applying fixed stress of 30 MPa, here the stress also starts at about 30 MPa but it decreases continuously with time. Similarly to the creep experiments, the stress relaxation measurements were performed isothermally at different temperatures.

In order to get more information under more temperature conditions, stress relaxation and recovery measurements of state B were performed on different samples. A stress relaxation time of 30 minutes and a following recovery of 30 minutes were performed. Each stress relaxation and recovery was performed at a certain temperature and higher temperatures are performed using the same sample. The characteristic result is shown on figure 5-20.

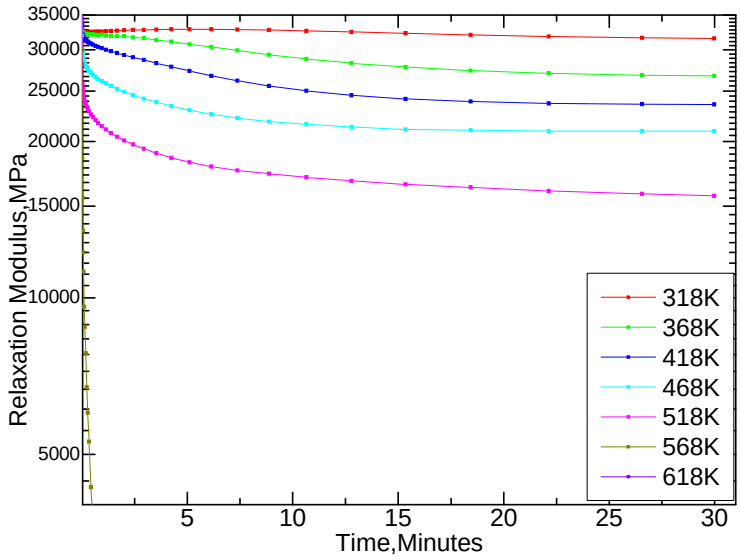

Figure 5-20 Stress relaxation of $Pd_{42.5}Ni_{7.5}Cu_{30}P_{20}$ in state B under isothermal conditions. Constant strain employed:0.1%.

5.2.4.1 Stress relaxation described by KWW function

The stress relaxation is often parameterized with a KWW function. Stress relaxation experiments were performed on different samples, the parameters obtained assuming a KWW-function are listed in table 5-5.

Table 5-5 KWW parameters for stress relaxation experiment.

Sample	T (K)	T (s)	β_{KWW}	ΔE (MPa)
1	368	720	1,5	5500
1	418	360	0,85	8700
1	468	240	0,5	10000
1	518	120	0,45	11000
1	568	4,2	0,55	22000
2	393	540	1,3	9500
2	443	420	0,65	13500
2	493	180	0,5	12000
3	423	168	0,6	11000
3	453	300	0,85	9000
3	483	192	0,5	11000
3	513	120	0,5	9000
4	543	240	0,55	14000
4	553	240	0,34	24000
4	563	48	0,4	22000
5	418	360	0,75	10000
5	468	150	0,5	11000
5	518	120	0,4	12000

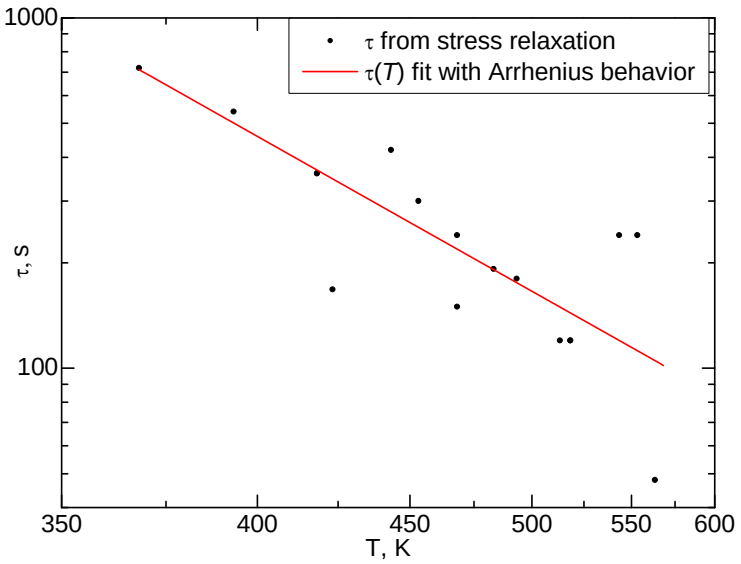

Figure 5-21 Typical relaxation time of $Pd_{42.5}Ni_{7.5}Cu_{30}P_{20}$ from stress relaxation measurements. Relaxation time τ calculated by fitting with KWW functions. Red line is the Arrhenius fitting of the τ(T) behavior.

The KWW function has three parameters: average relaxation time τ, stretching exponent β_{KWW} and relaxation intensity ΔE. These parameters are interdependent when fitting. When larger ΔE is employed, larger relaxation time τ fitted is obtained, together with smaller β_{KWW} which mathematically suggest a broader distribution of relaxation times. Beforehand, β_{KWW} was determined to be 0.5 in the fitting of the stress relaxation of $Cu_{46}Zr_{46}Al_8$ glass in section 5.1. The $\beta_{KWW}(T)$ behavior might be related with different mechanical deformation modes[205].

As can be seen from figure 5-20, at 518 K and after 30 minutes, there is still a remaining elastic-solid part of the relaxation modulus. The mechanical response can be viewed as an anelastic behavior. Below T_g, the anelastic events can be estimated to have a relaxation intensity of around 10^4 MPa, with average relaxation times that change from 10 to 2 minutes. $\tau(T)$ can be parameterized as $\tau=2.8\times\exp(2035/T)$ s. The KWW parameters are plotted in figures 5-21 and 5-22.

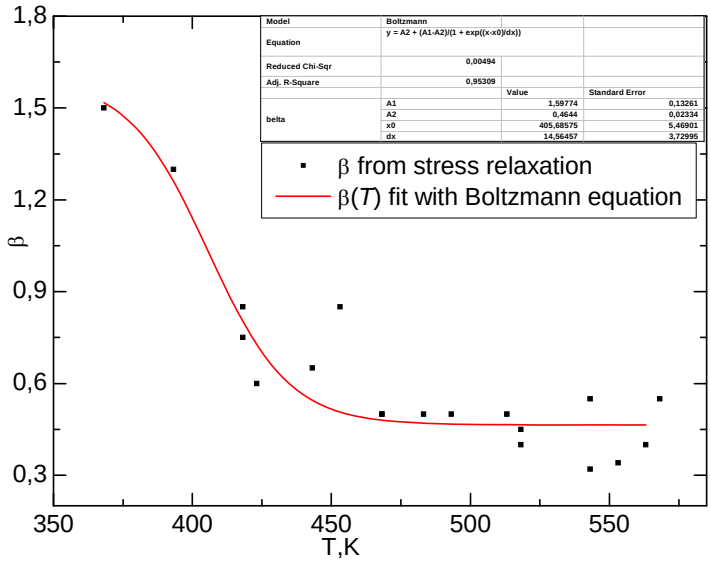

Figure5-22 β_{KWW} dependence of temperature from KWW fitting of stress relaxation

The behavior of β_{KWW} with temperature is shown in figure 5-22. Around T_g, β_{KWW} is around 0.4. It increases with decreasing temperature. At temperatures lower than 418 K, the relaxation can be fit only with $\beta_{KWW} \geq 1$. The compressed exponential is also observed from XPCS measurement [109].

Actually, $\beta_{KWW}(T)$ can be fit using a four parameter Boltzmann function which has an *s*-shape curve nature as shown in figure 5-22. At temperatures higher than T_g, the system flows and relaxation modulus changes from 2×10^4 MPa to 10^2 MPa. This is regarded as the α relaxation.

5.2.4.2 Stress relaxation described in relaxation spectrum

Actually, when calculating the relaxation time, the fitting is performed on the time scale of interest. As can be seen from figure 5-18 which shows the creep test on the logarithmic scale, at different time scale the slope is different. This can be regarded as an indication of the presence of a distribution of relaxation times. The relaxation spectrum can be obtained from the time response by Fourier transform or by a non-linear regression method. From the mathematical point of view, the problem of deconvolving the relaxation spectra is a particular case of the generic form of the first-kind Fredholm equation

$$\sigma(t) = \sigma_e + \int_0^\infty \sigma(\tau) e^{-t/\tau} d\tau \tag{5.5}$$

Where $e^{-t/\tau}$ is the kernel that describes the system, $\sigma(t)$ is the measured signal and $\sigma(\tau)$ is the unknown integral solution. The numerical solution of this equation is not a straightforward task since the Fredholm integral equation is a classical example of an ill-posed problem. In this work we used the renormalization technique described by Kontogiorgos[213]. It is based on the optimization of the residual and solution norms using the singular value decomposition of a matrix, which is the discrete representation of the kernel $e^{-t/\tau}$. This methodology was already applied to the deconvolution of static stress relaxation data for polymers.

The optimization of the residual and solution norms using the singular value decomposition method was performed for all the temperature conditions. How stress is relaxed at the different temperatures is shown in figure 5-20. The corresponding relaxation spectra are shown in figure 5-23.

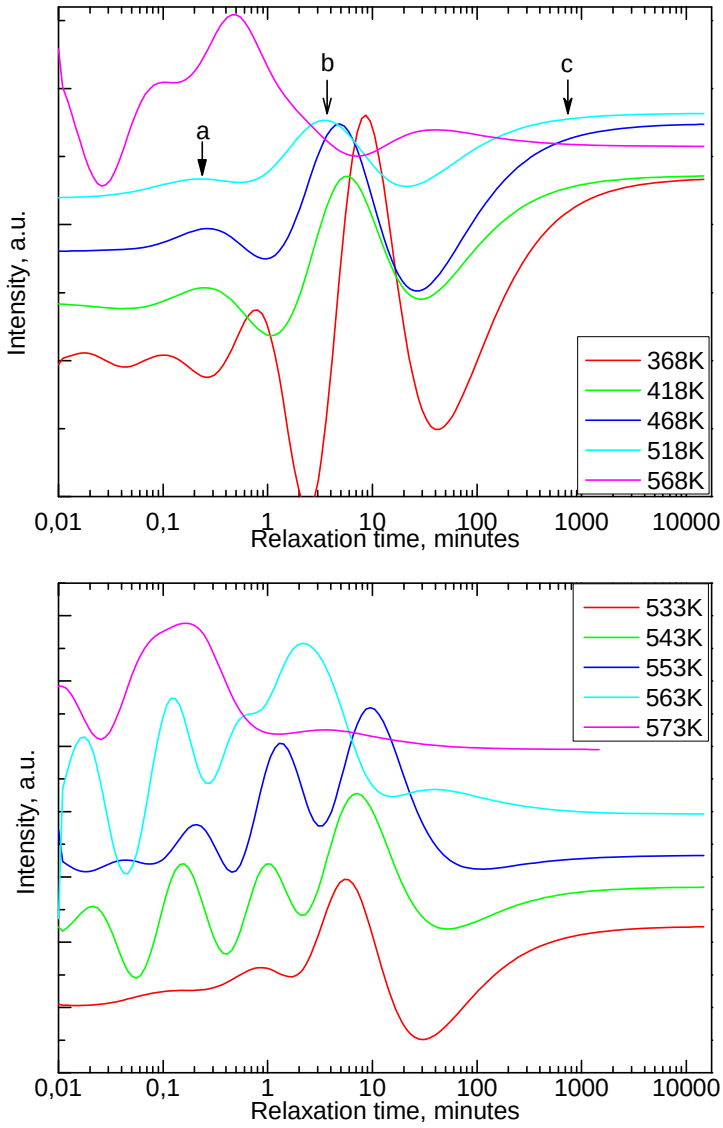

Figure 5-23 Relaxation time spectrum of $Pd_{42.5}Ni_{7.5}Cu_{30}P_{20}$ from stress relaxation.Up: with wide temperature span. Down: T_g region.

Using this method, it is found that, below the glass transition temperature, there are 3 main relaxation times which might suggest three different relaxation mechanisms or stages. At 368 K, three main events are perceptible which are located at around 1 minute, 10 minutes, and longer than 100 minutes. This behavior agrees with Ocelik's work[188] where they also obtained three well differentiated relaxation processes in MGs. One

explanation is to link the events with relaxation times around 1 and 10 minutes with the anelastic behavior. And the one with time larger than 100 minutes as the viscoplastic or viscous flow contribution described as annihilation of internal stresses or excess free volume by cooperative motions. Below T_g, the anelastic process with a relaxation time near 10 minutes shows a weak temperature dependence, decreasing the relaxation time with increasing temperature. At temperatures reaching the glass transition, more relaxation events are revealed under this methodology and the relaxation spectrum becomes more complex.

From our measurement and subsequent analysis, the typical relaxation time at around 10 minutes decreases with increasing temperature. However, at 533 K, 543 K, 553 K, the relaxation peak at around 10 minutes shifts to longer time with increasing temperature. This is originated by the physical aging of the system when reaching this temperature region. Above the glass transition temperature determined by both DSC and viscosity of value of 10^{12} Pa·s (553 K), the main relaxation time becomes shorter with increasing temperature. Actually, the main relaxation time can be fitted via VFT or Arrhenius temperature dependence. For the above-T_g data measured at 553, 563, 568 and 573 K, the corresponding τ obtained are 574, 137, 27 and 10 s respectively. These values follow a local Arrhenius behavior with apparent activation energy of E_α=546 kJ/mol and a corresponding fragility parameter of m=52.

For the relaxation spectra shown in figure 5-23, the vertical axis gives the relaxation relative intensity in arbitrary units. The relaxation relative intensity is only comparable with each other in the same stress relaxation measurement. The total relaxation intensity information can be obtained from original data as in figure 5-20, but the relative intensity shown in figure 5-23 is not comparable with each other for different temperatures. The relative intensity of the relaxation event at around 10 minutes might seem to be more or less the same from figure 5-23 at different temperatures, but actually the relaxation intensity is increased with temperature as can be seen from figure 5-20.

The results of stress relaxation part are plot on double log scale in figure 5-24.

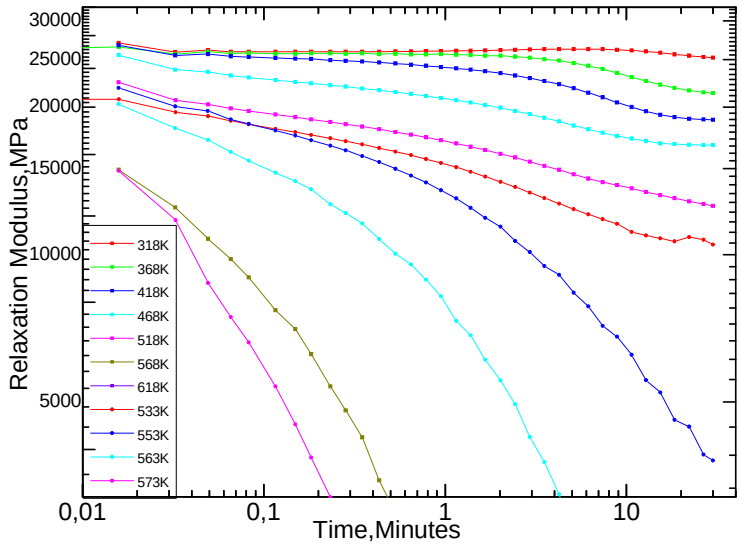

Figure 5-24 Stress relaxation behavior of $Pd_{42.5}Ni_{7.5}Cu_{30}P_{20}$ in state B. Strain employed:1%.

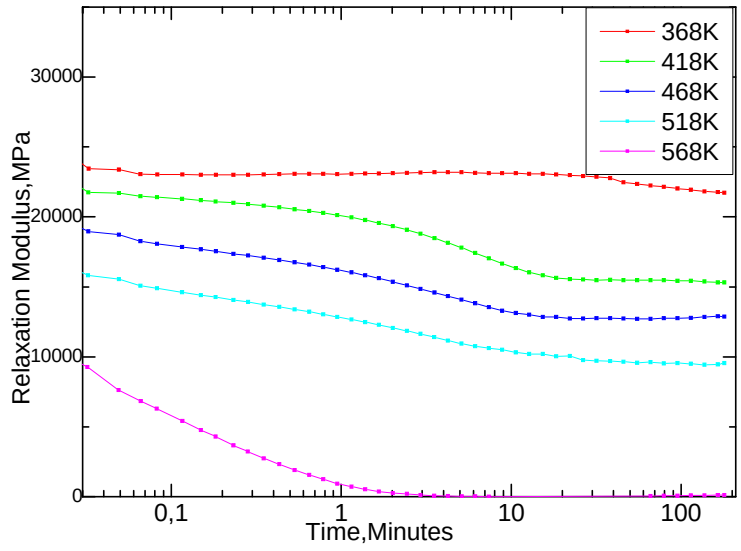

Figure 5-25 Relaxation modulus on log time scale. Strain: 0.1%. At each iso-thermal temperatures, a stress relaxation time of 3 hours is performed and followed by 2 hours of recovery.

From figure 5-24, it seems that at low temperatures, the modulus remains at finite instead of continuously decaying. Stress relaxation times of 3 hours at different temperatures were measured as illustrated in figure 5-25. The relaxation events with times around 10 minutes are clearly illustrated at

temperatures below T_g. Also below T_g, it can be clearly observed that applying recovery times longer than 120 minutes the relaxation modulus did not reduce but showed a saturated value. This means that the glass shows a solid behavior with a remaining elastic stress contribution at these temperatures.

5.2.5 Dynamic mechanical analysis

The analysis of the $E''(T)$ profile allows to realize that some relaxation processes get activated in MGs below the glass transition temperature. In order to differentiate from the α relaxation which reflects the movement of the whole structure, these processes are known as secondary relaxations [214][72]. A considerable amount of work has been done trying to understand the divergence between the α and secondary relaxation processes[179]. Originated from the molecular glasses, the Johari-Goldstein β relaxation is considered as the origin of events manifested on the low temperature DMA behavior. Beside molecular glasses, several different secondary relaxation processes have been found in different glassy systems[120]. Here we are will try to understand the DMA behavior of this MG, and to explain the observed secondary relaxation as a contribution of the anelastic events observed in the quasi-stationary measurement discussed in the previous experimental results.

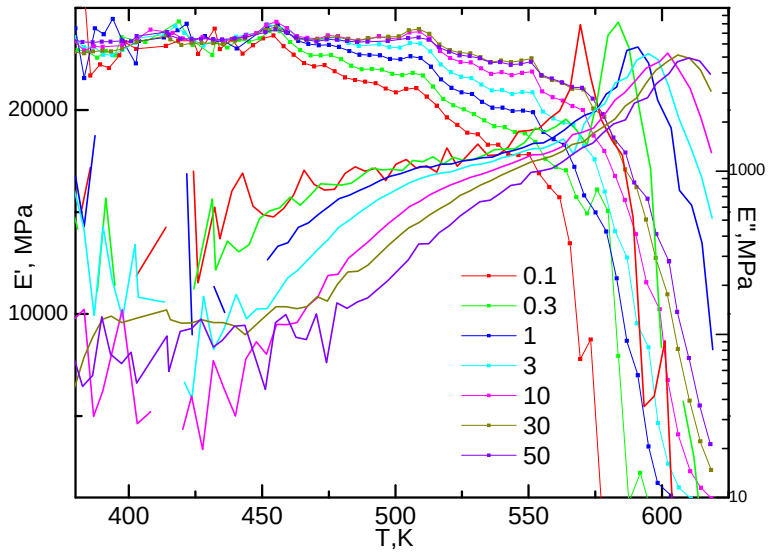

Figure 5-26 DMA of $Pd_{42.5}Ni_{7.5}Cu_{30}P_{20}$ measured under continuous heating. Different frequencies are performed at each temperature. Dots are storage modulus and lines are loss modulus. Heating rate:2K/min.

5.2.5.1 Temperature region below T_g

T_g is found at 553 K, determined from DSC with a heating rate of 2K/min. The typical mechanical spectroscopy of $Pd_{42.5}Ni_{7.5}Cu_{30}P_{20}$ in state A is shown in figure 5-26. The loss modulus starts to increase at around 400K under continuous heating. It is often described as a shoulder on $E''(T)$ profile. The origin of this shoulder has been explained as Johari-Goldstein β relaxation[121]. From a solid state mechanism point of view, it is regarded as a secondary relaxation and might be originated from anelastic events. The activation energy could be fitted considering a standard anelastic solid. In the current situation where the peak is not distinguishable, it is suggested that a fixed loss modulus value can be chosen and the corresponding temperature obtained can be used for fitting the activation energy[122].

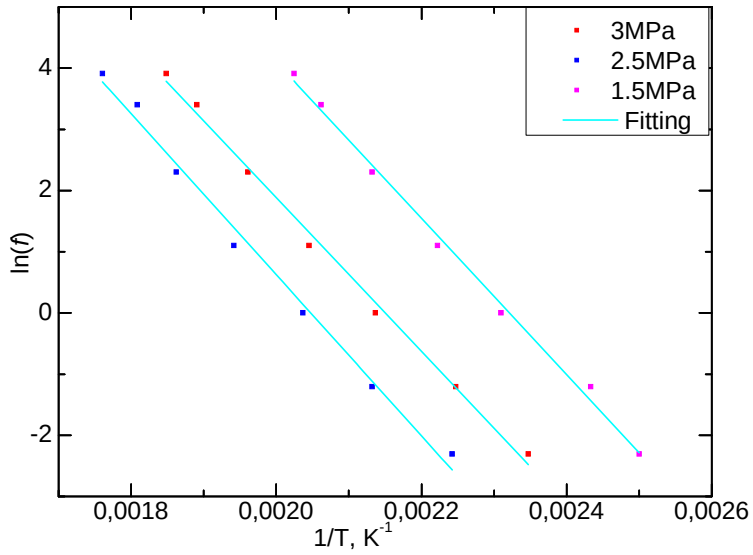

Figure 5-27 Secondary relaxation of as quenched $Pd_{42.5}Ni_{7.5}Cu_{30}P_{20}$ MG. Figure shows the temperatures and corresponding testing frequencies of a fixed value loss modulus,. The data is fitted with Debye equation (3.20). Different colors show different values of loss modulus employed.

Setting the loss modulus at a fixed value, we get the temperatures corresponding to each different testing frequency. The frequency dependent loss modulus is illustrated in figure 5-27. The activation energy is calculated according to equation 3.20. There are several factors influencing the determination of the activation energy: the state of the glass, the loss modulus employed to get the temperature, and the testing amplitude.

When applying an amplitude of 5μm, for the state A, the activation energy and pre-exponential factors are 106, 104, 109 kJ/mol and 7×10^{12} s^{-1}, 5×10^{11} s^{-1}, 5×10^{11} s^{-1} when the fixed values of loss modulus employed are 1.5 MPa, 2.5 MPa, 3 MPa respectively. As to state B, the activation energies obtained are 126 and 179 kJ/mol with pre-exponential factors of 2×10^{14} s^{-1} and 3.5×10^{18} s^{-1} for values of loss modulus of 1 and 2 MPa respectively.

It seems that a lower value of the loss modulus, which corresponds to a lower temperature, is more appropriate for the fitting. At higher temperatures where the loss modulus reaches 2 MPa, the fitting using this methodology gives higher activation energy and a pre-exponenntial factor of unclear physical meaning. It might originate from other events that may get activated at these higher temperatures and become overlapped on this temperature region.

Amplitude also influenced the fitting. With amplitude of 0.5 μm, the obtained activation energy and pre-exponential factors for the state A are 180, 270 kJ/mol and 3.5×10^{19} s^{-1}, 7×10^{26} s^{-1} for values of loss modulus of 1 and 2 MPa respectively. The relaxed sample shows activation energies of 225, 243 and 280 kJ/mol and pre-exponential factors of 1×10^{24} s^{-1}, 4×10^{25} s^{-1} and 5×10^{28} s^{-1} for chosen values of loss modulus of 1, 1.5 and 2 MPa respectively. The physical meaning of the obtained values when applying an amplitude of 5 μm is more clear. The activation energies of around 105 and 126 kJ/mol, for as-quenched and relaxed states respectively, agree with the values reported above. These values are also close to the activation energy of diffusion of small atoms in the system[158,215,216].

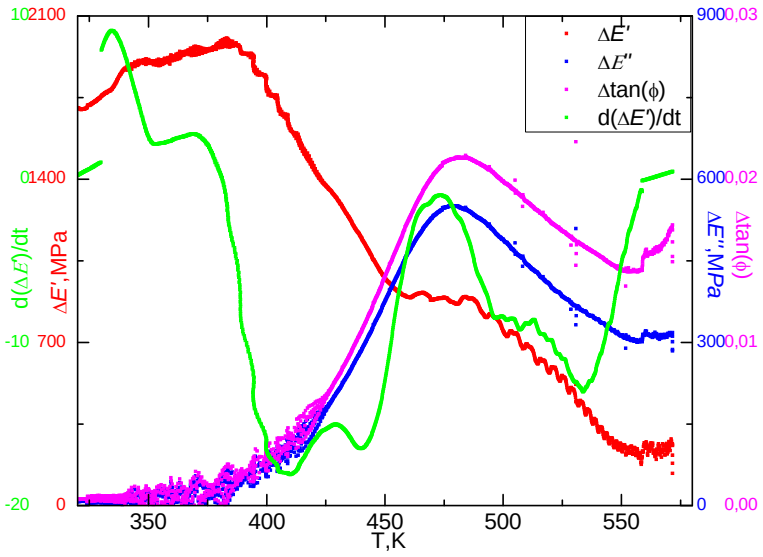

Figure 5-28 Difference of modulus between as quenched and relaxed state measured by DMA at a frequency of 3Hz. Red line is *ΔE'*. Blue line is *ΔE''*. Pink line is the Δ*tan(φ)*. Green line is the differential of the *ΔE'* with time: *d(ΔE')/dt* .

If we treat *E''*(*T*) of the relaxed state as a thermo-elastic background, the low temperature events can be more clearly analyzed by looking at the difference between as quenched and relaxed states as shown in figure 5-28. Here the relaxed state refers to the sample first heated to 573 K and cooled back to 313 K with cooling rate of 2K/min. Both Δ*E'*(*T*) and Δ*E''*(*T*) are shown in the figure. A single peak on Δ*E''*(*T*) profile suggests a single process with a broadened activation energy distribution. The shape of internal friction Δ*tan*(*φ*) has the same features than Δ*E''*(*T*).

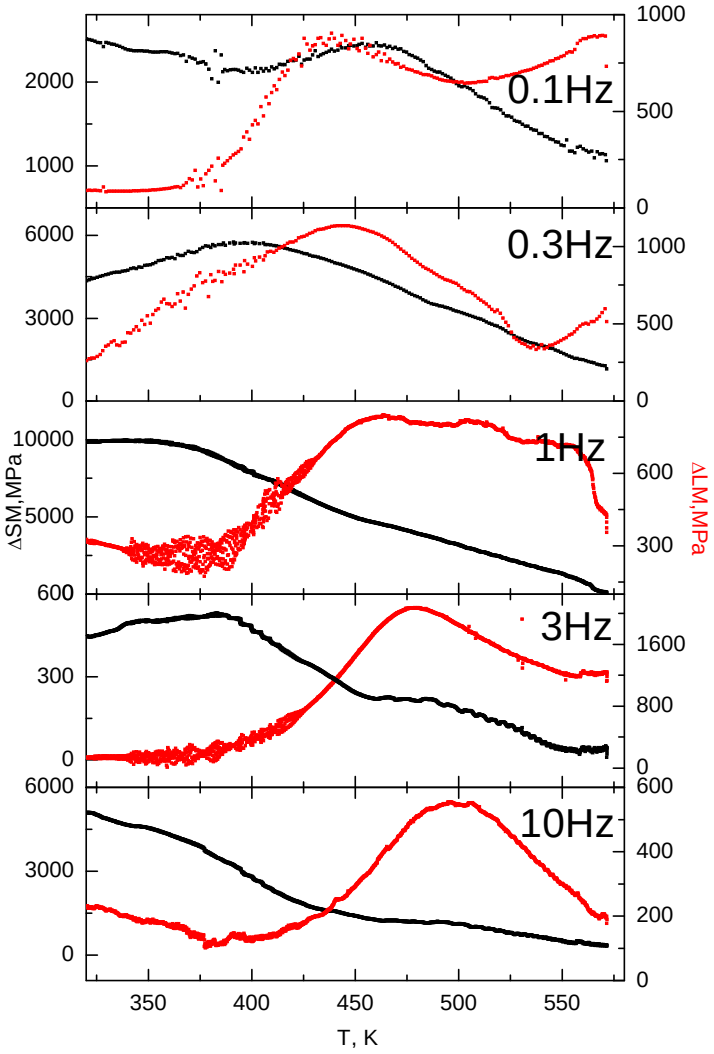

Figure 5-29 $\Delta E'(T)$ and $\Delta E''(T)$ at different frequencies. Black: $\Delta E'(T)$. Red: $\Delta E''(T)$.

As can be seen from figure 5-29, when increasing the testing frequency f, the peak temperature on the $\Delta E''(T)$ profile increases. The relationship between f and peak temperature could be fitted with an Arrhenius process. The activation energy fitted was 120 kJ/mol and the pre-exponential factor 2.9×10^{13}. The difference between the as quenched and relaxed state is an effect of physical aging. Under this methodology, the physical aging with apparent activation energy of 120 kJ/mol is close to the events manifested on

the beginning of the loss modulus increment (126 kJ/mol under amplitude of 5μm, fixed loss modulus of 1MPa in state B).

The overall difference of storage modulus between as quenched and relaxed state is an effect of all the relaxation events in all the temperature range. Differentiation is performed and the corresponding activation energy spectrum is obtained as shown in figure 5-28 as the green line. It can be explained by two relaxation processes with different activation energies[98,112].The physical aging is described by an activation energy spectrum generated by difference between the as quenched and relaxed state. The behavior of $E'(T)$ in figure 5-29 agrees with Tsyplakov's work[98] on $Pd_{41.25}Cu_{41.25}P_{17.5}$ MG.

5.2.5.2 Temperature region higher than T_g

In this region the peak of the α-relaxation is quite obvious. The relaxation time is obtained through the position of the peak maximum assuming the relationship $\ln(\omega\tau)=0$ where $\omega=2\pi f$ is the testing angular frequency. The relationship between the obtained relaxation time and temperature can be fitted via the VFT behavior (equation 3.1) using parameters $\tau_0 = 10^{-13}$, B=4000 and T_0=449 K; the parameters obtained are similar to those reported in ref. [129]. However, the fitting is not good at lower temperatures close to T_g where simple Arrhenius relationship fits better the relaxation time, with activation energy of 526 kJ/mol. Based on the relationship between fragility and activation energy (equation 3.22), when T_g is chosen as 553 K, the fragility parameter has a value of m=50. This value agrees with the results obtained by stress relaxation as discussed in section 5.2.4.

5.2.6 Physical aging explored by mechanical relaxation

5.2.6.1 Isothermal physical aging dynamics

As described in chapter 3, physical aging leads the glass to more relaxed states and produces important changes in many properties. Interestingly, there is a link between the activation energy of relaxations below T_g and the

initiation of mechanical flow events. Moreover, secondary relaxations are also considered the origin of physical aging or structural relaxation below T_g.

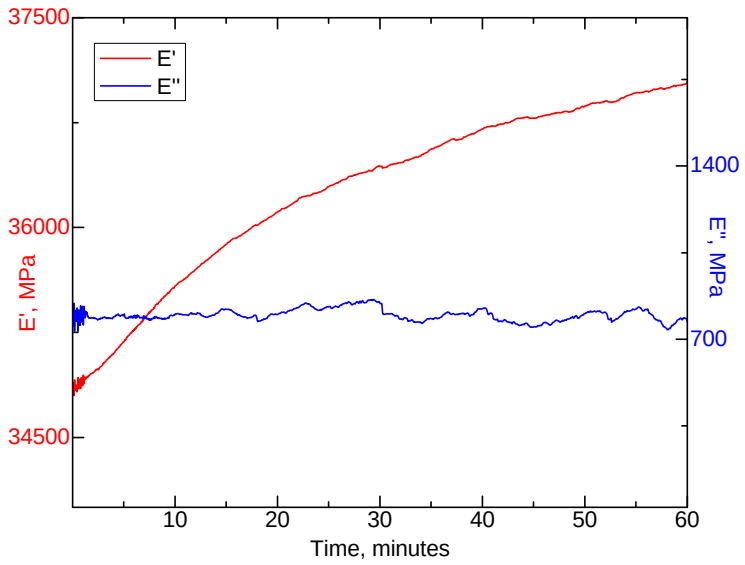

Figure 5-30 Time dependent modulus of $Pd_{42.5}Ni_{7.5}Cu_{30}P_{20}$ at 383 K. The as quenched sample is heated to 383 K with heating rate of 2K/min, then physical aging is monitored under isothermal conditions for 60 minutes. Amplitude: 5μm. Preload force: 0.8N.

Physical aging is explored by monitoring how the elastic modulus changes with time under isothermal conditions. As can be seen from figure 5-30, at 383 K the storage modulus *E'* increases with time while loss modulus *E''* decreases slightly. The storage modulus increasing behavior can be fitted by using a stretched exponential function, the obtained relaxation time τ is 2000 s with β_{KWW}=0.9. The viscosity is on the order of 10^{14} Pa·s at this temperature, by interpolation of the isothermal creep measurement in figure 5-17. According to the Maxwell relationship $\tau=\eta/G$ (which must be used with caution in the deep glassy state), the relaxation time would be around 3300 s, close to the one governing the aging process.

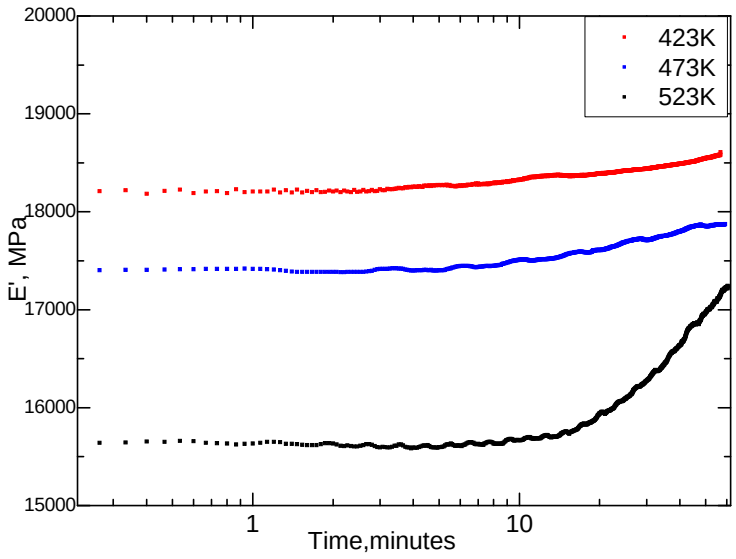

Figure 5-31 Isothermal physical aging dynamics manifest on storage modulus. As quenched sample is relaxed in the DMA at 423, 473 and 523K successively. DMA is measured with amplitude of 5μm and preload force of 0.8N.

Structural relaxation dynamics is explored isothermally at different temperatures. In the experimental time window, the storage modulus does not saturate, suggesting that physical aging is still proceeding. This behavior agrees with Khonik's work on shear modulus change as a function of time in the Zr-Ti-Cu-Ni-Al MGs[100]. Actually, aging time in the $Pd_{40}Ni_{10}Cu_{30}P_{20}$ MG is found on the order of 5000 s at 533 K as explored by monitoring the shear modulus change [217].

5.2.6.2 Physical aging explored under continuous heating

It has been suggested that the structural relaxation has an energy distribution nature. The amount and activation energy of relaxation centers are related to the specific temperature. At a given temperature, after the characteristic relaxation time, the relaxation process is finished and properties like loss modulus or viscosity would retain a metastable value. More relaxation sites can get activated at higher temperatures, because of the higher thermal energy available in the system, and get saturated after a certain relaxation time.

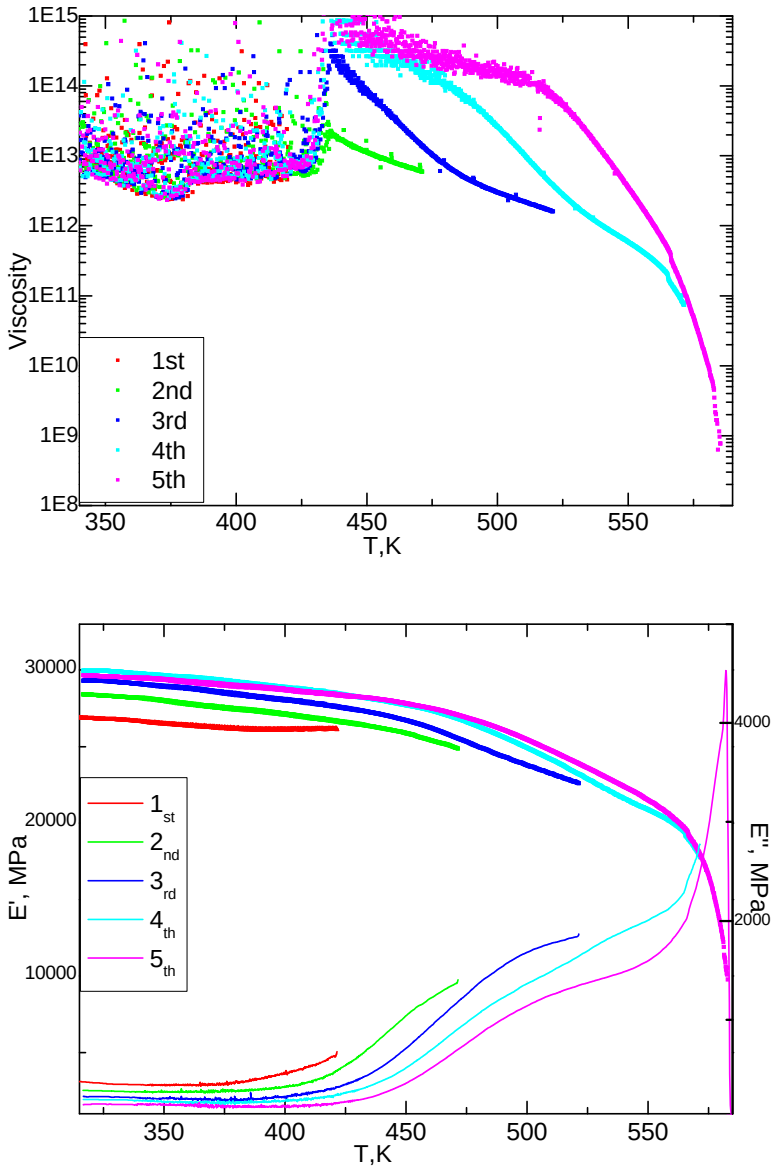

Figure 5-32 Influence of physical aging on viscosity (up) and elastic modulus (down). Thermal protocal as in figure 5-13 (c).

A series of thermal treatments on the same sample were performed, the viscosity as well as the mechanical spectroscopy were obtained *in situ*. The effect of physical aging on viscosity and modulus is illustrated in figure 5-32. It can be observed that physical aging reduces the internal friction, which was quite high even at low temperatures for the rapid quenched initial samples.

This result is similar to that found in $Pd_{40}Cu_{30}Ni_{10}P_{20}$ MG by Khonik[218,219].

The viscosity, the storage and the loss modulus in figure 5-32 show a clear aging behavior. After each run, the state of the system is progressively stabilized increasing viscosity and storage modulus while decreasing internal friction. After a certain run is performed, the next one starts from a more relaxed state. When the next run reaches the final temperature of the previous one, the properties correspond to a more relaxed state than the one measured at the end of the preceding run. This is because the physical aging occurs continuously during both the heating and cooling segments.

Regarding sub-T_g viscosity behavior, it is shown that the activation of physical aging changes the viscosity by two orders of magnitude. For each run, it is clearly observed that the abrupt reduction of $\eta(T)$ coincides with the presence of the secondary peak in the $E''(T)$. At temperatures below the activation of the secondary relaxation, the activation energy of viscous flow is the same as calculated in subsection 5.2.2.2.

5.3. Relaxation dynamics of $Fe_{55}Cr_{10}Mo_{14}C_{15}B_6$ MG

5.3.1 Activation energy spectrum by enthalpy relaxation

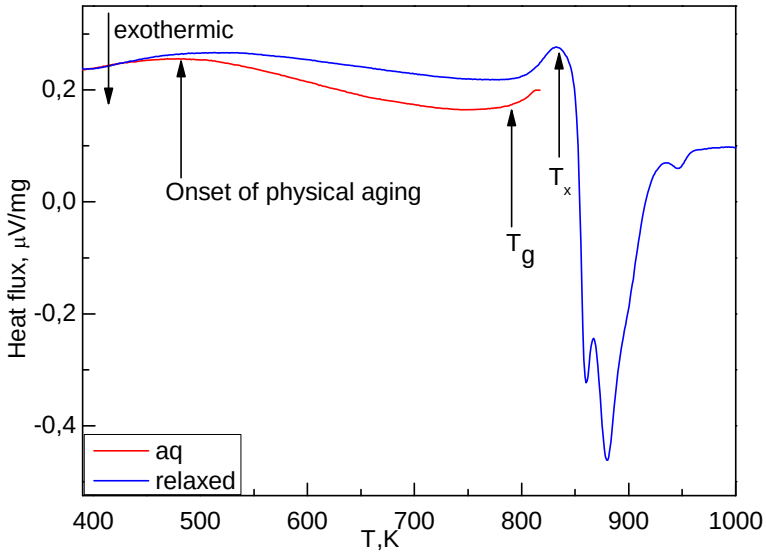

Figure 5-33 DSC of $Fe_{55}Cr_{10}Mo_{14}C_{15}B_6$ MG showing difference between as quenched and relaxed state

DSC results in figure 5-33 show that the glass transition starts at 790 K when applying a heating rate of 20 K/min. The crystallization process is a multistep process with the first step starting at 835 K. The second crystallization process is entangled with the first crystallization process, having its crystallization peak at 878 K. The third crystallization peak is 937 K. A detailed description ot the crystallization process of this material was studied by Madinehei[220].

It is well known that the structural relaxation influences many properties like viscosity and magnetic properties, as well as mechanical properties[221]. The mechanism is described as the annihilation of the free volume or shear transformation zones. The DSC of the as quenched and relaxed samples is shown in figure 5-33. The structural relaxation starts around 500 K. Here the relaxed sample is obtained by heating the as quenched sample up to 813 K and then cooling down, both heating and cooling applying the same rate of 20 K/min.

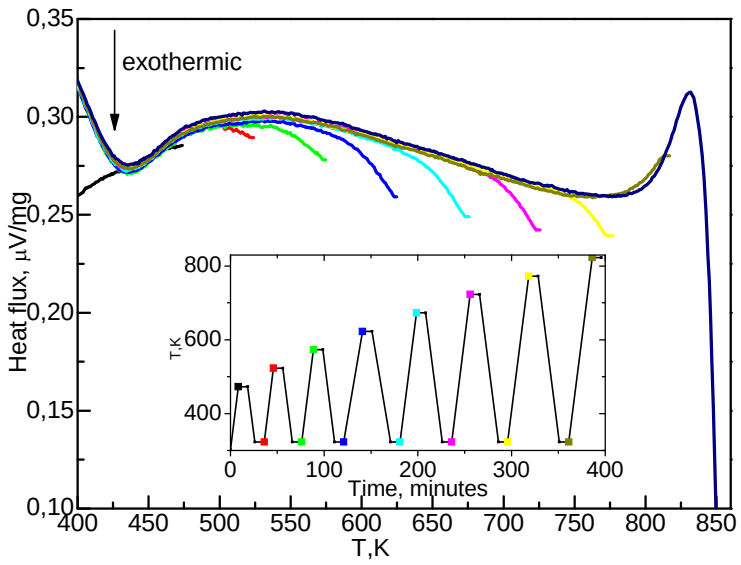

Figure 5-34 DSC of Fe based MG with different states with controlled heating and cooling protocol explained in the insert figure, suggesting the activation energy spectrum

A controlled physical aging was performed in the DSC, the recorded heat flow is depicted in figure 5-34. As it was observed on viscosity and elastic modulus of $Pd_{42.5}Ni_{7.5}Cu_{30}P_{20}$ MG, discussed in section 5.2, a physical aging with a distribution of activation energies is also manifested on the enthalpy experiment. At a given temperature, after the characteristic relaxation time, the structural relaxation process is finished and heat capacity retains a metastable value. When heating to higher temperature, more release of heat is observed. This behavior is continuous until the glass transition region, where the system reaches the configuration of the supercooled liquid equilibrium state and there is no more structural relaxation under the experimental heating rate conditions.

Recently, the activation energy spectrum (AES) has attracted great interest to study the plasticity of MGs [98,112]. The AES is constructed by difference between the as quenched and relaxed states, as first introduced by Primak[223] and later developed by Gibbs[224]. This method is applied to MGs as described by Chen and Khonik[97,100,222] where Khonik suggests that a continuous distribution of activation energies is a typical feature of the relaxation, and that the shear modulus is influenced by structural relaxation[100]. The structure relaxation spectrum is obtained by the

difference between C_p of the as quenched and the relaxed states[97], the result is shown in figure 5-35.

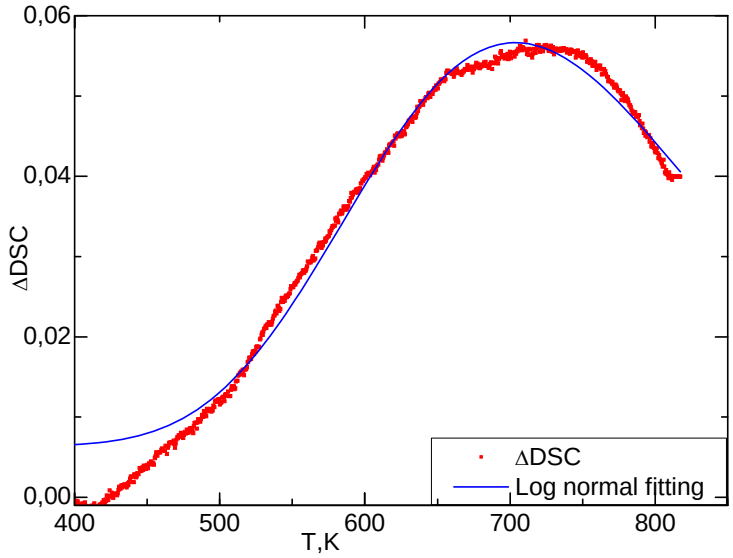

Figure 5-35 Activation energy spectrum of FeCrMoCB obtained by enthalpy relaxation. Red point is the difference of DSC between as quenched and relaxed state. Blue line shows a fit to a log normal distribution.

Unlike Pd-Ni-P glass where there are two events with separated activation energies[98,112], Fe-Cr-Mo-C-B MG has only one event with a wide activation energy distribution; the AES can be fitted to a log-normal distribution:

$$y = y_0 + \frac{A}{\sqrt{2\pi}wT}\exp\left(-\frac{\ln^2\left(T/T_c\right)}{2w^2}\right) \tag{5.6}$$

with fitting parameters y_0=0.006, T_c =724, w=0.17 and A=15.34. This experimental observed lognormal distribution agrees with Jiao's assumption used in fitting the stress relaxation of $Pd_{40}Ni_{10}Cu_{30}P_{20}$ metallic glass[125].

There is a relationship between activation energy and temperature in the form of $E=kT$, where k is between 0.002 and 0.003 depending on the heating rate[100,222]. Chen assumed k=0.0025 with a heating rate of 20 K/min[97]. From the lognormal fitting, the most probable activation energy is 724 K, thus the corresponding activation energy is 1.81 eV, namely 174 kJ/mol. This value is close to the Johari-Goldstein β relaxation activation energy 171

kJ/mol obtained using the empirical relationship E_β =26RT_g described in chapter 3.

5.3.2 Mechanical relaxation

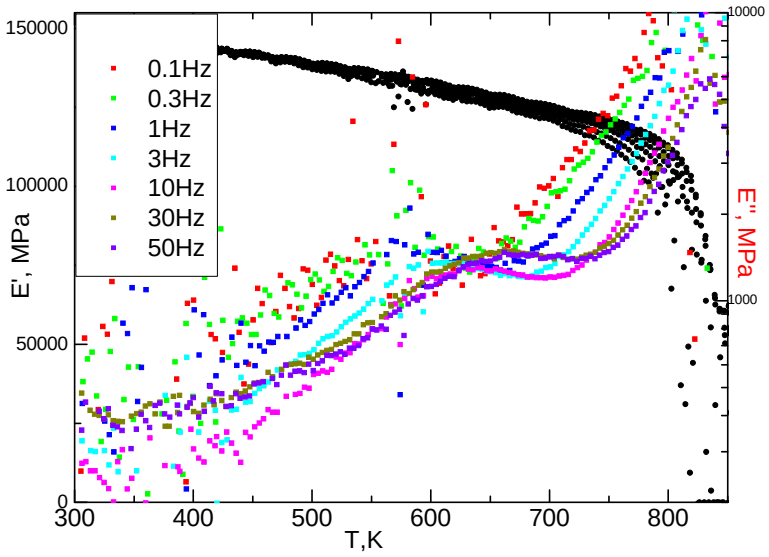

Figure 5-36 Modulus of $Fe_{55}Cr_{10}Mo_{14}C_{15}B_6$ MG at different frequencies varying between 0.1 to 50Hz. There an is obvious secondary relaxation at around 500K. The main peak is not α relaxation, but cut by crystallization.

The typical multi-frequency mechanical spectroscopy results obtained for $Fe_{55}Cr_{10}Mo_{14}C_{15}B_6$ MG are shown in figure 5-36. As described in section 5.1, $Cu_{46}Zr_{46}Al_8$ glass showed that the relaxation response can be fitted by a CC-function, and the relaxation time obtained followed a VFT behavior near and above T_g and an AGV behavior below it[203]. This Cole-Cole fitting was found also applicable to the $Mg_{65}Cu_{25}Y_{10}$ MG where $E''(T)$ showed a shoulder-like behavior of the loss modulus[162]. In that case, the induction of physical aging by annealing treatments eliminated the secondary peak of the loss modulus. However, in the current situation, a secondary relaxation process needs to be taken into consideration. From 450 K, the loss modulus starts to increase, indicating that some process gets activated. Unlike $Pd_{42.5}Ni_{7.5}Cu_{30}P_{20}$ where loss modulus increases continuously with temperature, in the current MG, there is an obvious peak on the temperature scale. This distinguishable peak is also reported in La-Ni-Y MGs where is

normally referred as β-relaxation. At even higher temperatures, the loss modulus increases continuously with temperature until it is cut by crystallization and starts to decrease.

As mentioned in chapter 3, the secondary relaxation peak is usually a thermally activated process whose relaxation time dependence on temperature follows an Arrhenius relationship. The frequency response can be then analyzed in the framework of the Debye equation (equation 3.20 in chapter 3).

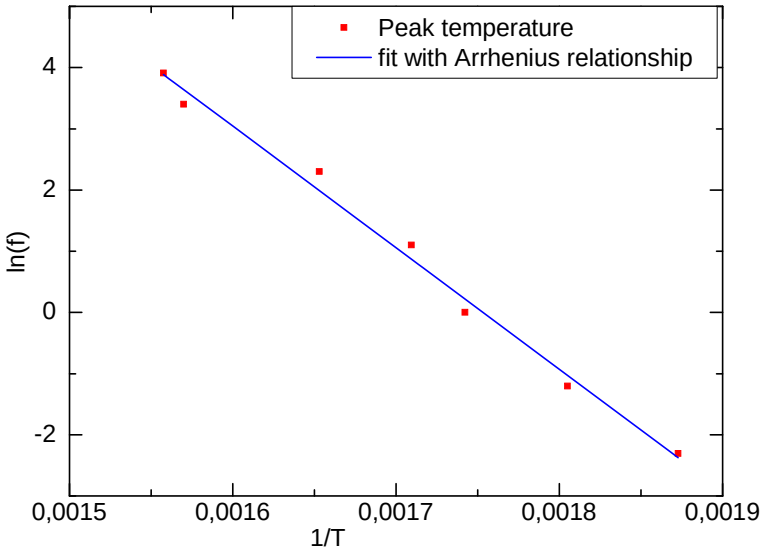

Figure 5-37 Peak temperature dependence of testing frequency showing secondary relaxation in $Fe_{55}Cr_{10}Mo_{14}C_{15}B_6$ MG. E_{act} =165KJ/mol.

The ln(f) is plotted against $1/T_{peak}$ in figure 5-37. For the as quenched state, using the peak temperature of the secondary relaxation, the fitted activation energy is 165 kJ/mol and the pre-exponential factor is 1.3×10^{15} s^{-1}. Using the commonly employed relationship E_β =26RT_g, the activation energy of the Johari-Goldstein relaxation would be around 171 kJ/mol, taking T_g = 790 K as obtained by calorimetry with a heating rate of 20 K/min. The activation energy of this process is close to the one proposed for Johari-Goldstein relaxations in metallic glasses; however, with only the activation energy it is difficult to tell whether the secondary relaxation is a JG-relaxation or not. This fitted activation energy is also close to the activation energy of physical aging (174 kJ/mol from AES model from section 5.3.1).

The samples relaxed at 723 K and 773 K were analyzed by DMA. It is noted that after relaxation at 773 K for 30 minutes, the β relaxation still can be perceived. This result suggests that physical aging has similar activation energy than the β-relaxation shown on *E''(T)*, but physical aging does not eliminate the β-relaxation. In the former case, the activation energy obtained from the secondary peak is 152 kJ/mol, with pre-exponential factor of 3.6×10^{13} s^{-1} while the latter gives an activation energy of 181 kJ/mol with pre-exponential factor of 7×10^{15} s^{-1}.

Actually, a similar activation energy is obtained by DMA in La-Ni-Al MGs as well as by NMR in Zr-Ti-Cu-Ni-Be metallic glass[225]. It has been suggested that these processes are dominated by the atomic motion introduced by the smallest atoms[158]. The activation energy of β-relaxation is comparable with the activation energy of the shear transformation zones, and it is believed that enhancing β-relaxation might be beneficial for mechanical properties of MGs like plasticity and toughness [149,150,226]. Our results here, with significant secondary relaxation, suggest that when the β-relaxation gets activated at elevated temperature, plasticity may get improved in this alloy. Since chemical composition influences both the intensity as well as the peak position of the β-relaxation[72], further research might include systematic work on reducing the activation energy of this β-relaxation with the aim of improving toughness, as achieved in La based MG system with notable β-relaxations[71].

In situations when the peak is not distinguishable, the temperatures at which the material shows the same loss modulus are employed to calculate the activation energy. When a fixed loss modulus value of 1500 MPa is chosen, the activation energy is computed to be 99 kJ/mol with pre-exponential factor of 4.9×10^{10} s^{-1}. The activation energy fitted with a fixed loss modulus value is lower than the one fitted from the peak position. This indicates that, as expected, the secondary peak is originated from a distribution of processes with a corresponding distribution of activation energies. Although an average relaxation time and activation energy may be calculated, the fastest processes of the distribution (which have the lowest activation energies) get activated at lower temperatures.

At higher temperatures, close to T_g, a peak is observed in the loss modulus. The peak temperature shifts to higher temperature when the frequency is increased. This increase of loss modulus can be ascribed to the α-relaxation involving the activation of collective movement. The peak here is cut by the crystallization process which further decreases the loss modulus at higher temperature.

Using a fixed loss modulus value of 9200 MPa, the temperatures corresponding to each frequency are determined. Using equation 3.20, the activation of this α-process is calculated as 461 kJ/mol. However, as illustrated above in the case of the anelastic event, the activation energy obtained by a fixed value is lower than that obtained fitting from peak temperatures; the activation energy of 461 kJ/mol might thus be underestimated. Using equation 3.22, this apparent activation energy of the viscous flow in the glass transition region gives a fragility parameter of m=30, which is quite low for a metallic glass.

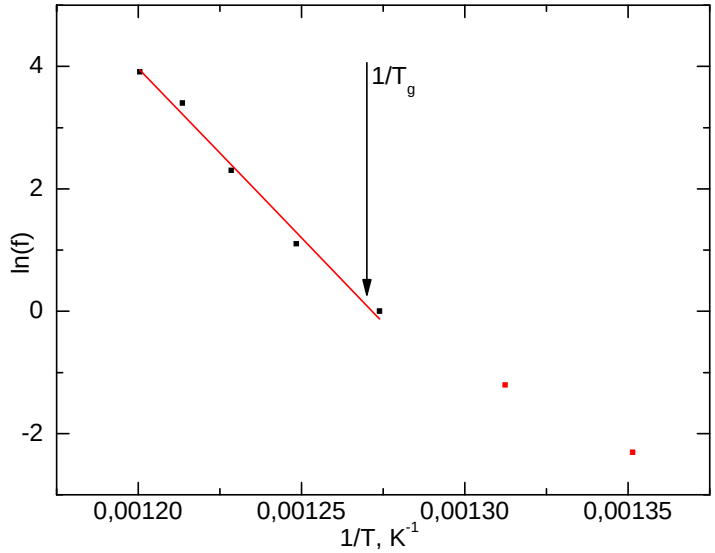

Figure 5-38 α-relaxation analyzed by equation 3.20. Temperatures are chosen as loss modulus reaches a fixed value of 9200 MPa at each frequency. Red line is fit with Arrhenius behavior with activation energy of 461 kJ/mol. Below T_g, the system is in a non-ergodic state and the behavior deviates from the equilibrates state.

As described in section 5.2, the viscosity during DMA measurement can be obtained in the framework of Maxwell viscosity. The dependence of

viscosity on temperature for this alloy is illustrated in figure 5-39. Viscosity decreases with increasing temperature. T_g, determined where viscosity reaches 10^{12}, is around 788 K. This is quite close to the 790 K obtained by DSC measurement under a heating rate of 20 K/min. At temperatures higher than 837 K, viscosity increases with temperature, this increase on viscosity is related to the crystallization. This agrees with the enthalpy measurements that showed that T_x=835 K.

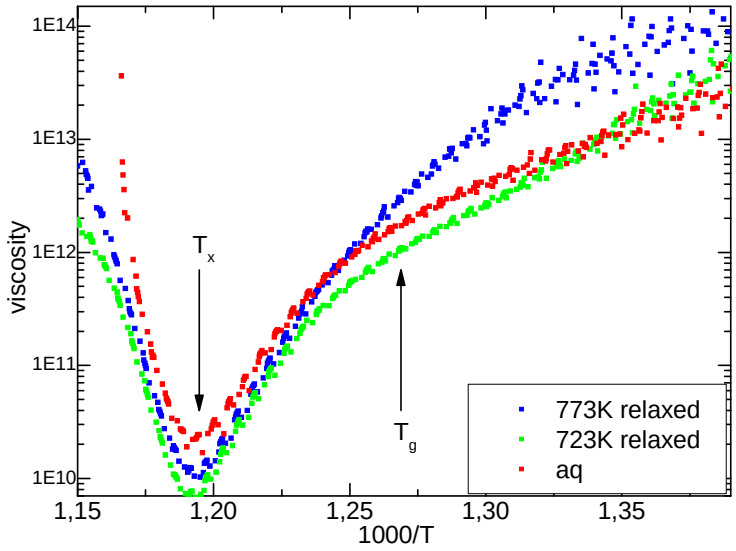

Figure 5-39 Viscosity of the Fe based metallic glass obtained by $\eta=\sigma/3*\dot{\varepsilon}$. The viscosity can be described by an Arrhenius behavior under T_g, while can be fit with to a VFT or Arrhenius behavior above T_g, Further heating above the crystallization temperature would increase viscosity. Measurement performed with heating rate of 2K/min.

The temperature dependent viscosity follows an Arrhenius relationship below T_g. As for the as quenched state, activation energy is found to be 180 kJ/mol, which is slightly larger than the 165 kJ/mol obtained from fitting the secondary relaxation peak of the loss modulus. The slope of the viscosity vs $1/T$ curve of the samples relaxed at 723 and 773 K are larger than that the one shown by the as-quenched ribbons, in agreement with the expected increase of the activation energy for sub-T_g viscous flow because of physical aging.

Above T_g, the temperature dependent viscosity can be described as VFT or also as local Arrhenius-like in a narrow range of temperatures. Fitting with

Arrhenius relationship leads to E_α=746 kJ/mol. With equation 3.22, the corresponding fragility parameter results to be m=49.

5.4 Discussion of the experimental results

Similar to dielectric spectroscopy studies of other glassy substances, like inorganic or polymeric glasses, mechanical spectroscopy is able to capture the characteristics of the relaxation dynamics of metallic glasses in the frequency domain. Within the explored frequency and temperature windows, the above DMA results show that the mechanical response of $Cu_{46}Zr_{46}Al_8$, $Pd_{42.5}Ni_{7.5}Cu_{30}P_{20}$ and $Fe_{55}Cr_{10}Mo_{14}C_{15}B_6$ shows the three typical secondary relaxation behaviors (termed as β relaxations) found in metallic glasses. To be more specific, the low temperature relaxation appeared as excess wing, shoulder or differentiated peak on the $E''(T)$ profile.

In the case of $Cu_{46}Zr_{46}Al_8$, the relaxation mechanism is proposed to involve only α-relaxation both in the liquid and glassy state, with dynamics given by the VFT and AGV (Arrhenius-like) functions respectively. It should be noted that the low frequency (high temperature) wing of the α-relaxation peak is not covered by this study. At 1 K/min the onset of crystallization is observed at T=745 K, inhibiting the access to the high-temperature wing. If the low frequency wing could be measured, it would be possible that a complete Havriliak–Negami function with an asymmetry parameter $\gamma \neq 1$ would be necessary for describing the shape of the peak. However, the estimation of the $\tau(T)$ values and the exponential decay of the high-frequency wing (given by the α parameter of the CC-function) would not change significantly.

Figure 5-40 resumes the proposed model for mechanical relaxation of the $Cu_{46}Zr_{46}Al_8$ metallic glass. The broadening of the CC-relaxation function has been found experimentally to be approximately constant. The excess wing observed experimentally agrees well with the tail of the α-relaxation when the average relaxation time follows a non-equilibrium AGV behavior. The solid thick black line in the figure shows the expected isochronal $E''(T)$ measurement showing the excess wing detected in experimental DMA measurements. In section 5.1, the validity of the relaxation times obtained from the DMA analysis has been assessed by independent measurements of stress relaxation quasi-static tests. The model proposed in figure 5-40 is for a relaxed glass, with fictive temperature near to the glass transition temperature

detected at heating rates of the order of 1-10 K/min, as the ones usually applied for DSC and DMA characterization.

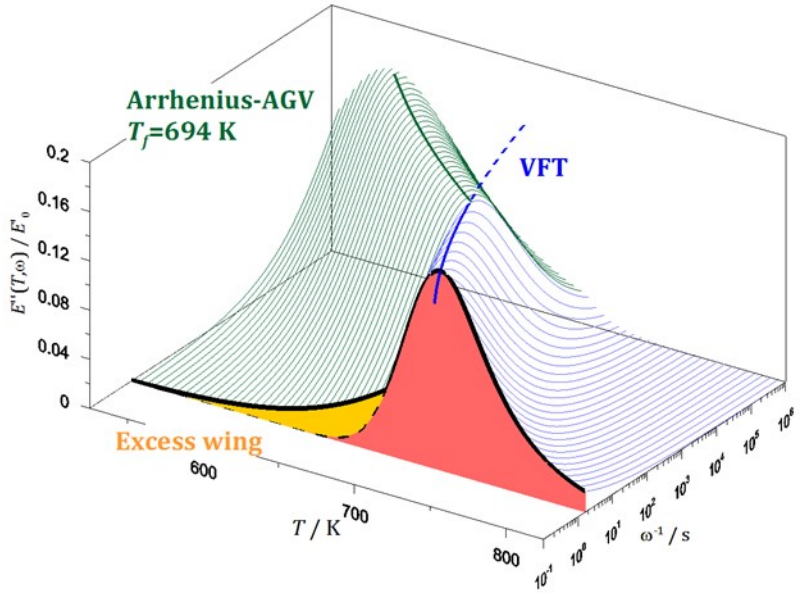

Figure 5-40 Model proposed for the relaxation spectrum of $Cu_{46}Zr_{46}Al_8$ glass. Blue lines stand for the CC-function following equilibrium VFT dynamics. Green lines stand for CC-function following AGV dynamics below T_g.

The results obtained are consistent with those obtained for $Mg_{65}Cu_{25}Y_{10}$, a MG with a very different chemistry[162]. In both cases, only a single relaxation process was necessary to understand the glass–liquid dynamics within the frequency and temperature window probed (0.1 Hz < f < 100 Hz). It should be noted that the AGV function is a good description of the glass dynamics only if the glass is in an isoconfigurational state. Physical aging of MGs has been recently studied by X-ray photon correlation spectroscopy (XPCS) in $Mg_{65}Cu_{25}Y_{10}$ and $Ni_{33}Zr_{67}$ glasses[109]. The complex aging behavior found in those works cannot be described by the simple VFT-AGV scheme proposed here. However, if the validity of the VFT-AGV description is verified for isoconfigurational MGs, it may give a useful tool to estimate the relaxation times and associated properties as function of the fictive temperature of the glass.

Although only the presence of the α-relaxation is needed to explain the excess wing of $Cu_{46}Zr_{46}Al_8$, a secondary relaxation with very low intensity

could be merged with the main loss peak. In fact, the presence of β-relaxation as a universal phenomenon in metallic glasses has been widely discussed. However, the intensity of this relaxation would be irrelevant as it is not needed to interpret the experimental results of this system. Many other metallic glass systems, basically the ones belonging to the very important families of Cu, Ti and Zr based metallic glasses, do only show an excess wing in their internal friction behavior. It is reasonable to suggest that a similar picture to the one presented in section 5.1 of this work may be applicable to most of these systems.

In the case of $Pd_{42.5}Ni_{7.5}Cu_{30}P_{20}$ glass analyzed in section 5.2, there are obvious secondary relaxations prior to the α-relaxation process on the temperature profile. At the lower temperature regions, loss modulus is fitted in the framework of a standard anelastic solid by a thermal activated process with activation energy of 126 kJ/mol and possible atomic jump origin. At a higher temperature region, the plateau shown on the loss modulus is related with events of varying relaxation times. The distribution parameters, as well as relaxation intensity, have been derived from the stress relaxation measurements. At even higher temperature, close to T_g, the mechanical response is due to α-relaxation which follows a VFT behavior.

The anelastic origin of the secondary relaxation is even more obvious in the case of $Fe_{55}Cr_{10}Mo_{14}C_{15}B_6$, where a thermal activated secondary relaxation occurs at temperatures 200 K below the glass transition region and the correspondent predominance of the α process. The activation energy of this low temperature anelastic event is 165 kJ/mol. As discussed in chapter 3, the presence of relaxations in conventional steels and other Fe-based crystalline materials with similar compositions have been reported since long ago. They are attributed to anelastic relaxations of crystalline materials and similar activation energies are reported. This may suggest a similar origin for the anelastic relaxation observed for the $Fe_{55}Cr_{10}Mo_{14}C_{15}B_6$ glass. However, the calculated activation energy is also close to the activation energy associated to Johari-Goldstein relaxations (171 kJ/mol), using the empirical $E_{act}=26RT_g$ rule.

Furthermore, it is interesting to note the two following points found in this work: Firstly, the physical aging explored by enthalpy measurements shows a log normal distribution of activation energies with a most probable value of activation energy of 174 kJ/mol. Secondly, the viscosity of this metallic glass, which was obtained by treating it as a Maxwell fluid, shows an activation energy of viscous flow slightly below T_g of around 180 kJ/mol. The apparent activation energies from different properties are therefore similar with each other, whether they come from the same microscopic mechanism still needs to be verified.

Isothermal creep measurements of $Pd_{42.5}Ni_{7.5}Cu_{30}P_{20}$ showed that in the glassy state viscous flow can be detected at quite low temperatures, as low as 200 K below T_g. By treating this alloy as a Newtonian liquid, the viscosity was also calculated in situ during the DMA measurements. The obtained viscosity agrees with the data from isothermal creep measurements. From the temperature dependent viscosity behavior, it is shown that at T_g the temperature dependent viscosity behavior changes from VFT to Arrhenius dynamics. A similar result has been also obtained for $Fe_{55}Cr_{10}Mo_{14}C_{15}B_6$ MG and it has been previously reported in other systems as discussed in chapter 3. We can conclude that microscopic movements leading to viscous flow are present in the system far below T_g. Furthermore, they have activation energies similar to those attributed to β-relaxation and physical aging. On the one hand this suggests the same microscopic origin for the three processes. On the other hand, this makes difficult the interpretation of the low temperature internal friction, termed as β-relaxation, as coming from reversible jumps between sub-basins of the potential energy landscape. In the classical picture, this type of secondary relaxations would not be able to activate viscous flow.

Based on continuous time random walk through meta basins in the potential energy landscape, Gupta developed a model which fits quite well the isostructural viscosity data[74]. It is also suggested that the viscous flow could be described in the framework of percolation theory[227]. Hunt suggested that transport occurs by atomic diffusion through thermally activated hopping over energy barriers at higher temperatures, while below a certain temperature T_c it becomes a percolative behavior[228]. From the solid state point of view, the

Arrhenius behavior of viscosity at low temperatures is also analyzed by Ferrarit in the framework of intrinsic defects with exponentially distributed activation energies[229]. It can also be explained in the framework of flow events[205]. The assessment of the predictions of these different models in order to elucidated the physical mechanisms responsible of sub-T_g viscous flow would be interesting to address in future work.

Stress relaxation is usually analyzed within the framework of KWW function. Within this approach, the underlying distribution of relaxation times is characterized by the value of the stretching exponent β_{KWW}, lower exponents implying a broader time distribution. In this work, the full relaxation behavior has been parameterized by a KWW function with all the parameters dependent on temperature: relaxation intensity, average relaxation time and stretching exponent. Results for the $Cu_{46}Zr_{46}Al_8$ and $Pd_{42.5}Ni_{7.5}Cu_{30}P_{20}$ glasses are given in sections 5.1 and 5.2. A more detailed analysis can also be performed within the framework of relaxation time spectrum. This methodology implies a relaxation time distribution as described in section 5.2.4 where viscous flow units can be regarded as having the longest relaxation time events on the relaxation time spectrum. This has been performed in this work for the $Pd_{42.5}Ni_{7.5}Cu_{30}P_{20}$ glass, finding three relaxation stages even near the glass transition temperature. As discussed in chapter 3, similar results have been already reported in metallic glasses when using similar techniques. The decomposition of the stretched relaxation into a fast and slow processes has been observed by Kursumovic[124,187], Ocelik[230] and Atzmon[189,190]. The results presented here show that, although the frequency response may show just one (α peak) or two (α and β peaks), the relaxation time spectrum is composed by different processes with differentiated times and activation energies. The convolution of all this processes results in the broad response functions collected in frequency-temperature DMA scans, i.e. the relaxation time in the KWW function is an average effect of all the three events found on the stress relaxation spectrum.

Besides of this, the mechanical relaxation of metallic glasses can be viewed as a merging of anelastic plus viscoplastic behaviors. As discussed above, the structural processes responsible of structural relaxation are linked

with the fundamental deformation events originating plastic deformation of MGs. These events could be associated to molecular rearrangements belonging to the broad peak of the α-relaxation, as in the case of $Cu_{46}Zr_{46}Al_8$, or to the secondary loss modulus peaks in $Pd_{42.5}Ni_{7.5}Cu_{30}P_{20}$ and $Fe_{55}Cr_{10}Mo_{14}C_{15}B_6$ glasses. In any case, the activation energies are similar to the ones expected for viscous flow (α-relaxation) once in the out-of-equilibrium (sub-T_g) glassy dynamics.

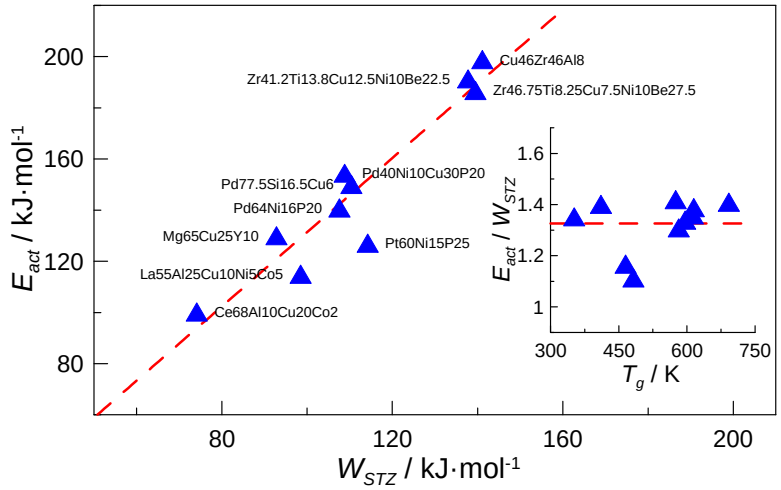

Figure 5-41 relationship between activation energy of shear transformation zone and apparent activation energy of α relaxation in non-equilibrium state in several MGs. Data of W_{STZ} and the VFT parameters obtained from reference[175,231].

Let us now discuss the implications of this point. Considering a well relaxed glass ($T_{fictive} \sim T_g$) and relaxation times following equation 3.3, the average activation energy of structural relaxation below T_g would be determined as $E_{act} = RB/(1-T_0/T_g)$. Considering MG systems with equilibrium dynamics above T_g determined by viscosity measurements and well described by a VFT behavior, the activation energy of the primary glass relaxation below T_g can be estimated from the B and T_0 parameters. This is performed and shown in figure 5-41, where for the calculation of the activation energies $T_{fictive}$ is chosen as T_g and data of the VFT parameters are obtained from references [175,231]. As shown in the figure, this estimated E_{act} is consistently well correlated with the W_{STZ}, the estimated work to activate a

shear transformation zone, with E_{act} being 30–40% higher in most of the systems.

Concerning to the effect of the fictive temperature, the ratio of activation energies between two isoconfigurational states can be estimated as $E_{act1}/E_{act2}=(1-T_0/T_{fictive1})/(1-T_0/T_{fictive2})$. For instance, in the $Cu_{46}Zr_{46}Al_8$ system of this work, an increase of 30 K of the fictive temperature produces a 10% reduction of the activation energy for primary relaxation (or viscous flow) below T_g. More significant than the changes in activation energy are the large changes in relaxation times between different glassy states. The effect of physical aging has been analyzed in the three metallic glasses examined in this work. In all three cases important changes of relaxation times and/or viscosity have been detected as shown in figures 5-11, 5-32 and 5-39. Our result shows that physical aging or structural relaxation influences viscosity, manifested on the fact that the more relaxed state has viscosity more than one order of magnitude higher than the as-quenched state.

However, the change from VFT to Arrhenius behavior happens in both relaxed and non-relaxed samples. The results from $Cu_{46}Zr_{46}Al_8$ showed that for the as-quenched state, due to the concurrent physical aging manifested on the changing of the fictive temperature, the average main relaxation time deviated from the Arrhenius behavior below T_g. On the contrary, the relaxed sample is expected to be in a nearly isoconfigurational state, i.e. with fixed fictive temperature, and it is then found to follow an Arrhenius behavior. Our result might favor the conclusion by Hunt that the major component of the curvature of the viscosity with decreasing temperature is from the change in transport type other than changes in structure[228].

Let us now consider that the system can sustain a maximum critical stress σ_c before inhomogeneous flow or fracture becomes activated. For deformation rates $\dot{\varepsilon} < \sigma_c/E\tau$, the glass is able to release stress via activation of primary relaxation rapidly enough to maintain the accumulated stress lower than σ_c. Therefore, the knowledge of the $\tau(T, T_{fictive})$ behavior can give an estimation of the limiting values of $\dot{\varepsilon}$ at a given working temperature. For instance, considering $Cu_{46}Zr_{46}Al_8$ at 500 K, an increase of the fictive temperature of 5 K would double the limiting deformation rate.

From the temperature dependent relaxation time, the fragility parameter *m* is usually employed to describe the dynamics. In the case of $Cu_{46}Zr_{46}Al_8$, using the temperature dependence of the relaxation time obtained from α relaxation we obtained *m*=57. In the case of $Pd_{42.5}Ni_{7.5}Cu_{30}P_{20}$, using relaxation time from α relaxation, in the framework of a local Arrhenius relationship, we obtained E_α=526 kJ/mol and *m*=50. Using relaxation times from stress relaxation spectrum, we obtained E_α=546 kJ/mol and *m*=52. In the case of $Fe_{55}Cr_{10}Mo_{14}C_{15}B_6$, α-relaxation manifested on the temperature dependence of viscosity gives E_α=746 kJ/mol and a corresponding *m*=49. They are all very similar values and correspond to metallic glasses able to sustain a certain degree of plastic deformation at temperatures well below T_g. The study of more rigid metallic glasses coming from stronger precursor liquids, for example with fragility parameters *m*<30, might be interesting as future work.

In section 5.1, the full shape of the experimental $E''(T)$ of $Cu_{46}Zr_{46}Al_8$ has been modeled considering a single Cole–Cole relaxation function with different relaxation time-temperature dependences above and below T_g. The validity of this model was confirmed by means of stress relaxation experiments, which gave direct access to the time domain response. In sections 5.2 and 5.3, the $Pd_{42.5}Ni_{7.5}Cu_{30}P_{20}$ and $Fe_{55}Cr_{10}Mo_{14}C_{15}B_6$ $E''(T)$ cannot be fitted with one single relaxation event. For $Pd_{42.5}Ni_{7.5}Cu_{30}P_{20}$, the α and β processes are close in a narrow temperature region, with the subsequent overlapping between the concurring mechanisms: thermally activated anelastic events, physical aging manifested as irreversible relaxation, and the viscosity related component which shows a change from an Arrhenius behavior to a VFT behavior at the glass transition. It is very difficult to distinguish between them, as the corresponding activation energies are close to each other. This does not allowed us to obtain a model able to reproduce the internal friction all over the whole frequency-temperature region probed in this work. For $Fe_{55}Cr_{10}Mo_{14}C_{15}B_6$, the lower temperature β process shows a conventional thermally activated anelastic behavior. At higher temperature, the increase of loss modulus comes from primary relaxation and reflects the flow of the whole structure. This system should be in principle more suitable to model, combining the two processes with well defined average relaxation

times and response functions. In both cases, achieving a detailed modeling of the $E''(\omega,T)$ behavior would be a good tool for predicting the different mechanical responses under different deformation rate and temperature conditions. Future work is being addressed in order to accomplish this objective.

6. Conclusions

The present knowledge and models for understanding the relaxation dynamics of metallic glasses have been discussed in this work, mainly in chapter 3. Above the glass transition temperature, this is in the metastable equilibrium region, the α-relaxation is responsible for viscous flow and shows a frequency-temperature behavior similar to that observed in other kinds of glass-forming substances. The relaxation in this temperature region is in general well understood. Below T_g, the system is arrested in the out-of-equilibrium, non-ergodic glassy state. In this temperature region the internal friction of metallic glasses shows different relaxation phenomena. Some of them, detected at temperature far below T_g can be thought as coming from microscopic processes similar to those already present in crystalline alloys. Approaching the glass transition, the presence of internal friction may have different aspects, going from just an excess wing of the principal α-peak to a well-defined loss peak with different degrees of overlapping with the α-relaxation.

The origin and characteristics of this sub-T_g internal friction of metallic glasses, as well as its relation to physical aging and mechanical deformation, has been revised. From the extensive study of experimental data and theoretical models performed in chapter 3, it is shown that β-relaxation, activation of shear transformation zones, physical aging, atomic diffusion, viscous flow and also sub-T_g α-relaxation all show very similar activation energies in a metallic glass. This tells that the microscopic movements implicated in all these processes may be very similar and it makes difficult to classify the different relaxations as coming from well differentiated origins.

The relaxation dynamics of MGs has been investigated using several techniques including differential scanning calorimetry, dynamic mechanical analysis, stress relaxation, creep and recovery. After production and basic characterization of many different metallic glass compositions, as it is described in chapter 4, the relaxation behavior was investigated in 3 different MGs On $E''(T)$ profile, in terms of β relaxation the three selected MGs ($Cu_{46}Zr_{46}Al_8$, $Pd_{42.5}Ni_{7.5}Cu_{30}P_{20}$ and $Fe_{55}Cr_{10}Mo_{14}C_{15}B_6$) show totally different behavior, namely excess wing, shoulder and differentiated peak respectively.

The characterization, modeling and origin of the sub-T_g internal friction has been presented and discussed in chapter 5.

In the case of $Cu_{46}Zr_{46}Al_8$, the relaxation behavior of this MG can be well described by a broad distribution of relaxation times. This distribution was modelled with a CC-function with a broadening parameter of value around 0.5 and an average relaxation time $\tau(T)$. The relaxation dynamics of the system can be then characterized by the $\tau(T)$ behavior, which follows VFT ($>T_g$) and AGV ($<T_g$) equations at least within the frequency and temperature windows explored. The results show that the low-temperature excess wing of internal loss is generated by the high-frequency tail of the α-relaxation. The induction of physical aging by annealing at temperatures near T_g and the comparison of the relaxation spectra for as quenched and aged samples allowed the characterization of the relaxation behavior of different glassy states. In this system, it is shown that the effect of physical aging on the relaxation dynamics can be well quantified through the definition of the glassy state by means of the fictive temperature parameter.

In the case of $Pd_{42.5}Ni_{7.5}Cu_{30}P_{20}$, the shoulder manifested on $E''(T)$ profile cannot be modeled by an empirical function because of its overlapping with the main relaxation. The intensity and temperature extension of the secondary peak is reduced by physical aging but, contrary to other systems reported in literature, the presence of the secondary peak is clear even in the well relaxed glassy states. The shoulder of the loss modulus obtained by DMA is related to the short time dynamics manifested from the stress relaxation experiments. Three different approaches have been applied to investigate the mechanical response of this MG. Stress, creep and recovery allowed us to separate the anelastic and viscoplastic part of the internal friction. The secondary relaxation is then mainly attributed to the anelastic part while the characteristics of the α-relaxation are coherent with the viscoplastic effect. However, both anelastic and viscoplastic contributions are merged in the response of this material. The relaxation time spectrum obtained by a proper fitting of the stress relaxation tests show a complex picture, with different time scales clearly involved in the relaxation processes. The longer time scale seems to dominate the viscous flow and α-relaxation while the shorter times are related to anelastic effects originating the loss shoulder.

In the case of $Fe_{55}Cr_{10}Mo_{14}C_{15}B_6$, the separate β relaxation on $E''(T)$ profile is clearly attributed to an anelastic event. The activation energy of this process is close to the activation energy for physical aging as well as the expected one for a Johari-Goldstein β-relaxation following the empirical relation between activation energy and T_g discussed in chapter 3.The microscopic origin of the β-relaxation in this material can be attributed to a process precursor of the main relaxation that controls viscous flow at higher temperatures within the standard picture of secondary-primary relaxations in glasses. The physical aging of this material is controlled by the same process, which is characterized by a broad distribution of relaxation times.

The temperature dependence of viscosity is also obtained for the $Pd_{42.5}Ni_{7.5}Cu_{30}P_{20}$ and $Fe_{55}Cr_{10}Mo_{14}C_{15}B_6$ MGs. The viscosity follows the expected glass-liquid transition when reaching values close to 10^{12} Pa·s in agreement with the T_g obtained by calorimetric measurements at similar heating rates. The determination of the viscosity from DMA measurements under continuous heating is coherent with that obtained from creep experiments in the steady flow regime, this confirming the validity of the measurements. The viscosity is found to follow Arrhenius behavior in the glassy state and shows a great influence of physical aging. The activation energy of viscous flow is found to be similar to the sub-T_g relaxation processes and to the physical aging, this confirming that in this temperature region the activation of any kind of structural rearrangement has to overcome the same energy barrier and, probably, it involves the same type of microscopic movements.

Finally, it has been discussed the intrinsic relationship between stress relaxation, viscous flow, internal friction and recovery tests with the mechanical behavior of metallic glasses. The author hopes that the extensive characterization of these processes presented in this work will help the understanding of physical aging effects, thermoplastic forming behavior and deformation microscopic mechanisms which are important issues for the application of metallic glasses as technological materials.

References

1. Klement, W.; Willens, R. H.; Duwez, P. Non-crystalline Structure in Solidified Gold-Silicon Alloys. *Nature* **1960**, *187*, 869–870.

2. Inoue, A.; Zhang, T.; Masumoto, T. Glass-forming ability of alloys. *J. Non. Cryst. Solids* **1993**, *156-158*, 473–480.

3. Inoue, A. Stabilization and high strain-rate superplasticity of metallic supercooled liquid. *Mater. Sci. Eng. A* **1999**, *267*, 171–183.

4. Inoue, A. Stabilization of metallic supercooled liquid and bulk amorphous alloys. *Acta Mater.* **2000**, *48*, 279–306.

5. Inoue, A.; Nishiyama, N.; Matsuda, T. Preparation of Bulk Glassy Pd40Ni10Cu30P20 Alloy of 40 mm in Diameter by Water Quenching. *Mater. Trans.* **1996**.

6. Inoue, A.; Nishiyama, N.; Kimura, H. Preparation and thermal stability of Bulk Amorophous Pd40Cu30Ni10P20 alloy cylinder of 72 mm in diameter. *Mater. Trans.* 1997, *38*, 179–183.

7. Peker, A.; Johnson, W. L. A Highly Processable Metallic Glass Zr41.2Ti13.8Cu12.5Ni10.0Be22.5. *Appl. Phys. Lett.* **1993**, *63*, 2342–2344.

8. Nishiyama, N.; Horino, M.; Haruyama, O.; Inoue, a. Undercooled liquid-to-glass transition during continuous cooling in Pd–Cu–Ni–P alloys. *Appl. Phys. Lett.* **2000**, *76*, 3914.

9. Li, Y.; Poon, S. J.; Shiflet, G. J.; Xu, J.; Kim, D. H.; Löffler, J. F. Formation of Bulk Metallic Glasses and Their Composites. *MRS Bull.* **2007**, *32*, 624–628.

10. Inoue, A. Bulk amorphous alloys with soft and hard magnetic properties. *Mater. Sci. Eng. A* **1997**, *226-228*, 357–363.

11. Mitera, M.; Masumoto, T.; Kazama, N. S. Effect of silicon additions on the magnetic properties of Fe-B-C amorphous alloys. *J. Appl. Phys.* **1979**, *50*, 7609–7611.

12. Demetriou, M.; Launey, M. E.; Garrett, G.; Schramm, J. P.; Hofmann, D. C.; Johnson, W. L.; Ritchie, R. O. A damage-tolerant glass. *Nat. Mater.* **2011**, *10*, 123–128.

13. Trexler, M. M.; Thadhani, N. N. Mechanical properties of bulk metallic glasses. *Prog. Mater. Sci.* **2010**, *55*, 759–839.

14. Zhang, B.; Zhao, D. Q.; Pan, M. X.; Wang, W. H.; Greer, a. L. Amorphous metallic plastic. *Phys. Rev. Lett.* **2005**, *94*, 205502.

15. Suryanarayana, C.; Inoue, A. Iron-based bulk metallic glasses. *Int. Mater. Rev.* **2013**, *58*, 131–166.

16. Ashby, M. F.; Greer, A. L. Metallic glasses as structural materials. *Scr. Mater.* **2006**, *54*, 321–326.

17. Greer, A. L. Metallic glasses. In *Physical metallurgy*; Elsevier, 2014; pp. 305–384.

18. Turnbull, D. Under what conditions can a glass be formed? *Contemp. Phys.* **1969**, *10*, 473–488.

19. Yang, B.; Du, Y.; Liu, Y. Recent progress in criterions for glass forming ability. *Trans. Nonferrous Met. Soc. China* **2009**, *19*, 78–84.

20. Cai, A.; Sun, G.; Pan, Y. Evaluation of the parameters related to glass-forming ability of bulk metallic glasses. *Mater. Des.* **2006**, *27*, 479–488.

21. Ma, C. S.; Zhang, J.; Chang, X. C.; Hou, W. L.; Wang, J. Q. Electronegativity difference as a factor for evaluating the thermal stability of Al-rich metallic glasses. *Philos. Mag. Lett.* **2008**, *88*, 917–924.

22. Guo, F. .; Poon, S. .; Shiflet, G. . Investigation of glass formability in Al-based multinary alloys. *Scr. Mater.* **2000**, *43*, 1089–1095.

23. Duan, G.; Xu, D.; Johnson, W. L. High Copper Content Bulk Glass Formation in Bimetallic Cu-Hf System. *Metall. Mater. Trans. A* **2005**, *36*, 455–458.

24. Cheung, T. L.; Shek, C. H. Thermal and mechanical properties of Cu-Zr-Al bulk metallic glasses. *J. Alloys Compd.* **2007**, *434-435*, 71–74.

25. Jia, P.; Guo, H.; Li, Y.; Xu, J.; Ma, E. A new Cu–Hf–Al ternary bulk metallic glass with high glass forming ability and ductility. *Scr. Mater.* **2006**, *54*, 2165–2168.

26. Gong, P.; Yao, K.; Wang, X.; Shao, Y. Centimeter-sized Ti-based bulk metallic glass with high specific strength. *Prog. Nat. Sci. Mater. Int.* **2012**, *22*, 401–406.

27. Ponnambalam, V.; Poon, S. J.; Shiflet, G. J. Fe-based bulk metallic glasses with diameter thickness larger than one centimeter. *J. Mater. Res.* **2004**, *19*, 1320–1323.

28. Yoshio, W. *The structure of non crystalline materials liquids and amorphous solids*; McGraw-Hill International Book Co.: New York, 1980.

29. Bernal, J. D. The Bakerian Lecture, 1962. The Structure of Liquids. *Proc. R. Soc. A Math. Phys. Eng. Sci.* **1964**, *280*, 299–322.

30. Ichitsubo, T.; Matsubara, E.; Yamamoto, T.; Chen, H. S.; Nishiyama, N.; Saida, J.; Anazawa, K. Microstructure of fragile metallic glasses inferred from ultrasound-accelerated crystallization in Pd-based metallic glasses. *Phys. Rev. Lett.* **2005**, *95*, 245501.

31. Kim, D. H.; Kim, W. T.; Park, E. S.; Mattern, N.; Eckert, J. Phase separation in metallic glasses. *Prog. Mater. Sci.* **2013**, *58*, 1103–1172.

32. Deng, D.; Argon, A. S. Structural relaxation and embrittlement of Cu59Zr41 and Fe80B20 glasses. *Acta Metall.* **1986**, *34*, 2011–2023.

33. Sun, B. B.; Wang, Y. B.; Wen, J.; Yang, H.; Sui, M. L.; Wang, J. Q.; Ma, E. Artifacts induced in metallic glasses during TEM sample preparation. *Scr. Mater.* **2005**, *53*, 805–809.

34. Deng, J. W.; Du, K.; Wu, B.; Sui, M. L. Nanometer to micrometer scaled inhomogeneous etching of bulk metallic glasses by ion sputtering. *Intermetallics* **2013**, *34*, 75–82.

35. Park, E. S.; Kyeong, J. S.; Kim, D. H. Phase separation and improved plasticity by modulated heterogeneity in Cu-(Zr, Hf)-(Gd, Y)-Al metallic glasses. *Scr. Mater.* **2007**, *57*, 49–52.

36. Chen, L.; Fu, Z.; Zhang, G.; Hao, X.; Jiang, Q.; Wang, X.; Cao, Q.; Franz, H.; Liu, Y.; Xie, H.; Zhang, S.; Wang, B.; Zeng, Y.; Jiang, J. New Class of Plastic Bulk Metallic Glass. *Phys. Rev. Lett.* **2008**, *100*, 075501.

37. Pan, J.; Liu, L.; Chan, K. C. Enhanced plasticity by phase separation in CuZrAl bulk metallic glass with micro-addition of Fe. *Scr. Mater.* **2009**, *60*, 822–825.

38. Tian, L.; Cheng, Y.-Q.; Shan, Z.-W.; Li, J.; Wang, C.-C.; Han, X.-D.; Sun, J.; Ma, E. Approaching the ideal elastic limit of metallic glasses. *Nat. Commun.* **2012**, *3*, 609.

39. Yang, B. J.; Yao, J. H.; Zhang, J.; Yang, H. W.; Wang, J. Q.; Ma, E. Al-rich bulk metallic glasses with plasticity and ultrahigh specific strength. *Scr. Mater.* **2009**, *61*, 423–426.

40. Guo, H.; Yan, P. F.; Wang, Y. B.; Tan, J.; Zhang, Z. F.; Sui, M. L.; Ma, E. Tensile ductility and necking of metallic glass. *Nat. Mater.* **2007**, *6*, 735–739.

41. Schuh, C. A.; Hufnagel, T. C.; Ramamurty, U. Mechanical behavior of amorphous alloys. *Acta Mater.* **2007**, *55*, 4067–4109.

42. Trexler, M. M.; Thadhani, N. N. Mechanical properties of bulk metallic glasses. *Prog. Mater. Sci.* **2010**, *55*, 759–839.

43. Lewandowski, J. J.; Wang, W. H.; Greer, A. L. Intrinsic plasticity or brittleness of metallic glasses. *Philos. Mag. Lett.* **2005**, *85*, 77–87.

44. Spaepent, F. A MECHANISM FOR STEADY STATE INHOMOGENEOUS FLOW IN METALLIC GLASSES. *Acta Metall.* **1976**, *25*, 407–145.

45. Inoue, A.; Fan, C.; Saida, J.; Zhang, T. High-strength Zr-based bulk amorphous alloys containing nanocrystalline and nanoquasicrystalline particles. *Sci. Technol. Adv. Mater.* **2000**, *1*, 73–86.

46. Ito, H.; Yamamoto, T.; Hasegawa, M.; Inoue, A. Effect of Nanocrystal Distribution on Mechanical Properties of Ti-Based Metallic Glasses. *Mater. Trans.* **2007**, *48*, 1288–1291.

47. Foley, J. C.; Allen, D. R.; Perepezko, J. H. strategies for the development of nanocrystalline materials through devitrification. *Mater. Sci. Eng.* **1997**, *226-228*, 569–573.

48. He, G.; Eckert, J.; Löser, W.; Schultz, L. Novel Ti-base nanostructure-dendrite composite with enhanced plasticity. *Nat. Mater.* **2003**, *2*, 33–37.

49. Guo, S. F.; Liu, L.; Li, N.; Li, Y. Fe-based bulk metallic glass matrix composite with large plasticity. *Scr. Mater.* **2010**, *62*, 329–332.

50. Hofmann, D. C.; Suh, J.-Y.; Wiest, A.; Duan, G.; Lind, M.-L.; Demetriou, M. D.; Johnson, W. L. Designing metallic glass matrix composites with high toughness and tensile ductility. *Nature* **2008**, *451*, 1085.

51. Hofmann, D. C.; Suh, J.-Y.; Wiest, A.; Lind, M.-L.; Demetriou, M. D.; Johnson, W. L. Development of tough, low-density titanium-based bulk metallic glass matrix composites with tensile ductility. *Proc. Natl. Acad. Sci. U. S. A.* **2008**, *105*, 20136–20140.

52. Xu, Y. K.; Xu, J. Ceramics particulate reinforced Mg 65 Cu 20 Zn 5 Y 10 bulk metallic glass composites. *Scr. Mater.* **2003**, *49*, 843–848.

53. Xu, Y. K.; Ma, H.; Xu, J.; Ma, E. Mg-based bulk metallic glass composites with plasticity and gigapascal strength. *Acta Mater.* **2005**, *53*, 1857–1866.

54. Brothers, A. H.; Dunand, D. C. Ductile bulk metallic glass foams. *Adv. Mater.* **2005**, *17*, 484–486.

55. Sarac, B.; Schroers, J. Designing tensile ductility in metallic glasses. *Nat. Commun.* **2013**, *4*, 2158.

56. Pauly, S.; Das, J.; Bednarcik, J.; Mattern, N.; Kim, K.; Kim, D.; Eckert, J. Deformation-induced martensitic transformation in Cu–Zr–(Al,Ti) bulk metallic glass composites. *Scr. Mater.* **2009**, *60*, 431–434.

57. Ding, S.; Liu, Y.; Li, Y.; Liu, Z.; Sohn, S.; Walker, F. J.; Schroers, J. Combinatorial development of bulk metallic glasses. *Nat. Mater.* **2014**, *13*, 494.

58. Battezzati, L.; Greer, A. L. The viscosity of Liquid Metals and Alloys. *Acta Metall.* **1989**, *37*, 1791–1802.

59. Volkert, C. A.; Spaepen, F. Crossover relaxation of the viscosity of Pd40Ni40P19Si1 near the glass transition. *Acta Metall.* **1989**, *37*, 1355–1362.

60. Taub, A. I.; SPAEPEN, F. The kinetics of structural relaxation of a metallic glass. *Acta Metall.* **1980**, *28*, 1781–1788.

61. Taub, A. I.; Spaepen, F. Ideal elastic, anelastic and viscoelastic deformation of a metallic glass. *J. Mater. Sci.* **1981**, *16*, 3087–3092.

62. Tsao, S. .; Spaepen, F. Structural relaxation of a metallic glass near equilibrium. *Acta Metall.* **1985**, *33*, 881–889.

63. Spaepen, F. A microscopic mechanism for steady state inhomogeneous flow in metallic glasses. *Acta Metall.* **1977**, *25*, 407–415.

64. Mckenna, G. B. Glass dynamics: Diverging views on glass transition. *Nat. Phys.* **2008**, *4*, 673.

65. Stickel, F.; Fischer, E. W.; Richert, R. Dynamics of glass-forming liquids. II. Detailed comparison of dielectric relaxation, dc-conductivity, and viscosity data. *J. Chem. Phys.* **1996**, *104*, 2043.

66. Alba-Simionesco, C. Salient properties of glassforming liquids close to the glass transition. *Comptes Rendus l'Académie des Sci. - Ser. IV - Phys.* **2001**, *2*, 203–216.

67. Evenson, Z.; Schmitt, T.; Nicola, M.; Gallino, I.; Busch, R. High temperature melt viscosity and fragile to strong transition in Zr–Cu–Ni–Al–Nb(Ti) and Cu47Ti34Zr11Ni8 bulk metallic glasses. *Acta Mater.* **2012**, *60*, 4712–4719.

68. Fan, G. J.; Fecht, H. J.; Lavernia, E. J. Viscous flow of the Pd43Ni10Cu27P20 bulk metallic glass-forming liquid. *Appl. Phys. Lett.* **2004**, *84*, 487–489.

69. Ott, R. T.; Heggen, M.; Feuerbacher, M.; Park, E. S.; Kim, D. H.; Kramer, M. J.; Besser, M. F.; Sordelet, D. J. Anelastic strain and structural anisotropy in homogeneously deformed Cu64.5Zr35.5 metallic glass. *Acta Mater.* **2008**, *56*, 5575–5583.

70. Suryanarayana, C.; Inoue, A. *Bulk metallic glasses*; Taylor& Francis group, 2011.

71. Yu, H. B.; Shen, X.; Wang, Z.; Gu, L.; Wang, W. H.; Bai, H. Y. Tensile Plasticity in Metallic Glasses with Pronounced beta Relaxations. *Phys. Rev. Lett.* **2012**, *108*, 015504.

72. Yu, H. Bin; Samwer, K.; Wang, W. H.; Bai, H. Y. Chemical influence on β-relaxations and the formation of molecule-like metallic glasses. *Nat. Commun.* **2013**, *4*, 2204.

73. Yu, H. B.; Wang, W. H.; Bai, H. Y.; Wu, Y.; Chen, M. W. Relating activation of shear transformation zones to β relaxations in metallic glasses. *Phys. Rev. B* **2010**, *81*, 220201.

74. Gupta, P. K.; Heuer, A. Physics of the iso-structural viscosity. *J. Non. Cryst. Solids* **2012**, *358*, 3551–3558.

75. Das, J.; Tang, M.; Kim, K.; Theissmann, R.; Baier, F.; Wang, W.; Eckert, J. "Work-Hardenable" Ductile Bulk Metallic Glass. *Phys. Rev. Lett.* **2005**, *94*, 205501.

76. Pauly, S.; Gorantla, S.; Wang, G.; Kühn, U.; Eckert, J. Transformation-mediated ductility in CuZr-based bulk metallic glasses. *Nat. Mater.* **2010**, *9*, 473–477.

77. Amir, A.; Oreg, Y.; Imry, Y. On relaxations and aging of various glasses. *Proc. Natl. Acad. Sci.* **2012**, *109*, 1850–1855.

78. Duarte, M. J.; Klemm, J.; Klemm, S. O.; Mayrhofer, K. J. J.; Stratmann, M.; Borodin, S.; Romero, A. H.; Madinehei, M.; Crespo, D.; Serrano, J.; Gerstl, S. S. A.; Choi, P. P.; Raabe, D.; Renner, F. U. Element-resolved corrosion analysis of stainless-type glass-forming steels. *Science (80-.).* **2013**, *341*, 372.

79. Chen, M. Mechanical Behavior of Metallic Glasses: Microscopic Understanding of Strength and Ductility. *Annu. Rev. Mater. Res.* **2008**, *38*, 445–469.

80. Liu, C.; Pineda, E.; Crespo, D. Mechanical Relaxation of Metallic Glasses: An Overview of Experimental Data and Theoretical Models. *Metals (Basel).* **2015**, *5*, 1073–1111.

81. Angell, C. A. Relaxation in liquids, polymers and plastic crystals strong/fragile patterns and problems. *J. Non. Cryst. Solids* **1991**, *131-133*, 13–31.

82. Stillinger, F. H.; Debenedetti, P. G. Glass Transition Thermodynamics and Kinetics. *Annu. Rev. Condens. Matter Phys.* **2013**, *4*, 263–285.

83. Debenedetti, P. G.; Stillinger, F. H. Supercooled liquids and the glass transition. *Nature* **2001**, *410*, 259–67.

84. Dyre, J. C. Colloquium: The glass transition and elastic models of glass-forming liquids. *Rev. Mod. Phys.* **2006**, *78*, 953–972.

85. Angell, C. A.; Ngai, K. L.; McKenna, G. B.; MaMillan, P. F.; Martin, S. W. Relaxation in glassforming liquids and amorphous solids. *J.Appl.Phys.* **2000**, *88*, 3113–3157.

86. Böhmer, R.; Ngai, K. L.; Angell, C. A.; Plazek, D. J. Nonexponential relaxations in strong and fragile glass formers. *J. Chem. Phys.* **1993**, *99*, 4201–4209.

87. Johari, G. P.; Goldstein, M. Viscous liquids and the glass transition. II. Secondary relaxations in glasses of rigid molecules. *J. Chem. Phys.* **1970**, *53*, 2372–2388.

88. Gotze, W.; Sjogren, L. Relaxation processes in supercooled liquids. *Reports Prog. Phys.* **1992**, *55*, 241–370.

89. Borrego, J. M.; Conde, C. F.; Conde, a. Structural relaxation processes in FeSiB-Cu(Nb, X), X=Mo, V, Zr, Nb glassy alloys. *Mater. Sci. Eng. A* **2001**, *304-306*, 491–494.

90. Kumar, G.; Neibecker, P.; Liu, Y. H.; Schroers, J. Critical fictive temperature for plasticity in metallic glasses. *Nat. Commun.* **2013**, *4*, 1536.

91. Hodge, I. M. Enthalpy relaxation and recovery in amorphous materials. *J. Non. Cryst. Solids* **1994**, *169*, 211–266.

92. Hodge, I. M. Effects of Annealing and Prior History on Enthalpy Relaxation in Glassy-Polymers .6. Adam-Gibbs Formulation of Nonlinearity. *Macromolecules* **1987**, *20*, 2897–2908.

93. Tool, A. Q. Relation Between Inelastic Deformability and Thermal Expansion of Glass in Its Annealing Range. *J. Am. Ceram. Soc.* **1946**, *29*, 240–253.

94. Moynihan, C. T.; Macedo, P. B.; Montrose, C. J.; Gupta, P. K.; DeBolt, M. a.; Dill, J. F.; Dom, B. E.; Drake, P. W.; Easteal, A. J.; Elterman, P. B.; Moeller, R. P.; Sasabe, H.; Wilder, J. A. Structural Relaxation in Vitreous Materials. *Ann. N. Y. Acad. Sci.* **1976**, *279*, 15–35.

95. Narayanaswamy, O. S. A Model of Structural Relaxation in Glass. *J. Am. Ceram. Soc.* **1971**, *54*, 491–498.

96. Lunkenheimer, P.; Wehn, R.; Schneider, U.; Loidl, A. Glassy aging dynamics. *Phys. Rev. Lett.* **2005**, *95*, 055702.

97. Chen, H. S.; Coleman, E. Structure relaxation spectrum of metallic glasses. *Appl. Phys. Lett.* **1976**, *28*, 245–247.

98. Tsyplakov, A. N.; Mitrofanov, Y. P.; Makarov, A. S.; Afonin, G. V.; Khonik, V. A. Determination of the activation energy spectrum of structural relaxation in metallic glasses using calorimetric and shear modulus relaxation data. *J. Appl. Phys.* **2014**, *116*, 123507.

99. Granato, A. V.; Khonik, V. A. An interstitialcy theory of structural relaxation and related viscous flow of glasses. *Phys. Rev. Lett.* **2004**, *93*, 155502.

100. Khonik, S. V.; Granato, A. V.; Joncich, D. M.; Pompe, A.; Khonik, V. A. Evidence of distributed interstitialcy-like relaxation of the shear modulus due to structural relaxation of metallic glasses. *Phys. Rev. Lett.* **2008**, *100*, 065501.

101. Nagel, C.; Rätzke, K.; Schmidtke, E.; Faupel, F.; Ulfert, W. Positron-annihilation studies of free-volume changes in the bulk metallic glass Zr65Al7.5Ni10Cu17.5 during structural relaxation and at the glass transition. *Phys. Rev. B* **1999**, *60*, 9212–9215.

102. Van den Beukel, A.; Radelaar, S. On the Kinetics of Structural Relaxation in Metallic Glasses. *Acta Mater.* **1983**, *31*, 419–427.

103. Van den Beukel, A.; van der Zwaag, S.; Mulder, A. L. A semi quantitative description of the kinetics of structural relaxataion in amorphous Fe40Ni40B20. *Acta Metall.* **1984**, *32*, 1895–1902.

104. Borrego, J. M.; Blázquez, J. S.; Lozano-Pérez, S.; Kim, J. S.; Conde, C. F.; Conde, a. Structural relaxation in Fe(Co)SiAlGaPCB amorphous alloys. *J. Alloys Compd.* **2014**, *584*, 607–610.

105. Gibbs, M. R. J.; Sinning, H. R. A critique of the roles of TSRO and CSRO in metallic glasses by application of the activation energy spectrum model to dilatometric data. *J. Mater. Sci.* **1985**, *20*, 2517–2525.

106. Khonik, V. A.; Kosilov, A. T.; Mikhailov, V. A.; Sviridov, V. V. Isothermal creep of metallic glasses: a new approach and its experimental verification. *Acta Mater.* **1998**, *46*, 3399–3408.

107. Khonik, V. A. The Kinetics of Irreversible Structural Relaxation and Homogeneous Plastic Flow of Metallic Glasses. *Phys. Status Solidi A* **2000**, *177*, 173–189.

108. Khonik, V. A. The kinetics of irreversible structural relaxation and rheological behavior of metallic glasses under quasi-static loading. *J. Non. Cryst. Solids* **2001**, *296*, 147–157.

109. Ruta, B.; Baldi, G.; Monaco, G.; Chushkin, Y. Compressed correlation functions and fast aging dynamics in metallic glasses. *J. Chem. Phys.* **2013**, *138*, 054508.

110. Zhai, F.; Pineda, E.; Ruta, B.; Gonzalez-Silveira, M.; Crespo, D. Aging and structural relaxation of hyper-quenched Mg65Cu25Y10 metallic glass. *J. Alloys Compd.* **2014**, *615*, s9–s12.

111. Hu, L.; Zhou, C.; Zhang, C.; Yue, Y. Thermodynamic anomaly of the sub-Tg relaxation in hyperquenched metallic glasses. *J. Chem. Phys.* **2013**, *138*, 174508.

112. Tsyplakov, A. N.; Mitrofanov, Y. P.; Khonik, V. A.; Kobelev, N. P.; Kaloyan, A. A. Relationship between the heat flow and relaxation of the shear modulus in bulk PdCuP metallic glass. *J. Alloys Compd.* **2015**, *618*, 449–454.

113. Chen, H. S. GLASS TRANSITION AND SECONDARY RELAXATION IN METAL GLASSES. In *amorphous metals and semiconductors*; Haasen, P.; Jaffee, R. I., Eds.; Pergamon Press: Coronado, 1985; pp. 126–150.

114. Maddin, R.; Masumoto, T. The deformation of amorphous palladium-20 at.% silicon. *Mater. Sci. Eng.* **1972**, *9*, 153–162.

115. Cohen, M. H.; Turnbull, D. Molecular Transport in Liquids and Glasses. *J. Chem. Phys.* **1959**, *31*, 1164–1169.

116. Turnbull, D.; Cohen, M. H. Free Volume Model of the Amorphous Phase: Glass Transition. *J. Chem. Phys.* **1961**, *34*, 120–125.

117. Turnbull, D.; Cohen, M. H. On the Free-Volume Model of the Liquid-Glass Transition. *J. Chem. Phys.* **1970**, *52*, 3038–3041.

118. Jackle, J. Models of the glass transition. *Reports Prog. Phys.* **1986**, *49*, 171–231.

119. Goldstein, M. Viscous Liquids and the Glass Transition: A Potential Energy Barrier Picture. *J. Chem. Phys.* **1969**, *51*, 3728.

120. Ngai, K. L.; Paluch, M. Classification of secondary relaxation in glass-formers based on dynamic properties. *J. Chem. Phys.* **2004**, *120*, 857–873.

121. Ngai, K. L. Johari-Goldstein relaxation as the origin of the excess wing observed in metallic glasses. *J. Non. Cryst. Solids* **2006**, *352*, 404–408.

122. Nowick, A. S.; Berry, B. S. *Anelastic relaxation in Crystalline solids*; Academic Press, Inc: New York and London, 1972.

123. Ngai, K. L. *Relaxation and Diffusion in Complex systems*; Springer, 2011.

124. Kuršumović, a.; Cantor, B. Anelastic crossover and creep recovery spectra in Fe40Ni40B20 metallic glass. *Scr. Mater.* **1996**, *34*, 1655–1660.

125. Jiao, W.; Wen, P.; Peng, H. L.; Bai, H. Y.; Sun, B. a.; Wang, W. H. Evolution of structural and dynamic heterogeneities and activation energy distribution of deformation units in metallic glass. *Appl. Phys. Lett.* **2013**, *102*, 101903.

126. Hermida, É. B. Description of the Mechanical Properties of Viscoelastic Materials Using a Modified Anelastic Element. *Phys. Status Solidi* **1993**, *178*, 311–327.

127. Alvarez, F.; Alegria, A.; Colmenero, J. relationship between the time domain Kohlrausch Williams Watts and frequency domain Havriliak Negami relaxation functions. *Phys. Rev. B* **1991**, *44*, 7306–7312.

128. Svanberg, C. Correlation function for relaxations in disordered materials. *J. Appl. Phys.* **2003**, *94*, 4191–4197.

129. Qiao, J.; Casalini, R.; Pelletier, J.-M. M.; Kato, H. Characteristics of the structural and Johari-Goldstein relaxations in Pd-based metallic glass-forming liquids. *J. Phys. Chem. B* **2014**, *118*, 3720–3730.

130. Blanter, M. S. S.; Neuhauser, H.; Golovin, I. S. S.; Sinning, H.-R.-R.; Neuhauser, H.; Sinning, H.-R.-R. *Internal friction in metallic materials*; springer, 2001; Vol. 3.

131. Wen, P.; Zhao, D. Q.; Pan, M. X.; Wang, W. H.; Huang, Y. P.; Guo, M. L. Relaxation of metallic Zr46.75Ti8.25Cu7.5Ni10Be27.5 bulk glass-forming supercooled liquid. *Appl. Phys. Lett.* **2004**, *84*, 2790–2792.

132. Magalas, L. B. Mechanical spectroscopy, internal friction and ultrasonic attenuation: Collection of works. *Mater. Sci. Eng. A* **2009**, *521-522*, 405–415.

133. Castellero, A.; Moser, B.; Uhlenhaut, D. I.; Dalla Torre, F. H.; Löffler, J. F. Room-temperature creep and structural relaxation of Mg–Cu–Y metallic glasses. *Acta Mater.* **2008**, *56*, 3777–3785.

134. Wang, W. H. The elastic properties, elastic models and elastic perspectives of metallic glasses. *Prog. Mater. Sci.* **2011**, *57*, 487–656.

135. Qiao, J. C.; Pelletier, J. M. Dynamic mechanical analysis in La-based bulk metallic glasses: Secondary (β) and main (α) relaxations. *J. Appl. Phys.* **2012**, *112*, 083528.

136. Ruta, B.; Chushkin, Y.; Monaco, G.; Cipelletti, L.; Pineda, E.; Bruna, P.; Giordano, V. M.; Gonzalez-Silveira, M. Atomic-scale relaxation dynamics and aging in a metallic glass probed by X-ray photon correlation spectroscopy. *Phys. Rev. Lett.* **2012**, *109*, 165701.

137. Wang, L.-M.; Liu, R.; Wang, W. H. Relaxation time dispersions in glass forming metallic liquids and glasses. *J. Chem. Phys.* **2008**, *128*, 164503.

138. Meyer, A.; Busch, R.; Schober, H. Time-Temperature Superposition of Structural Relaxation in a Viscous Metallic Liquid. *Phys. Rev. Lett.* **1999**, *83*, 5027–5029.

139. Qiao, J. C.; Pelletier, J. M. Dynamic universal characteristic of the main (α) relaxation in bulk metallic glasses. *J. Alloys Compd.* **2014**, *589*, 263–270.

140. Casalini, R.; Roland, C. M. Aging of the secondary relaxation to probe structural relaxation in the glassy state. *Phys. Rev. Lett.* **2009**, *102*, 035701.

141. Berry, B. S.; Pritchet, W. C.; Tsuei, C. C. Discovery of an internal-friction peak in the metallic glass Nb3Ge. *Phys. Rev. Lett.* **1978**, *41*, 410–413.

142. Berry, B. S.; Pritchet, W. C. C. Hydrogen related internal friction peaks in metallic glasses. *Scr. Mater.* **1981**, *15*, 637–642.

143. Yoon, H. N.; Eisenberg, A. Dynamic mechanical properties of metallic glasses. *J. Non. Cryst. Solids* **1978**, *29*, 357–364.

144. Fukuhara, M.; Wang, X.; Inoue, A.; Yin, F. Low temperature dependence of elastic parameters and internal frictions for glassy alloy Zr55Cu30Al10Ni5. *phys. stat. sol.(RRL)* **2007**, *1*, 220–222.

145. Kunzi, H. U. U.; Agyeman, K.; Guntherodt, H.-J. internal friction peaks in metallic glasses. *Solid State Commun.* **1979**, *32*, 711–714.

146. Zdaniewski, W. A.; Rindone, G. E.; Day, D. E. The internal friction of glasses. *J. Mater. Sci.* **1979**, *14*, 763–775.

147. Khonik, V. A.; Spivak, L. V. On the nature of low temperature internal friction peaks in metallic glasses. *Acta Mater.* **1996**, *44*, 367–381.

148. Egami, T.; Maeda, K.; Vitek, V. Structural defects in amorphous solids A computer simulation study. *Philos. Mag. A* **1980**, *41*, 883–901.

149. Okumura, H.; Inoue, A.; Masumoto, T. Glass transition and viscoelastic behaviors of La55Al25Ni20 and La55Al25Cu20 amorphous alloys. *Mater. Trans.* **1991**.

150. Okumura, H.; Chen, H. S.; Inoue, A.; Masumoto, T. Sub-Tg mechanical relaxation of a La55A125Ni20 amorphous alloy. *J. Non. Cryst. Solids* **1991**, *130*, 304–310.

151. Qiao, J.; Pelletier, J.-M.; Casalini, R. Relaxation of bulk metallic glasses studied by mechanical spectroscopy. *J. Phys. Chem. B* **2013**, *117*, 13658–13666.

152. Wang, Z.; Yu, H. B.; Wen, P.; Bai, H. Y.; Wang, W. H. Pronounced slow beta-relaxation in La-based bulk metallic glasses. *J. PHYSICS-CONDENSED MATTER* **2011**, *23*, 142202.

153. Chen, H. S.; Morito, N. Sub-Tg α′ relaxation in a PdCuSi glass; internal friction measurements. *J. Non. Cryst. Solids* **1985**, *72*, 287–299.

154. Evenson, Z.; Naleway, S. E.; Wei, S.; Gross, O.; Kruzic, J. J.; Gallino, I.; Possart, W.; Stommel, M.; Busch, R. β relaxation and low-temperature aging in a Au-based bulk metallic glass: From elastic properties to atomic-scale structure. *Phys. Rev. B* **2014**, *89*, 174204.

155. Okumura, H.; Inoue, A.; Masumoto, T. heating rate dependence of two glass transitions and phase separation for a La55Al25Ni20 amorphous alloy. *Acta Met. mater* **1993**, *41*, 915–921.

156. Louzguine-Luzgin, D. V.; Seki, I.; Yamamoto, T.; Kawaji, H.; Suryanarayana, C.; Inoue, A. Double-stage glass transition in a metallic glass. *Phys. Rev. B* **2010**, *81*, 144202.

157. Cohen, Y.; Karmakar, S.; Procaccia, I.; Samwer, K. The nature of the β-peak in the loss modulus of amorphous solids. *EPL (Europhysics Lett.* **2012**, *100*, 36003.

158. Yu, H. B.; Samwer, K.; Wu, Y.; Wang, W. H. Correlation between belta relaxation and self-diffusion of the smallest constituting atoms in metallic glasses. *Phys. Rev. Lett.* **2012**, *109*, 095508.

159. Liu, Y. H.; Fujita, T.; Aji, D. P. B.; Matsuura, M.; Chen, M. W. Structural origins of Johari-Goldstein relaxation in a metallic glass. *Nat. Commun.* **2014**, *5*, 3238.

160. Morito, N.; Egami, T. Internal friction and reversible structural relaxation in the metallic glass Fe32Ni36Cr14P12B6. *Acta Metall.* **1984**, *32*, 603–613.

161. Bohonyey, A.; Kiss, L. F. A quantitative study on reversible structural relaxation of metallic glasses. *J. Phys. Condens. Matter* **1999**, *3*, 4523–4531.

162. Pineda, E.; Bruna, P.; Ruta, B.; Gonzalez-Silveira, M.; Crespo, D. Relaxation of rapidly quenched metallic glasses: Effect of the relaxation state on the slow low temperature dynamics. *Acta Mater.* **2013**, *61*, 3002–3011.

163. Hettwer, K. J.; Haessner, F. Influence of heat treatment on the internal friction of metglas Fe32Ni36Cr14P12B6. *Mater. Sci. Eng.* **1982**, *52*, 147–154.

164. Kiss, S.; Posgay, G.; Harangozo, I. Z.; Kedves, F. J. structural relaxation and crystallization of FeB and NiP metallic glasses followed by internal friction and modulus measurements. *J. Phys.* **1981**, *10*, C5–529.

165. Hausch G Internal friction and ultrasonic attenuation in solids, 1977.

166. Morito, N.; Egami, T. internal friction of a glassy metal Fe32Ni36Cr14P12B6. In *IEEE TRANSACTIONS ON MAGNETICS*; 1983; Vol. 5, pp. 1898–1900.

167. Morito, N. Internal friction study on structural relaxation of glassy metal Fe32Ni36Cr14P12B6. *Mater. Sci. Eng.* **1983**, *60*, 261–268.

168. Deng, D.; Argon, a. S. Analysis of the effect of aging on distributed relaxations, hardness, and embrittlement in Cu59Zr41 and Fe80B20 glasses. *Acta Metall.* **1986**, *34*, 2025–2038.

169. Olsen, N. B.; Christensen, T.; Dyre, J. C. Time-temperature superposition in viscous liquids. *Phys. Rev. Lett.* **2001**, *86*, 1271–1274.

170. Pelletier, J. M.; Van de Moortèle, B.; Lu, I. R. Viscoelasticity and viscosity of Pd–Ni–Cu–P bulk metallic glasses. *Mater. Sci. Eng. A* **2002**, *336*, 190–195.

171. Jeong, H. T.; Fleury, E.; Kim, W. T.; Kim, D. H.; Hono, K. Study on the Mechanical Relaxations of a Zr36Ti24Be40 Amorphous Alloy by Time-Temperature Superposition Principle. *J. Phys. Soc. Japan* **2004**.

172. Jeong, H. T.; Kim, J.-H.; Kim, W. T.; Kim, D. H. The mechanical relaxations of a Mm55Al25Ni10Cu10 amorphous alloy studied by dynamic mechanical analysis. *Mater. Sci. Eng. A* **2004**, *385*, 182–186.

173. Guo, L.; Wu, X.; Zhu, Z. Mechanical relaxation studies of α and slow β processes in Nd65Fe15Co10Al10 bulk metallic glass. *J. Appl. Phys.* **2011**, *109*, 113524.

174. Ngai, K. L.; Capaccioli, S. Relation between the activation energy of the Johari-Goldstein belta relaxation and Tg of glass formers. *Phys. Rev. E - Stat. Nonlinear, Soft Matter Phys.* **2004**, *69*, 031501.

175. Wang, W. H. Correlation between relaxations and plastic deformation, and elastic model of flow in metallic glasses and glass-forming liquids. *J. Appl. Phys.* **2011**, *110*, 053521.

176. Liu, X. F.; Zhang, B.; Wen, P.; Wang, W. H. The slow β-relaxation observed in Ce-based bulk metallic glass-forming supercooled liquid. *J. Non. Cryst. Solids* **2006**, *352*, 4013–4016.

177. Wang, W. H.; Wen, P.; Liu, X. F. The excess wing of bulk metallic glass forming liquids. *J. Non. Cryst. Solids* **2006**, *352*, 5103–5109.

178. Rosner, P.; Samwer, K.; Lunkenheimer, P. Indications for an excess wing in metallic glasses from the mechanical loss modulus in Zr65Al7.5Cu27.5. *Europhys. Lett.* **2004**, *68*, 226–232.

179. Hachenberg, J.; Bedorf, D.; Samwer, K.; Richert, R.; Kahl, A.; Demetriou, M. D.; Johnson, W. L. Merging of the alpha and beta relaxations and aging via the Johari-Goldstein modes in rapidly quenched metallic glasses. *Appl. Phys. Lett.* **2008**, *92*, 131911.

180. Hachenberg, J.; Samwer, K. Indications for a slow β-relaxation in a fragile metallic glass. *J. Non. Cryst. Solids* **2006**, *352*, 5110–5113.

181. Cavaille, J. Y.; Perez, J. Molecular theory for the rheology of glasses and polymers. *Phys. Rev. B* **1989**, *39*, 2411–2422.

182. Gauthier, C.; Pelletier, J. M.; David, L.; Vigier, G.; Perez, J. Relaxation of non-crystalline solids under mechanical stress. *J. Non. Cryst. Solids* **2000**, *274*, 181–187.

183. Qiao, J. C.; Pelletier, J. M. Mechanical relaxation in a Zr-based bulk metallic glass: Analysis based on physical models. *J. Appl. Phys.* **2012**, *112*, 033518.

184. Hecksher, T.; Nielsen, A. I.; Olsen, N. B.; Dyre, J. C. Little evidence for dynamic divergences in ultraviscous molecular liquids. *Nat. Phys.* **2008**, *4*, 737–741.

185. Martinez-Garcia, J. C.; Rzoska, S. J.; Drozd-Rzoska, A.; Martinez-Garcia, J. A universal description of ultraslow glass dynamics. *Nat. Commun.* **2013**, *4*, 1823.

186. Wang, Z.; Wen, P.; Huo, L. S.; Bai, H. Y.; Wang, W. H. Signature of viscous flow units in apparent elastic regime of metallic glasses. *Appl. Phys. Lett.* **2012**, *101*, 121906.

187. Kuršumović, A.; Scott, M. G.; Cahn, R. W. Creep recovery spectra in Fe40Ni40B20 metallic glass. *Scr. Mater.* **1990**, *24*, 1307–1312.

188. Ocelík, V.; Csach, K.; Kasardová, A.; Bengus, V. Z. Anelastic deformation processes in metallic glasses and activation energy spectrum model. *Mater. Sci. Eng. A* **1997**, *226-228*, 851–855.

189. Ju, J. D.; Jang, D.; Nwankpa, A.; Atzmon, M. An atomically quantized hierarchy of shear transformation zones in a metallic glass. *J. Appl. Phys.* **2011**, *109*, 053522.

190. Ju, J. D.; Atzmon, M. A comprehensive atomistic analysis of the experimental dynamic-mechanical response of a metallic glass. *Acta Mater.* **2014**, *74*, 183–188.

191. Xi, X. K.; Zhao, D. Q.; Pan, M. X.; Wang, W. H.; Wu, Y.; Lewandowski, J. J. Fracture of brittle metallic glasses: Brittleness or plasticity. *Phys. Rev. Lett.* **2005**, *94*, 125510.

192. Kahl, A.; Koeppe, T.; Bedorf, D.; Richert, R.; Lind, M. L.; Demetriou, M. D.; Johnson, W. L.; Arnold, W.; Samwer, K. Dynamical and quasistatic structural relaxation paths in Pd40Ni40P20 glass. *Appl. Phys. Lett.* **2009**, *95*, 201903.

193. Harmon, J. S.; Demetriou, M. D.; Johnson, W. L.; Samwer, K. Anelastic to plastic transition in metallic glass-forming liquids. *Phys. Rev. Lett.* **2007**, *99*, 135502.

194. Spaepen, F. Homogeneous flow of metallic glasses: A free volume perspective. *Scr. Mater.* **2006**, *54*, 363–367.

195. Johnson, W. L.; Demetriou, M. D.; Harmon, J. S.; Lind, M. L.; Samwer, K. Rheology and Ultrasonic Properties of Metallic Glass-Forming Liquids: A Potential Energy Landscape Perspective. *MRS Bull.* **2007**, *32*, 644–650.

196. Zhao, Z. F.; Wen, P.; Shek, C. H.; Wang, W. H. Measurements of slow β - relaxations in metallic glasses and supercooled liquids. *Phys. Rev. B - Condens. Matter Mater. Phys.* **2007**, *75*, 174201.

197. Liu, S. T.; Wang, Z.; Peng, H. L.; Yu, H. B.; Wang, W. H. The activation energy and volume of flow units of metallic glasses. *Scr. Mater.* **2012**, *67*, 9–12.

198. Pan, D.; Inoue, A.; Sakurai, T.; Chen, M. W. Experimental characterization of shear transformation zones for plastic flow of bulk metallic glasses. *Proc. Natl. Acad. Sci. U. S. A.* **2008**, *105*, 14769.

199. Greaves, G. N.; Greer, A. L.; Lakes, R. S.; Rouxel, T. Poisson's ratio and modern materials. *Nat. Mater.* **2011**, *10*, 823–838.

200. Yu, H. B.; Shen, X.; Wang, Z.; Gu, L.; Wang, W. H.; Bai, H. Y. Tensile plasticity in metallic glasses with pronounced β relaxations. *Phys. Rev. Lett.* **2012**, *108*, 015504.

201. Lu, Z.; Jiao, W.; Wang, W. H.; Bai, H. Y. Flow unit perspective on room temperature homogeneous plastic deformation in metallic glasses. *Phys. Rev. Lett.* **2014**, *113*, 045501.

202. Ruta, B.; Giordano, V. M.; Erra, L.; Liu, C.; Pineda, E. Structural and dynamical properties of Mg65Cu25Y10 metallic glasses studied by in situ high energy x-ray diffraction and time resolved x- ray photon correlation spectroscopy. *J. Alloys Compd.* **2014**.

203. Liu, C.; Pineda, E.; Crespo, D. Characterization of mechanical relaxation in a Cu–Zr–Al metallic glass. *J. Alloys Compd.* **2014**, *In press*.

204. Pauly, S.; Das, J.; Mattern, N.; Kim, D. H.; Eckert, J. Intermetallics Phase formation and thermal stability in Cu – Zr – Ti (Al) metallic glasses. *Intermetallics* **2009**, *17*, 453–462.

205. Wang, Z.; Sun, B. a.; Bai, H. Y.; Wang, W. H. Evolution of hidden localized flow during glass-to-liquid transition in metallic glass. *Nat. Commun.* **2014**, *5*, 5823.

206. Ulfert, W.; Kronmuller, H. Anelastic and viscoelastic behaviour of amorphous Zr(65)Cu(17.5)Ni(10)A(17.5) in the range of the glass transition. *J. Phys. Iv* **1996**, *6*, 617–620.

207. Chen, H. S.; Goldstein, M. Anomalous viscoelastic behavior of metallic glasses of Pd-Si-based alloys. *J. Appl. Phys.* **1972**, *43*, 1642–1648.

208. Taub, A. I. Stress-strain rate dependence of homogeneous flow in metallic glasses. *Acta Metall.* **1980**, *28*, 633–637.

209. Berlev, A.; Bobrov, O.; Khonik, V.; Csach, K.; Juríková, A.; Miškuf, J.; Neuhäuser, H.; Yazvitsky, M. Viscosity of bulk and ribbon Zr-based glasses well below and in the vicinity of Tg: A comparative study. *Phys. Rev. B* **2003**, *68*, 132203.

210. Csach, K.; Bobrov, O.; Khonik, V.; Lyakhov, S.; Kitagawa, K. Relationship between the shear viscosity and heating rate of metallic glasses below Tg. *Phys. Rev. B* **2006**, *73*, 092107.

211. Kramer, M. J.; Ott, R. T.; Sordelet, D. J. Anisotropic atomic structure in a homogeneously deformed metallic glass. *J. Mater. Res.* **2007**, *22*, 382–388.

212. Gibbs, M. R. J.; Stephens, D. W.; Evetts, J. E. log time relaxation kinetics and the activation energy spectrum model. *J. Non. Cryst. Solids* **1984**, *61-62*, 925–930.

213. Kontogiorgos, V. Calculation of Relaxation Spectra from Stress Relaxation Measurements. In *biopolymers*; Magdy Elnashar, Ed.; 2010; p. 495.

214. Yu, H. Bin The β relaxation in metallic glasses. 1–75.

215. Faupel, F.; Frank, W.; Macht, M. P.; Mehrer, H.; Naundorf, V.; Ratzke, K.; Schober, H.; Sharma, S.; Teichler, H. Diffusion in metallic glasses and undercooled metallic melts. *Rev. Mod. Phys.* **2003**, *75*, 237–280.

216. Tang, X. P.; Geyer, U.; Busch, R.; Johnson, W. L.; Wu, Y. Diffusion mechanisms in metallic supercooled liquids and glasses. *Nature* **1999**, *402*, 160–162.

217. Harms, U.; Jin, O.; Schwarz, R. B. Effects of plastic deformation on the elastic modulus and density of bulk amorphous Pd40Ni10Cu30P20. *J. Non. Cryst. Solids* **2003**, *317*, 200–205.

218. Khonik, S. V.; Sviridov, V. V.; Bobrov, O. P.; Yazvitsky, M. Y.; Khonik, V. A. Structural relxation and recovery of bulk and ribbon glassy Pd40Cu30Ni10P20 monitored By Measurements of Infralow-Frequency Internal Friction. *J. Phys. Condens. Matter* **2008**, *20*, 165204.

219. Nguyen, N. T. N.; Khonik, S. V.; Khonik, V. A. Isochronal shear stress relaxation and recovery of bulk and ribbon glassy Pd40Cu30Ni 10P20. *Phys. Status Solidi* **2009**, *206*, 1440–1446.

220. Madinehei, M.; Bruna, P.; Duarte, M. J.; Pineda, E.; Klemm, J.; Renner, F. U. Glass-formation and corrosion properties of Fe-Cr-Mo-C-B glassy ribbons with low Cr content. *J. Alloys Compd.* **2014**, *615*, S128–S131.

221. Greer, A. L. Atomic transport and structural relaxation in metallic glasses. *J. Non. Cryst. Solids* **1984**, *61-62*, 737–748.

222. Khonik, V. a.; Kitagawa, K.; Morii, H. On the determination of the crystallization activation energy of metallic glasses. *J. Appl. Phys.* **2000**, *87*, 8440.

223. Primak, W. Kinetics of processes distributed in activation energy. *Phys. Rev.* **1955**, *100*, 1677–1689.

224. Gibbs, M. R. J.; Gibbs, M. R. J.; Evetts, J. E.; Evetts, J. E.; Leake, J. a; Leake, J. a Activation energy spectra and relaxation in amorphous materials. *J. Mater. Sci.* **1983**, *18*, 278–288.

225. Yuan, C. C.; Xiang, J. F.; Xi, X. K.; Wang, W. H. NMR signature of evolution of ductile-to-brittle transition in bulk metallic glasses. *Phys. Rev. Lett.* **2011**, *107*, 236403.

226. Jiang, W. H.; Atzmon, M. Room-temperature flow in a metallic glass - Strain-rate dependence of shear-band behavior. *J. Alloys Compd.* **2011**, *509*, 7395–7399.

227. Sen, S.; Mukerji, T. Diffusion and viscosity in silicate liquids: Percolation and effective medium theories. *Geophys. Res. Lett.* **1997**, *24*, 1015–1018.

228. Hunt, A. G. Fragility of liquids using percolation-based transport theories - correlation between limiting slope of the viscosity and non-exponentiality of relaxation. *J. Non. Cryst. Solids* **2000**, *274*, 93–101.

229. Ferrari, L.; Mott, N. F.; Russo, G. A defect theory of the viscosity in glass-forming liquids. *Philos. Mag. A* **1989**, *59*, 263–272.

230. Juríková, A.; Csach, K.; Ocelík, V.; Miškuf, J.; Bengus, V. Z. Spectral analysis of creep recovery process in finemet type amorphous alloy. *Czechoslov. J. Phys.* **2002**, *52*, A125–A128.

231. Johnson, W.; Samwer, K. A Universal Criterion for Plastic Yielding of Metallic Glasses with a (T/Tg)2/3 Temperature Dependence. *Phys. Rev. Lett.* **2005**, *95*, 195501.